Dissertation

Investigation of the effect of Enhanced Oil Recovery by polymers on corrosion processes in oil and gas production

Durchgeführt zum Zwecke der Erlangung des akademischen Grades eines Doktors der technischen Wissenschaften unter der Leitung von

Ao.Univ.Prof. Dipl.-Ing. Dr.techn. Paul Linhardt

E164
Institut für chemische Technologie und Analytik

Eingereicht an der Technischen Universität Wien
Fakultät für Technische Chemie

durch

Dipl.-Ing. Moritz Schwingenschlögl, BSc
Matrikelnummer e1226108

Wien, am 30.05.2023

Danksagung

Ein großes Dankeschön gilt meinem Betreuer **Prof. Paul Linhardt**, der mich in den Jahren immer unterstützt und betreut hat, für die vielen wertvollen Ratschläge in und außerhalb der Arbeit und das angenehme Miteinander, das mir meine gesamte Arbeitszeit mehr als angenehm gestaltet hat. Danke für die Ermutigungen auch bei Rückschlägen nicht nachzugeben und positiv weiterzuarbeiten.

Bei **DI Günther Ball** möchte ich mich für die Unterstützung, den großartigen fachlichen Input und die zahlreichen „Bastelstunden" bedanken. Auch für das ein oder andere graue Haar, bei dir und mir, einige Glasscherben aber immer viel Spaß in den gemeinsamen Arbeitsstunden, Danke.

Ein herzliches Dankeschön geht auch an meine Kooperationspartner der OMV Austria, allem voran **Dr. Stefan Hönig**, der mich in fachlichen und praktischen Fragestellungen immer wieder tatkräftig unterstützt und weitergebracht hat. Auch dem restlichen Team des TechCenters gebührt hier ein Dankeschön für die angenehmen Monate in Gänserndorf.

Für die vielen Messungen am Rheometer und die unzähligen last-minute Terminbuchungen geht ein großes Dankeschön an **Dr. Lisa Sinawehl**.

Bei allen Kollegen am **Institut für chemische Technologie und Analytik**, die mich während meiner Zeit an der TU begleitet haben, für die unzähligen Diskussionen beim Kaffee, die mehr oder weniger fachlichen Ratschläge und einige entspannende Partien am Tischfußballtisch. Danke für diese Zeit!
Die Kollegen, die sich mit mir ein Büro teilen mussten: **Robert, Tobi, Ella, Lena, Elisabeth Andi und Nico** für alles, was wir erlebt haben- während und außerhalb der „normalen Arbeitszeiten". Für die heiteren Abende und jeden Arbeitstag an dem ich gern in Büro gekommen, vielen Dank!
Dem zweiten „Stockwerks-Papa" **Markus** fürs Mitorganisieren, Aufräumen und die fachmännische Betreuung unseres Elektrolyt-Getränke Kühlschranks.
Auch alle anderen Kollegen: **Stefan, Pret, Gregor, Beda, Therry, Essi, Johannes, Lisa, Kathi, Vinc, Anna, Basti, Irina, Ufuk, Berni, Sebi, Karo, Felix x2 und David**, die in unserem Institut immer eine Atmosphäre geschaffen haben, die mich auch an schlechten Arbeitstagen immer wieder aufgeheitert hat. Danke und hoffentlich auf noch viele weiter Nachmittage/Abende/Nächte, die wir noch gemeinsam verbringen werden!

Auch allen anderen **Institutsangehörigen und Professoren**, die immer ein angenehmes und offenes Miteinander gepflegt und auch außerhalb der Arbeitszeiten für einige lustige Stunden gesorgt haben.

Der wohl größte Dank gilt meinen **Eltern**, die mir mein Studium ermöglicht haben und mich in allen erdenklichen Situationen tatkräftigt unterstützt und ermutigt haben weiter zu machen und auf die ich mich immer verlassen konnte.

Danke auch an **Simone**, die mich einen beträchtlichen Teil meiner Zeit begleitet hat, mir Ratschläge, Aufmunterungen und Ermunterungen mitgegeben hat; vielen Dank.

Weiters gilt mein Dank meiner **restlichen Familie und meinen Freunden**, die mich in den letzten Jahren immer wieder ausgehalten, ermutigt und unterstützt haben.

Vielen lieben Dank euch **ALLEN** für 3,5 Jahre, „auf und abs", viel Kaffee und das ein oder andere Bier, viel Spaß und lustige Aktionen die ich nicht missen möchte!

DANKE!

Kurzfassung

Im Bereich der Erdöl- und Erdgasförderung wird Enhanced Oil Recovery (EOR) eingesetzt, um die Förderungsraten zu steigern. Eine Methode besteht darin, ein Polymer, in der Regel hydrolisiertes Polyacrylamid oder Polysaccharide, im Flutwasser zu lösen oder zu quellen und die so entstandene hoch viskose Lösung in die Lagerstätte zu pumpen. Indem Verdrängung und Emulsionsbildung ausgenutzt werden, kann der Anteil an geförderten Kohlenwasserstoffen erhöht werden. In Pilotprojekten der OMV Austria wird hydrolisiertes-Polyacrylamid (HPAM) verwendet. Während kontinuierlicher Korrosionsüberwachung bei der Erdölförderung wurden erhöhte Korrosionsraten am eingesetzten Kohlenstoffstahl beobachtet, obwohl die üblichen Korrosionsschutzmaßnahmen unverändert blieben. Zudem änderte sich das Korrosionsangriffsbild von einer akzeptablen gleichmäßig niedrigen Korrosiosrate zu einer kritischen erhöhten Lokalisierung. Da bei EOR-Methoden, Chemikalien zum Einsatz kommen, die bei der Öl- und Gasförderung normalerweise nicht vorkommen, sollten die Auswirkungen dieser Chemikalien, Polymere und Korrosionsinhibitoren auf das Korrosionssystem bewertet und verstanden werden.

Diese Arbeit beschäftigt sich mit der Untersuchung der Wechselwirkungen von EOR-Polymeren mit Kohlenstoffstahl und verschiedenen Korrosionsinhibitoren auf Basis dieser Beobachtungen. Elektrochemische Impedanzspektroskopie und potentiodynamische Scans mit einer rotierenden Zylinderelektrode in einer CO_2-gesättigten Salzlösung wurden eingesetzt, um die komplexen Wechselwirkungen zwischen Stahloberfläche, Inhibitor und Polymer zu untersuchen. Die entwickelte Methode, soll robuste und reproduzierbare Daten, den Polarisationswiderstand Rp liefern, welcher die durchschnittliche Korrosionsrate repräsentiert. Um auch Phänomene wie die Veränderung des Korrosionsangriffs hin zu einer Lokalisierung des Schadensbilds, zu verstehen wurde die Korrosion an der Rotating-cylinder electrode (RCE) mittels einer Potential Verschiebung beschleunigt. Dadurch konnte die Heterogenität des Oberflächenzustands deutlich dargestellt werden. Rheologische Messungen, Fourier-Transform Infrarot-Spektroskopie und Raster-Elektronenmikroskopie sollten helfen, die Polymerlösungen und die entstandenen Korrosionsschäden sowie Korrosionsprodukte zu untersuchen.

Es konnte gezeigt werden, dass die Wechselwirkung von Polymer mit Kohlenstoffstahl und Korrosionsinhibitor zu unerwünschten Veränderungen der Korrosionsprozesse führen kann. Diese unerwünschten Veränderungen treten aufgrund der Absorption und Wechselwirkung von Polymeren in Korrosionsinhibitoren und der daraus resultierenden Heterogenität der Metalloberfläche auf. Bei der Auswahl von Polymeren, Korrosionsinhibitoren und deren gewünschten Konzentrationen für die Anwendung in der Praxis müssen diese Faktoren berücksichtigt werden.

Abstract

Enhanced Oil Recovery (EOR) is used in the oil and gas industry to increase recovery rates. One technique involves dissolving or swelling a polymer, typically hydrolysed polyacrylamide or polysaccharides, in floodwater and pumping this highly viscous solution into the reservoir. This allows a higher proportion of hydrocarbons to be recovered by taking advantage of displacement and emulsion formation. Hydrolysed polyacrylamide (HPAM) is used in OMV Austria's pilot projects. However, during continuous corrosion monitoring at oil production, increased corrosion rates were observed on the carbon steel used, despite unchanged conventional corrosion protection by corrosion inhibitors is applied. In addition, the corrosion pattern changed from acceptable uniform corrosion to severe localization. As the EOR process involves the use of chemicals regimes not typically encountered in oil and gas production, it is critical to evaluate and understand the impact of these chemicals, i.e. polymers and corrosion inhibitors on the corrosion system.

This study focuses on investigating the interactions between EOR polymers and carbon steel and various corrosion inhibitors based on these observations.

Electrochemical impedance spectroscopy and potentiodynamic scans using a rotating cylinder electrode (RCE) in a CO_2-saturated artificial brine were used to investigate the complex interactions between the steel surface, inhibitor, and polymer. A special procedure was developed to provide robust and reproducible data on the polarisation resistance Rp, which represents the average corrosion rate. To understand phenomena such as the change in corrosion attack towards localised damage, corrosion on the RCE cylinder was accelerated by applying an anodic potential shift. This highlighted the heterogeneity of the surface condition. Rheological measurements, Fourier transformed infrared spectroscopy (FTIR) and scanning electron microscopy were used to study the polymer solutions, the resulting corrosion damage and the corrosion products.

It could be shown that the interaction between polymer, carbon steel and corrosion inhibitor can lead to undesirable changes in the corrosion processes. These modifications occur due to the adsorption and interaction of polymers and corrosion inhibitors causing heterogeneity at the metal surface. These factors must be considered when selecting polymers, corrosion inhibitors and their desired concentrations for practical application.

1 Introduction and fundamentals 1

1.1 Oil and Gas 1

1.1.1 Formation & composition of oil and gas 1

1.1.2 Exploration of oil and gas 2

1.1.3 Oil and gas production 3

1.1.4 Corrosion and corrosion protection in Oil field facilities 5

1.1.5 Corrosion rate assessment in oil and gas industry 8

1.2 Corrosion 10

1.2.1 Fundamentals 10

1.2.2 Thermodynamic considerations 12

1.2.3 Kinetic considerations 14

1.2.4 Corrosion phenomena 16

1.2.5 CO_2 Corrosion 18

1.2.6 Corrosion protection 21

1.2.7 Corrosion testing 23

2 Subjects of investigation 28

2.1 Considerations on the influence of polymer EOR on corrosion 30

3 Experimental procedures 32

3.1 Polymer brine preparation 32

3.2 Corrosion inhibitors 33

3.3 Rheological measurements 34

3.4 Specimen preparation 34

3.5 Metallographic preparation 36

3.6 Scanning electron microscopy 36

3.7 Pickling of carbon steel specimen 36

3.8 Fourier-transform infrared spectroscopy (FTIR) 37

3.9 Rotating cylinder electrode (RCE)- with Electrochemical Impedance spectroscopy (EIS) 37

3.9.1 Test cell setup 37

3.9.2 RCE and EIS Setup 38

3.9.3 Setting up the electrochemical experiments 39

3.10 Potentiodynamic scans 40

3.11 Potentiostatically accelerated corrosion (PAC) 40

4 Results 41

4.1 Characterisation of carbon steel specimen 41

4.2 Methodology development of EIS experiments 42

4.2.1 Setting up a new method 43

4.2.2 Round robin test with different EIS equipment and single measurement procedure 46

4.3 Influence of polymer 1 in laboratory tests 53

4.4 Comparison of different corrosion inhibitors and their influence 56

4.4.1 Comparison of CI1 and CI2 58

4.5 Influence of the polymer type and chain length on corrosion behaviour 60
4.5.1 Influence of different polymer samples on the carbon steel surface 60
4.5.2 Polymer type influence on CI1 62
4.5.3 Polymer type influence on CI2 63
4.6 Difference in polymer batches and their influence on corrosion behaviour 65
4.7 Influence of the chain length of EOR polymer 67
4.7.1 Polymer without inhibitor 67
4.7.2 Polymer with inhibitor 70
4.8 Potentiodynamic scans 72
4.9 Potentiostatically accelerated corrosion PAC 73
4.9.1 Localized corrosion patterns in P1-AfB electrolyte 73
4.9.2 Influence of P1 and its chain length on PAC tests 79
4.9.3 Influence of P5 and its chain length on PAC tests 81
4.9.4 Influence of CI1 concentration on P1 83
4.9.5 Influence of oxygen traces 85
5 Conclusions 88
6 References 91
7 Table of Figures 97

1 Introduction and fundamentals

1.1 Oil and Gas

1.1.1 Formation & composition of oil and gas

Formation of hydrocarbons is a long-term process, which took place millions of years ago when certain conditions were met. First, due to movement of the earth crust a sedimentary basin can be formed. Second, the created basin must contain a high amount of organic material, which becomes part of the sedimentary material, this sedimentary layer can be called “source rock”. The organic matter can originate from single celled plankton, algae, invertebrates, fish and organic material carried into ancient oceans, which is transformed under initial microbial action to a waxy material called kerogen. Third, by high pressure and elevated temperatures kerogen and the remaining organic matter in the source rock can be converted into mature oil. This maturing process takes place over millions of years and the maturity of the oil depends on the prevailing temperature: this so-called oil window is in a temperature range between 80-220°C but can vary with the resulting pressure. Heavy oil (immature oil) is considered to be built under lower temperatures, while the less viscous mature oil is formed at higher temperatures. After this maturation process, hydrocarbons migrate through faults and fractures into a permeable "reservoir rock" where due to geologic activity (formation of highly impermeable formations) it can be trapped and allows the crude oil to accumulate for years, Figure 1 gives a schematic overview. Depending on the rock formation in which the petroleum is found, it often comes together with a natural gas cap above the petroleum and saline water with higher density which thus sinks to the bottom. Tar sands and oil sands are crude oil in semi-solid form, where it is mixed with sand and water and may contain bitumen [1].

Petroleum or crude oil consists mostly of hydrocarbons, these are organic compounds from carbon and hydrogen only. Due to the decomposition of organic matter, which is described above, a variety of hydrocarbons can be formed, for example straight chain, branched chain, or cyclic molecules. The simplest one is methane CH_4 which is also the major component of natural gas. By contrast, crude oil is a mixture of longer hydrocarbon chains such as alkanes (paraffines, saturated hydrocarbons), alkenes (olefins, unsaturated hydrocarbons), alkynes (acetylenes, triple bond between C atoms), aromatic hydrocarbons (containing an aromatic nuclei) cycloalkanes (naphtenes) and asphaltenes (alkenes with 35 or more C atoms) [1-3]. These hydrocarbons determine the physical and chemical properties of crude oil, i.e. color, viscosity, boiling point etc. Further components which are often present in petroleum are sulfur, oxygen and nitrogen or traces of metals such as iron, copper, nickel and vanadium.

The oil industry classifies crude oil into three major categories: the geographic location where it is produced, the American Petroleum Institute (API) gravity which differs by the oils density and the sulfur content where sweet oil contains relatively little sulfur amount (often high amounts of carbon dioxide) and sour crude oil with high sulfur content. Each of these classifications will influence the costs of transportation, the refinery process and the quality of products made from crude oil[1, 3].

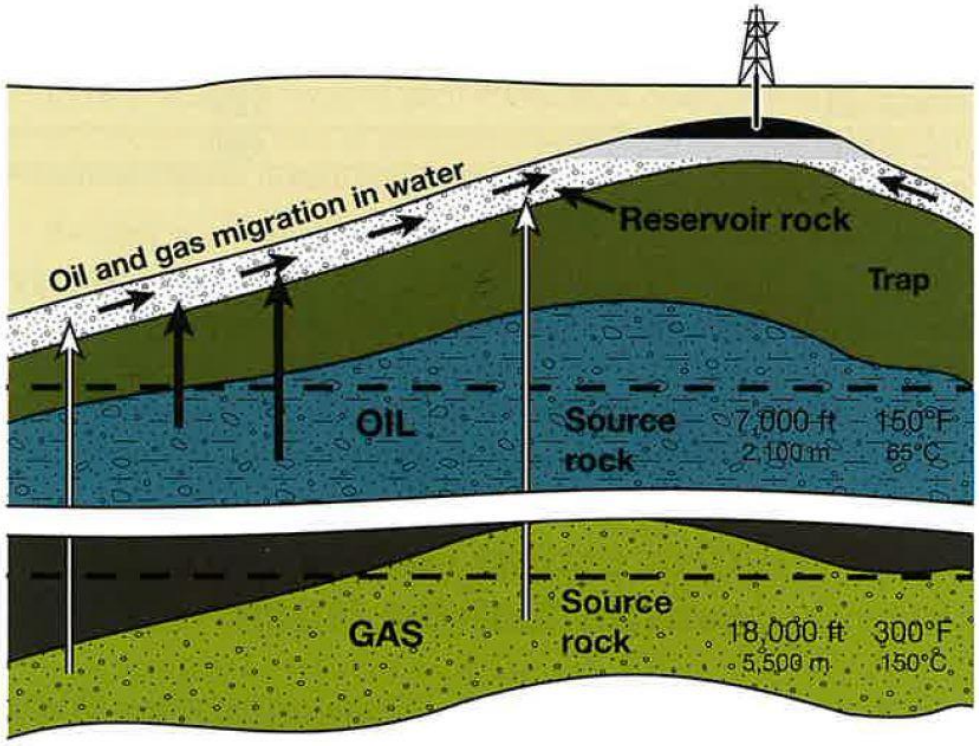

Figure 1: Formation and migration of oil and gas [1].

1.1.2 Exploration of oil and gas

This chapter should only give a short overview of used methods as exploration of oil and gas formations is not part of this thesis.

There are different techniques and survey methods to gain a detailed picture of the subsurface and therefore, possible oil and gas formations. Geological methods include mapping and sampling of rock formations, these are often available from earlier drilling activities for other resources such as water, coal or minerals. Geophysical methods should help to identify subsurface depth, thickness and properties of rock formations. These includes gravimetry, magnetometry and seismographic methods.

With data from above mentioned methods, companies start formation evaluation by drilling one or more exploratory wells to determine the geological structures and locate possible mineral deposits. The variety of assessment operations during exploration drilling are widely spread including well logging and real-time methods. Well logging allows geologists to gain a picture of subsurface formation and gives drill operators the possibility to monitor the drilling process. This includes methods such as lithographic, drill-time, mud and wireline logs.

To sum up, after exploration and the possible findings, companies need to evaluate costs and benefits of discovered formations before they can start drilling development and production wells. If the drilling is finished and drill equipment and rig have been removed from the wellbore, a production tree ("Christmas tree") is connected to it. Further explanation of oil drilling is beyond the scope of this thesis[1, 3].

1.1.3 Oil and gas production

The chronological way of oil and gas production is traditionally subdivided into three stages: primary, secondary and tertiary. These descriptions changed over time and where adapted to the conditions of the oil reservoir.[4] For the definition of enhanced oil recovery EOR we have to differentiate between improved oil recovery (IOR) and enhanced oil recovery (EOR). IOR is an overall term to increase oil production. For example, operation and injection strategies, field redevelopment and pressure support. EOR is considered a subset of IOR and is used to reduce the oil saturation below residual oil saturation of the reservoir obtained after earlier IOR. EOR is commonly equalled to tertiary recovery. [5], [6]

The exploitation of oil reservoirs can be divided as described above, Figure 2 shows the three stages of oil recovery, the acronym OOIP stands for original oil-in-place and refers to the total oil content of an oil reservoir. [6]

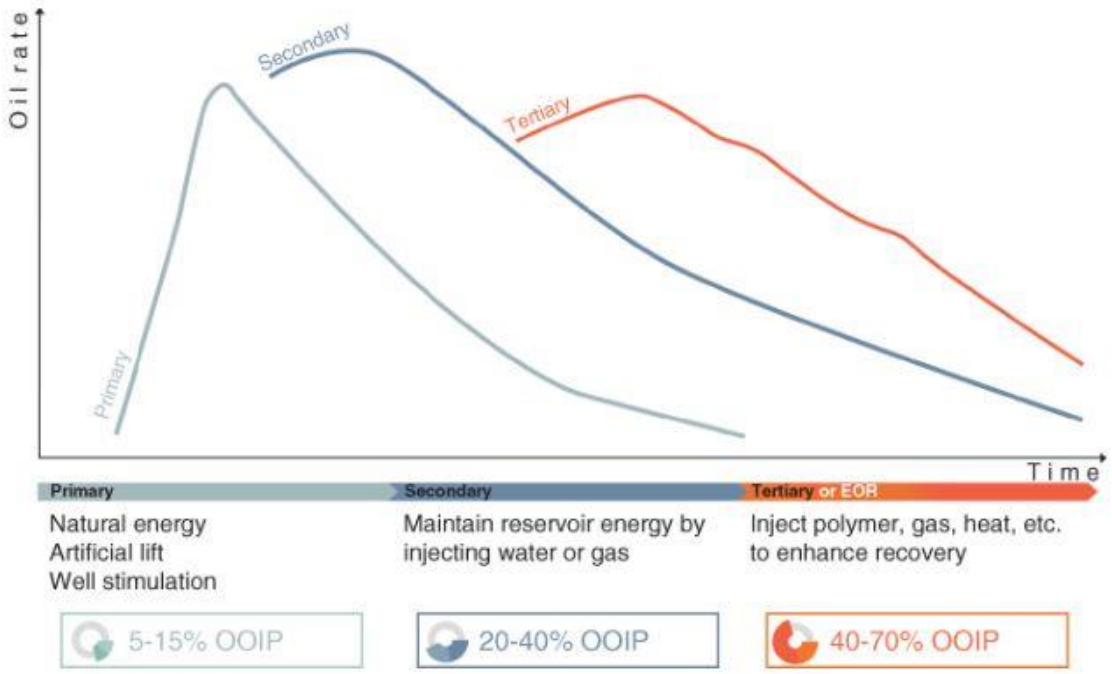

Figure 2: Hydrocarbon recovery mechanisms[6].

Primary recovery uses the natural energy present in a reservoir as a main source for crude oil displacement of oil producing wells. These energies are for example, fluid and rock expansion, solution gas drive, gas-cap drive, natural water drive, and gravity drainage. As long as the reservoir pressure remains high enough a production tree can be used to connect the well with tanks, or a distribution network of pipelines. If the pressure drops, for example if water (higher density than oil and gas) penetrates the subsurface formation, artificial lift methods can be applied to the well. A surface pump is a common approach to increase the production again, these "pumpjacks" (motor-driven sucker rod pumps) look like horse heads slowly going up and down [1, 3]. To maintain production a workover has to be done after a certain time. This includes the removal of water, drilling mud, scale (salt scales, e.g. sulphates and carbonates), paraffine scales and sand. Also repair and replacement actions of pumps, valves

tubing's and casings are performed to increase the production of hydrocarbons again[1].
If natural energy runs low and pumpjacks effectivity decreases, secondary recovery is used to enhance the energy through injecting water or gas into formation via injection wells to drive the fluids in the reservoir towards production wells. Injecting water is called waterflooding, where pre-treated water (removal of solids, bacteria, and oxygen) is introduced through several injection wells. It is necessary that this process is carefully adjusted to the target rock formation. A further method is a so-called gas lift, where compressed gas is injected and dissolves in the produced liquid forming bubbles, decreasing the density [1, 3, 4].
At tertiary recovery or Enhanced Oil Recovery (EOR), gases, liquid chemicals, and thermal energy can be used to enhance the displacement of reservoir fluids. Hydrocarbon gases, CO_2, nitrogen and flue gases are among the gases used in these processes. These gases have to be miscible with the oil.
Examples for liquid chemicals are polymers, surfactants and hydrocarbon solvents. For thermal processes, steam or hot water is typically used to supplement the natural energy in the reservoir. Primarily, the displacement of oil in the reservoir is enhanced but the injected fluids can also interact with reservoir rock/oil system to create favourable conditions for the recovery. Possible interactions are oil swelling or viscosity reduction and wettability modification. The line between secondary and tertiary oil recovery varies over time [4].

1.1.3.1 EOR processes and classification

Different sources divide EOR into categories, for example Green and Willhite [4] classify five categories while Lake [7] only differs three categories. Thomas [5] divides it into thermal and non-thermal EOR methods. For this thesis a short description of chemical, thermal and miscible processes appear sufficient. It should be mentioned that most of the mechanisms have some overlap, as chemicals are used in all categories, not only in chemical processes. [4]

1.1.3.1.1 Chemical Processes

These methods utilize a chemical formulation as displacing fluid to promote a decrease in mobility ratio. Major processes are polymer flooding, surfactant flooding, alkaline flooding, micellar flooding and alkaline-surfactant flooding.[5]

Polymer flooding

This mobility-control process uses a polymer-augmented waterflood, typically a solution of partially hydrolysed polyacrylamide (HPAM) polymer or polysaccharides which is injected to displace the oil towards production wells. [5] The concentration of the polymer brine depends on the reservoir characteristics and should be designed to develop a favourable mobility ratio between polymer solution and the oil/water bank and to improve the overall sweep efficiency. Polymers have two possible ways to affect the mobility. First, the injected polymer brine has a higher viscosity than injection water. Second, they can adsorb on porous media and/or are entrapped as a result of their large physical size. This effect would reduce the amount of polymer in the solution but causes a decrease in the effective permeability of the porous medium which increases the mobility of oil. [4]

Surfactant flooding

Surfactants like petroleum sulfonates are often used to lower the interfacial tension between oil and water. The surfactant slug is followed by a polymer slug with low polymer concentration (a few 100 ppm [4]) and further chemical slugs to enhance the recovery. [5]

Alkaline flooding

This is a complex process due to various reactions between alkaline chemicals and reservoir rock and fluids. A slug consisting of hydroxide, carbonate or orthosilicate of sodium are injected into the reservoir and reacts with acidic components of the crude oil to produce a surfactant insitu. The interfacial tension reduction described above takes place and increases oil recovery rates. [5]

1.1.3.1.2 Thermal Processes

This includes hot water injection, steam injection and in situ combustion. The recovery rate is increased mainly due to thermal heat transfer resulting in oil viscosity reduction, oil swelling and steam flashing. [6] Thermal methods are usually used for heavy oil and tar sand reservoirs. [5]

1.1.3.1.3 Miscible Processes

There are two types of miscible flooding, the displacing fluid is miscible with the reservoir oil either at the first contact (first contact miscible process, FCM) or after multiple contacts (multiple contact miscible process, MCM). During FCM the injected fluid is directly miscible with the reservoir oil under prevailing conditions (pressure and temperature). At MCM processes the fluid is not miscible at the first contact, the miscibility depends on the modification of composition of the injected fluid or the oil. This is possible due to multiple contacts between the pases and mass transfer of components between them under proper conditions of pressure and temperature [4].

Regardless of the method a transition zone or mixing zone between the displacing fluid and the reservoir oil induces a piston-like displacement. Various miscible flooding methods exist, e.g. miscible slug processes, enriched gas drive, vaporizing gas drive and high pressure gas injection [5].

1.1.4 Corrosion and corrosion protection in Oil field facilities

There are three major areas where corrosion problems can occur and cause severe damage in the oil and gas industry: production, transportation and storage, and refinery operations [8]. For this chapter we will focus on production and transportation. A proper equipment design, materials selection and corrosion monitoring can result in economic advantages but more important in environmental safety [9]. Corrosion is therefore one of the outstanding challenging problems in industry. Catastrophies caused by material failure due to corrosion cost companies several millions of euros and the ecological damage can't be measured in money [10]. Carbon dioxide (CO_2), hydrogen sulphide (H_2S) and free water, especially the water salinity and the water cut, and other sulfur containing species are examples of components in crude oil and natural gas which are inherently corrosive for materials used in oil and gas facilities. Oxygen is usually only a problem in connection with surface equipment, as it's unlikely to occur naturally in downhole formations but nevertheless must not be

ignored [9, 11]. Further factors can be the fluid temperature, fluid dynamics and pH which are influencing the corrosivity of the environment.
When metal (mostly carbon steel is used) comes in contact with an electrolyte, the formation of anodes and cathodes is possible. Oxidation processes take place at anodic sites, where the metal loses electrons which are transferred through the metal to cathodic sites and used there for reduction processes. Typical for carbon steel is the oxidation of iron; see Equation1 with a parallel reduction depending on available species. Hydrogen evolution (Equation2) or oxygen reduction (depending on the pH, Equation 3 and Equation 4) or a metal ion reduction or deposition are possible (Equation 5).

Equation1: iron oxidation.

$$Fe \rightarrow Fe^{2+} + 2e^{-}$$

Equation2: Hydrogen evolution.

$$2H^{+} + 2e^{-} \rightarrow H_2$$

Equation 3: Oxygen reduction in acidic environment.

$$O_2 + 4H^{+} + 4e^{-} \rightarrow 2H_2O$$

Equation 4: Oxygen reduction in neutral or basic environment.

$$O_2 + 2H_2O + 4e^{-} \rightarrow 4OH^{-}$$

Equation 5: iron reduction or deposition.

$$Fe^{3+} + e^{-} \rightarrow Fe^{2+}$$

$$Fe^{2+} + 2e^{-} \rightarrow Fe$$

As described above, oxygen is regularly not available, CO_2 and H_2S are commonly present in aqueous solution and following reactions can be formed [12]:

Equation 6: Sweet corrosion (Carbon dioxide).

$$Fe + H_2CO_3 \rightarrow FeCO_3 + H_2$$

Equation7: Sour corrosion (H_2S)[13].

$$Fe + H_2S \rightarrow FeS + 2H$$

The major forms of corrosion in oil and gas industry described in this thesis will be sweet corrosion, sour corrosion and oxygen corrosion.

1.1.4.1 Sweet corrosion

Carbon dioxide is called sweet gas in petroleum industry and is not corrosive provided it stays dry. In aqueous solution, depending on the pH (Bjerrum plot, Figure 3) a protective scale can be formed. At high pH a carbonate film can be formed at the metal surface; lowering the pH will lead to a break down and the bare metal is exposed to carbonic acid. Elevated temperatures will enhance the formation of iron carbonate layer and therefore the corrosion of the carbon steel. The impact of sweet corrosion is rising in recent years due to increased CO_2 concentrations found in the wells, but this can be controlled using corrosion inhibitors. Other possibilities to prevent sweet corrosion are the use of martensitic stainless steels (>12% chromium) in environments with increased temperatures, where organic chemical-based corrosion inhibitors fail. During drilling the pH can be controlled with sodium hydroxide.[9, 11]

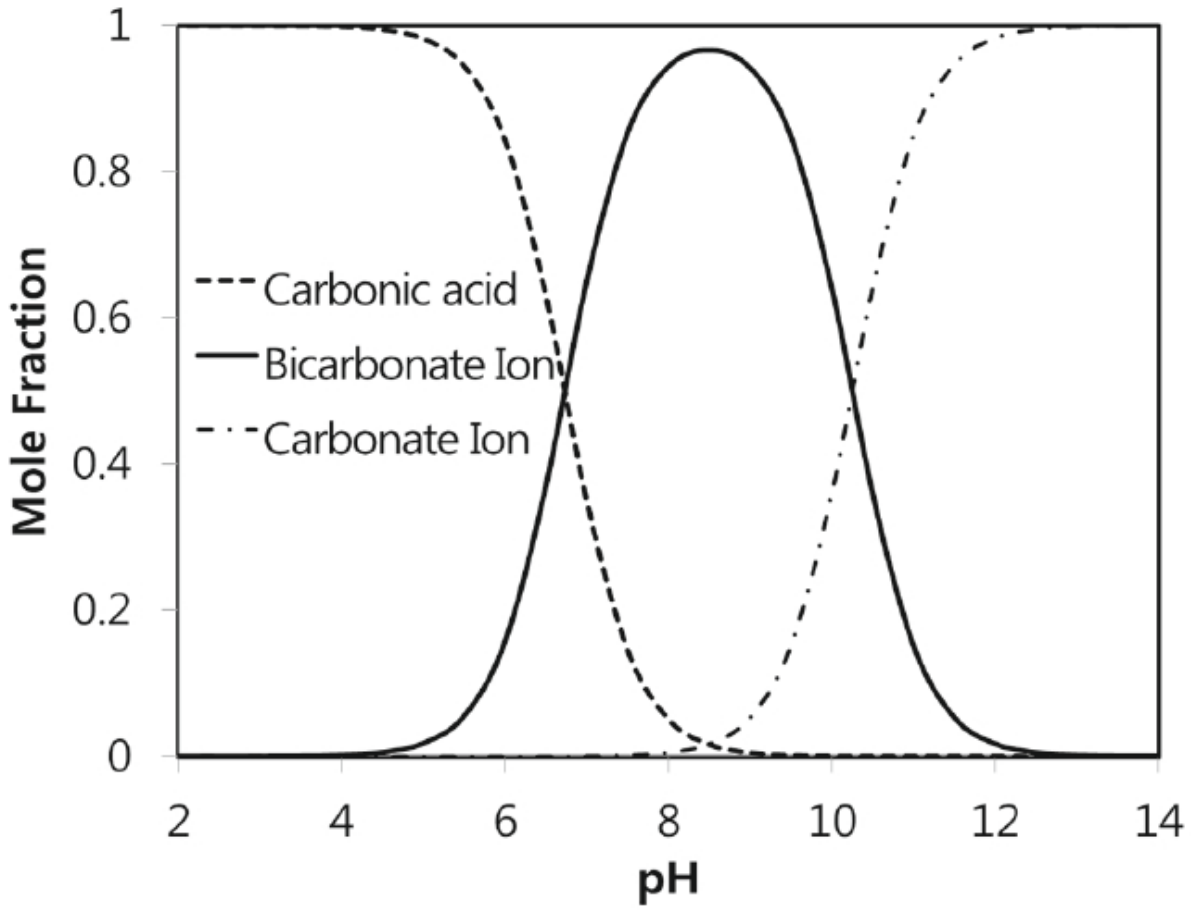

Figure 3: Bjerrum plot, pH vs. mole fraction of carbonate species[14].

1.1.4.2 Sour corrosion

Sulphur containing oil and gas are named sour crude or sour gas - the most common species containing sulphur is H_2S gas [15]. These sour conditions can originate from hydrogen sulphide in the downhole formation or from surface sources. H_2S toxic and more soluble in crude oil than in water, where a common concentration of 100-200 ppm is possible [16]. Further it can form a weak mineral acid when dissolved in water. With low pH values and microorganism reducing sulphate to sulphide which is called microbiologically induced corrosion (MIC) a corrosive regime is established [9]. Sour corrosion can occur as uniform or pitting corrosion and may lead to several forms of metal cracking, especially sulphide stress cracking and hydrogen stress cracking [11]. To control sour corrosion, corrosion inhibitors and H_2S scavengers or a combination of both can be used. For cracking control an appropriate material selection and stress design is necessary[13].

1.1.4.3 Oxygen corrosion

As mentioned before it's unlikely that oxygen naturally appears in oil and gas wells, but due to leaking seals, pumps, process vents, leaking injection systems and shallow wells oxygen ingress can take place. The solubility of oxygen in surface water is approximately 10 ppm but oxygen levels of 50-100 ppb are enough to start corrosion processes. Oxygen not only serves as an oxidant, it also accelerates CO_2 and H_2S induced corrosion mechanisms. The best way

to prevent oxygen corrosion is keeping it out of the system, either by preventing leakages or using oxygen scavengers to bind oxygen traces. Further methods are corrosion inhibitors in combination with oxygen scavengers, protective coatings and cathodic protection [9, 11].

1.1.4.4 Corrosion control

There are different approaches for corrosion mitigation in oil and gas industries. Among the important ones are the use of protective coatings, water treatment and corrosion inhibitors, cathodic protection and material selection. If existing materials are prone to corrosion attack it's possible to change the materials to one which suits the specific need, such as different alloyed steels [17]. If this is economically not reasonable, the materials already used have to be protected by other methods. To shorten it up the use of corrosion inhibitors will be discussed only.

Corrosion inhibitors are substances which are added in oil and gas industry to protect the oil field facilities, especially preventing the metal surfaces from corrosion. They can merge with the metal or react with impurities in the environment. Therefore, the liquid inhibitors are dispersed through the fluid in the pipelines and form a thin layer or film on available surfaces, either metal surfaces, already built scale surfaces or on dispersed particles in the fluid [11, 18]. Corrosion inhibitors are classified into groups based on how they control corrosion [9]:

- Adsorption and film-forming inhibitors
- Precipitation inhibitors
- Oxidizing or anodic passivation inhibitors
- Cathodic corrosion inhibitors
- Volatile or vapor-phase inhibitors

Practically, commercial corrosion inhibitors are multicomponent liquids with a variety of substances like: imidazolines, quaternary ammonium compounds, amines, long hydrocarbon chains, sulfur and phosphor components etc. Due to heteroatoms (sulfur, nitrogen, and phosphor) the inhibitor is able to adsorb on the metal surface and builds the protective film. The effectivity of corrosion inhibitor is strictly connected to the adsorption properties of its species. Further influencing factors for inhibitor efficiency are the inhibitor concentration, the exposure period, the temperature and the composition of the inhibitor product. Rajeev et al. predicts when two or more inhibiting substances (may be organic or inorganic) are added in a corrosive environment, the inhibiting effect can be enhanced compared to the inhibiting effect achieved by either of the two (or more) substances individually. This is called a synergistic effect of inhibition [18].

1.1.5 Corrosion rate assessment in oil and gas industry

There are different concepts to prevent corrosion in oil and gas industry including inspection, monitoring and testing. While they often overlap in practice, they have slightly different definitions. Inspection is used to determine the conditions of a system, monitoring and testing is for assessing corrosion control or the effectiveness of corrosion control in the field and tests

are performed to determine the suitability of materials and chemicals, often carried out in laboratories. Possible inspection methods are visual inspection, magnetic particle inspection, ultrasonic inspection, radiography and magnetic flux leakage inspection to name some non-destructive techniques (NDT). Methods for monitoring and testing will be described in more detail. Monitoring and testing allows to analyse corrosion rates and possible changes in corrosion behaviour [9].

1.1.5.1 Weight-loss coupons

For this monitoring and test method pre-weighed coupons or probes are inserted into the environment of interest. Usually, they could be made out of the same material as the surrounding facilities or from carbon steel which is the most susceptible material for corrosion attack. Online monitoring should therefore be mounted in the appropriate location, top for gas-phase and bottom for water/oil-phase. In laboratory tests the test solution should be, if possible, field based. The coupons are exposed for a period of time, usually between weeks and month. Afterwards the coupons are visually analysed for the developed corrosion pattern and by weight-loss measurement an average corrosion rate can be calculated. But it's inevitable to be aware that this average corrosion rate and pattern over a period of time may not reveal possible changes of mechanism before or during the exposure time. However, short term mass loss experiments tend to overestimate corrosion rates and therefore predicting a shorter life time for materials used. This method is a relatively simple procedure, can be used in any corrosive environment and provides information to the corrosion mechanism and rate. Limits are the overestimation of corrosion rate and the possible missing of pitting and MIC during short-term exposure [8, 9, 19].

1.1.5.2 Electrochemical corrosion rate monitoring

A possible online monitoring method are electrical resistance probes (ER), which is mostly used in combination with mass-loss measurements. These probes are commercially available and can be installed directly into the region of interest. The used metal probes have a characteristic resistance against to an applied electrical current, which would increase if corrosion or erosion decrease the metal amount of the probe. As the resistivity changes with temperature, probes have usually a temperature compensation system. This method can also be used to monitor corrosion inhibitor persistence's. However, ER can only detect corrosion in general but not distinguish corrosion patterns and is therefore used in combination with other methods like weight-loss coupons.

Another technique is the linear polarization resistance (LPR) measurement, which can be used online or as a laboratory test method. This technique takes advantage of the fact that the voltage/current diagram is frequently linear when the potential variations (±20 mV) near the corrosion potential are very small. With the polarization resistance Rp (Equation 8), resulting from the linear slope of the current/voltage diagram, it's possible to calculate the corrosion current (i_{corr}) through the Stern-Geary equation (Equation 9, β = Stern-Geary constants). The mass loss of corroding material can be calculated with the corrosion current due to the relation of the Faraday law with electrochemical processes. This technique can be only used

in aqueous environment; therefore, hydrocarbons and microorganism would disturb the measurement [9].

Equation 8: Polarization resistance.

$$R_p = \frac{\Delta E}{\Delta i}$$

Equation 9: Stern-Geary equation.

$$i_{corr} = \frac{\beta}{R_p}$$

Further techniques are potentiodynamic measurements, which lead to Tafel extrapolation, electrochemical noise measurement und electrochemical impedance spectroscopy (EIS). These are requiring more complex equipment and measurement conditions. Potentiodynamic scans and EIS will be discussed in the experimental procedure section.

1.2 Corrosion

We live in a metal-based society where various types of metals are used in our environment. Different steel grades are used in construction, the automobile industry, pipelines and tanks etc. In aerospace and food industries aluminium alloys are used, as well in electronic applications where copper is a main component. Even in the human body metals are used for replacements, arterial stents, screws and wires. E. McCafferty[20] divides into three main reasons to study corrosion: human life and safety, the costs of corrosion and conservation of corrosion.

Corrosion is an economic problem, the annual global cost of corrosion in 2022 was 2,5 trillion USD [21]. In general, the costs vary between 3 to 4 % of the worlds gross domestic product (GDP), but more than 15% of these costs can be saved with state-of-the-art technology for corrosion prevention and control[22].

In this thesis, we will only deal with metallic materials and aqueous electrolytes.

1.2.1 Fundamentals

The standard ISO 8044:2020 [23] gives some definitions to corrosion and all processes included:

Corrosion

> Physicochemical interaction between a metallic material and its environment. This can lead to a change in the metal's properties and a possible deterioration of the material [23].
>
> Corrosion usually occurs not by direct chemical reaction of the metal with its environment but rather by the coupled electrochemical half-cell reaction. Therefore, corrosion in aqueous environment is an electrochemical oxidation process[20, 24].

Corrosion system

> Consisting of environmental components (including coatings, surface layers and additional electrodes) which are influencing the metals in the system. This can be a positive or negative influence [23].

Corrosion effect

> Measurable change of the material, which may lead to a loss of its properties [23].

Corrosion damage

> Impairment of the function of a component or an entire system due to corrosion [23].

As defined above corrosion is an electrochemical process, divided into half-cell reactions linked at the interface material and environment (electrolyte). The presence of an electrolyte is a condition for corrosion to occur, i.e. conductive liquids, salt melts, or 50-70% humidity for atmospheric corrosion. If electrons are products in this half-cell reaction it is an oxidation process and an anodic reaction. Vice versa, if electrons are reactants it is a reduction process and cathodic reaction.

The anodic oxidation reaction leads to a metal loss, due to the oxidation process a positive metal ion is released. This causes a positive charge in the electrolyte (metal ion) and a negative charge (electrons) are left in the metal. Equation 10 are examples for possible anodic oxidation reactions.

Equation 10: Anodic oxidation reactions of iron and aluminum.

$$Fe(s) \rightarrow Fe^{2+}(aq) + 2e^{-}$$
$$Al(s) \rightarrow Al^{3+}(aq) + 3e^{-}$$

During cathodic reduction reaction an oxidizing agent (H^+ ions, O_2) is reduced with electrons provided from the metal and building a negative charge in the electrolyte. Possible reaction is provided in Equation 11, the formation of hydrogen gas after reduction of two hydrogen ions or the reduction of dissolved oxygen to hydroxyl ions. These reaction ´s are dependent on the pH.

Equation 11: Possible cathodic reduction reactions.

$$2H^{+} + 2e^{-} \rightarrow H_2$$
$$O_2(g) + 2H_2O + 4e^{-} \rightarrow 4OH^{-}$$

Both half-cell reactions may occur on different places of the metal surfaces in an aqueous electrolyte, because of its heterogeneous nature (impurities, different orientated grains or defects). Metal atoms located at the edges and corners of crystal planes (high energy sites) or at stressed surfaces have high possibility to pass into solution. Figure 4 gives a schematic overview on reactions at metal/electrolyte interfaces. Ions are transported through the electrolyte, while electrons are transported through the metal but the corrosion current flows through both, electrolyte and metal [20, 23-25].

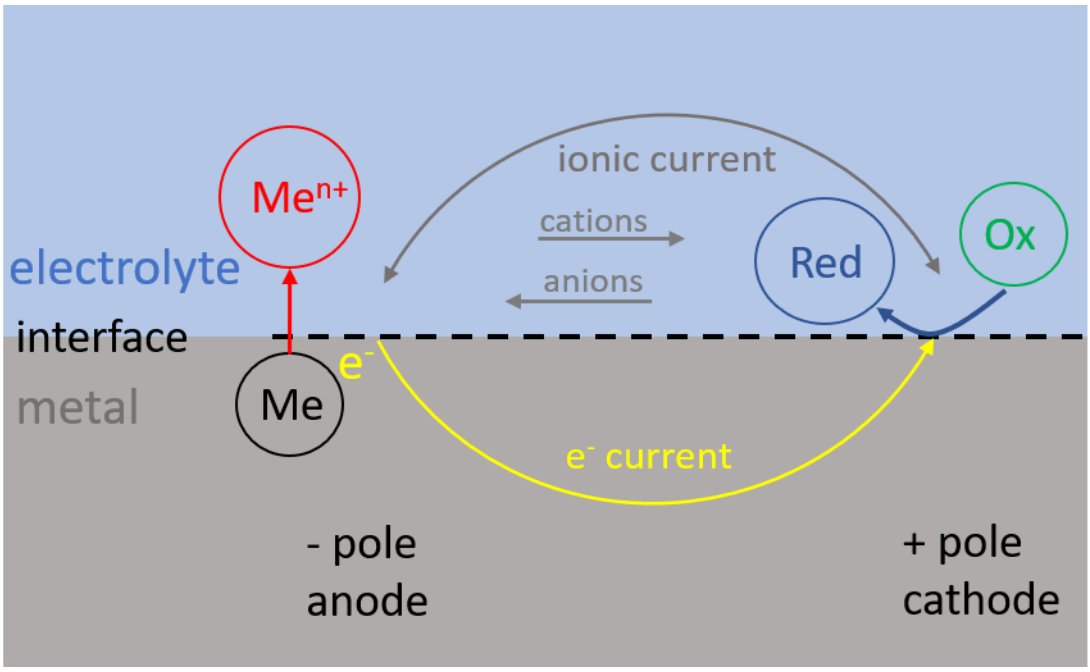

Figure 4: Schematic drawing of electrochemical processes at the metal/electrolyte interface modified after personal communication[26].

1.2.2 Thermodynamic considerations

As described above corrosion processes are electrochemical cells with at least one anode and one cathode generating and consuming electrons. These electrochemical cells are divided into half-cells, each half-cell reaction will be in an equilibrium state where the rates of forward and revers reaction are equal at a reversible potential ($E_{half\text{-}cell}$). Connecting both gives an overall electrochemical cell potential: $E^0_{cell} = E^0_{cathode} - E^0_{anode}$ where the E^0 is the standard potential of each half-cell reactions where the more negative electrode potential is the anode. The potential of these redox reactions describes the motivation of donating or accepting electrons. In a general case, electrodes or cells are not in their standard state therefore, the electrode potentials, depending on environmental conditions, can be calculated through the Nernst equation (Equation 12):

Equation 12: Nernst equation for half-cell potentials [27].

$$E = E^0 + \frac{RT}{nF} ln\left\{\frac{\prod(a_{ox})^j}{\prod(a_{red})^k}\right\}$$

Standard potential E^0 are given versus the standard hydrogen electrode (SHE), which is a universal reference electrode under standard state conditions (a_{H^+}=1, p_{H_2}=1 bar→ $E^0_{SHE} \equiv 0$). R is the gas constant, T the prevailing temperature, n the number of electrons of the reaction, F the Faraday constant and $\prod(a_{ox})^j$ and $\prod(a_{red})^k$ the products of the activities of oxidized and reduced species respectively, to the power of the stoichiometric coefficients in the half cell reactions.

With the calculated electrode potentials and the resulting electrochemical cell potential the free Gibbs Energy (ΔG) can be calculated as follows: ΔG = -n*F*E. Reactions with negative Gibbs Energy tend to be spontaneous[20, 24, 27].

To summarize these thermodynamic data and to simplify them, Marcel Pourbaix developed potential-pH diagrams, so called Pourbaix diagrams [28]. The ordinate is the electrode potentials E (electrochemical environment) and the abscissa is the pH of the aqueous solution (chemical environment) in these diagrams. These electrochemical maps, indicating the stability of ions, oxides and hydroxides are suitable for studies of electroplating, hydrometallurgy, electrolysis, electrical cells and corrosion. For corrosion studies, it's possible to determine areas where the electrochemical system is in an active state (corrosion), in a passivation state or in an immune state. Figure 5 is an example for a Pourbaix diagram (iron in water) where dashed line (a) is for anodic evolution of oxygen and dashed line (b) for cathodic evolution of hydrogen, i.e. the stability of the aqueous electrolyte. Regions where dissolved ions are stable (dotted regions), for example Fe^{2+} and Fe^{3+}, corrosion takes place. If the unreacted metal (Fe) is the stable species it is an immune region and if solid oxides, Fe_2O_3 and Fe_3O_4 (or hydroxides) are the stable phases, it's a region of passivation[20, 24, 29].

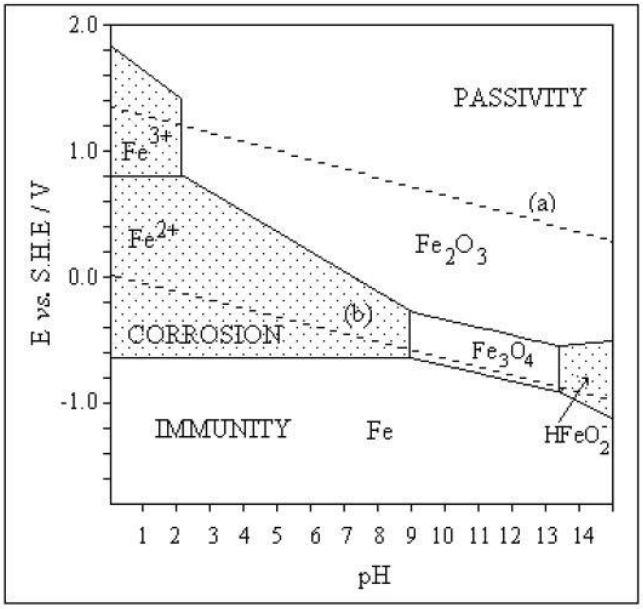

Figure 5: Pourbaix diagram of iron in water (25°C) [29].

A practical example for the different stable phases and passivating layers are potentiodynamic scans of steels. Therefore, Figure 6 shows schematic shape of the current-potential relationship of passivating steels and the influence of alloying elements and environmental conditions. Bold arrows indicating a positive influence, while normal arrows are unfavourable, respectively. Starting at U_R which corresponds to the open circuit potential (E_{OC}) and increasing the potential (to a more positive one) will lead to an increase in current I till the passivating potential U_{pas} is reached. This point can vary with environmental conditions and depending on the alloying elements it's possible that a passivating layer is build, i.e. chromium oxide. A dense passive layer stops iron dissolution but is able to transport electrons, the current decreases again, with increasing potential, and reaches a stable value which is called the passive region. If U_d is reached, the trans passive region where the passive layer breaks down begins and with increasing potential water decomposition to oxygen and hydrogen ions starts which determines the current increase[30].

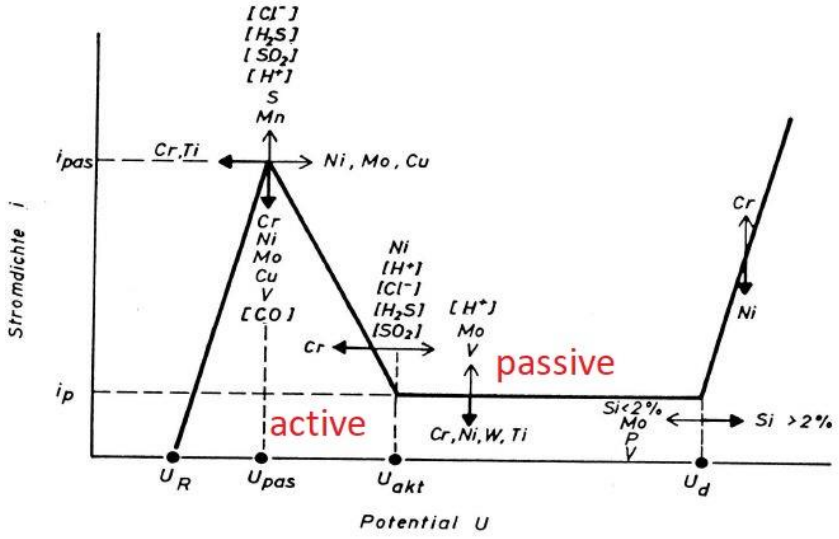

Figure 6: Schematic Current-potential curve indicating possible effects of alloying elements and electrolyte compositions.[30].

1.2.3 Kinetic considerations

With the thermodynamic considerations and Pourbaix diagrams above, we are able to determine if a reaction may be spontaneous or which phases are stable at certain conditions. But it gives no information about corrosion rates or if reactions proceed "slowly" or "quickly", therefore kinetic considerations will give information about reaction rates. Corrosion reaction rates depend on the electron flow rate to or from an electrode interface. At the equilibrium, i.e. anodic and cathodic reactions equal each other, the net electron rate is zero, i.e. negligible low, in an electrochemical system. Electron rate per time corresponds to the current density i_{corr} and with the corrosion potential E_{corr} of the system they are related with a corrosion rate through the 1. Faradaic law (Equation 13). Q is the quantity of charge transferred, I the current, t the time, M the molar mass of the electrode material and m the mass of the metal and z the electrons converted in the corrosion reaction [24, 31].

Equation 13: 1. Faradaic law with transformation to corrosion rate.

$$Q = n * z * F$$
$$Q = I * t$$
$$\frac{m}{t} = \frac{M * I}{z * F}$$

Cathodic and anodic reactions are limited due to the rate of reaction itself, the diffusion of educts and products to or from the electrode surface and the current transport in metal and electrolyte. While the metal has a high conductivity, the conductivity of electrolyte is lower and variable by its composition.

In electrochemical systems, the availability of electrons can be expressed as the potential while the reaction rate (electrons per time unit) corresponds to the current. As described above, each cathodic and anodic reaction (Equation 10 and Equation 11) is in a steady state with it reverse reaction, and exchange current rates ($\vec{\imath}_a = \overleftarrow{\imath_a} = i_{o,M}$, $\vec{\imath}_c = \overleftarrow{\imath_c} = i_{0,x}$, Figure 7)

are equal at the Nernst-potential (E_c and E_a) [20, 24, 32].

If the net rates of cathodic and anodic reaction are equal, and a steady state potential is established, the open circuit potential (OCP, E_{OC}, E_{corr}) with $\vec{\imath}_a + \vec{\imath}_c = \overleftarrow{\imath_a} + \overleftarrow{\imath_c} = i_{corr}$. Is there an overpotential η, i.e. a sufficient deviation from the corrosion potential, the backreactions $\overleftarrow{\imath_a}$ and $\vec{\imath}_c$ are neglectable. This overpotential is the difference between polarized and unpolarized electrode potentials $\eta = (E-E_{corr})$.

The reaction rate is determined by the charge transfer at the metal/electrolyte interface in electrochemical systems. With Butler-Volmer equation (Equation 14) the current to voltage relation can be described during corrosion measurements near E_{corr}[24, 32-34].

Equation 14: Butler-Volmer equation

$$i = i_{corr}\left\{exp\left[\frac{\alpha nF}{RT}\eta\right] - exp\left[\frac{(1-\alpha)nF}{RT}\eta\right]\right\}$$

The current density of the complete reaction is i, α is the transfer coefficient ranging between 0 and 1 and the other parameters were already described above. Rearranging and taking the logarithm to the basis 10 of Equation 14 a linear equation for η can be achieved, where two constants β_a and β_c (Tafel constants) can be defined [24, 32-34].

Equation 15: Tafel equation and Tafel slopes, respectively[34].

$$\eta = -\frac{RT}{\alpha nF}2{,}3 * \log i_{corr} + \frac{RT}{\alpha nF}2{,}3log|i|$$

$$\beta_a = \frac{2{,}30\ RT}{\alpha nF}, \qquad \beta_c = \frac{2{,}30\ RT}{(1-\alpha)nF}$$

Measuring the polarization curve and plotting in a half logarithmic diagram will give access to the Tafel-extrapolation, see Figure 7. For this, Tafel behaviour is assumed for individual oxidation (red) and reduction (Blue) reaction polarization curves. The slopes $B_{red,X}$ and $B_{ox,M}$ in this diagram correspond to the before mentioned Tafel constants, β_a and β_c respectively. E'_M and E'_X are the respective equilibrium half-cell potentials with their exchange current densities $i_{0,M}$ and $i_{0,X}$. The oxidation and reduction current density $i_{ox,M}$ and $i_{red,X}$ can be expressed with the logarithmic Butler-Volmer equation. As can be seen in Figure 7 if the overpotential approaches zero, the measured current i_{meas} also approaches zero, this is where oxidation and reduction reaction rates are equal. In a theoretical approach, a sufficient large positive or negative overpotential reduces the Tafel equation (logarithmic Butler-Volmer equation) to single oxidation or reduction reaction, the other one becomes negligible, and the branches become linear. For practical corrosion systems the branches deviate from this linear Tafel behaviour due to diffusion limitation, kinetic inhibition, passive layer formation etc [20, 24, 32-35].

Nevertheless, for very small overpotentials $\eta < 10$ mV and assuming equal transfer coefficients for oxidation und reduction Equation 14 can be simplified to Equation 16. The slope of these linear current-potential curves become linear and can be expressed as seen in Equation 17, where Rp is the polarization resistance, respectively. With this simplification Rp can be used for determination of i_{corr} and with Faradaic law above the corrosion rate can be estimated[24, 32, 33, 35].

Equation 16: Simplified Butler-Volmer equation for η<10 mV.

$$i = i_{corr} \frac{\alpha n F}{RT} \eta$$

Equation 17: Polarization resistance Rp.

$$\frac{d\eta}{di} = R_p = \frac{\beta_a |\beta_c|}{2{,}3 * (\beta_a + |\beta_c| \quad)} * i_{corr}$$

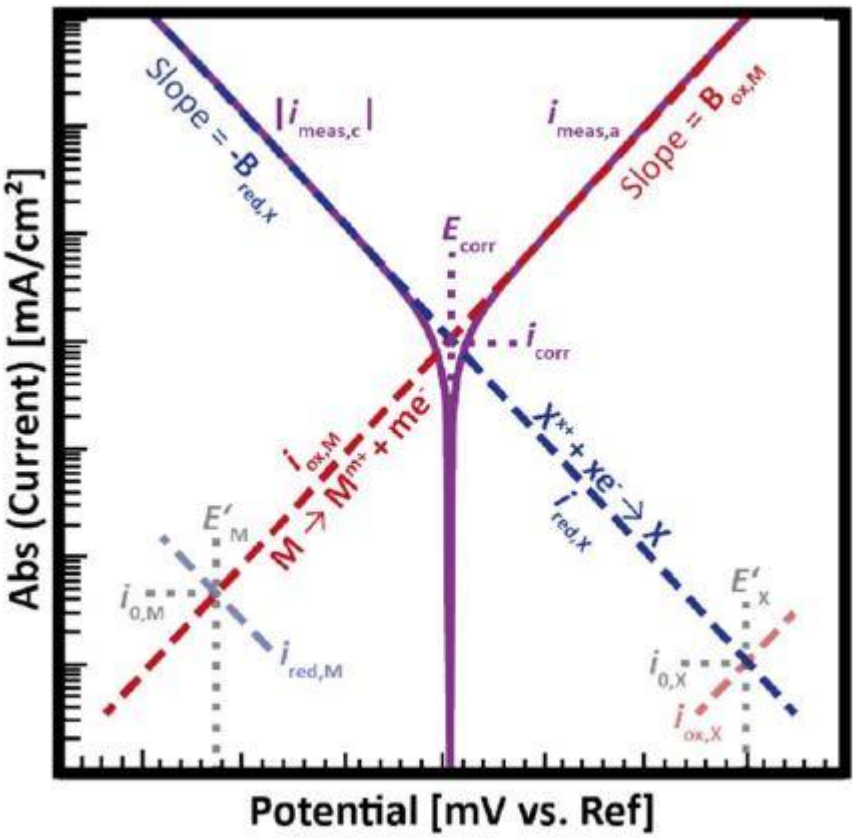

Figure 7: schematic experimental polarization curve [33].

1.2.4 Corrosion phenomena

In this chapter different types of corrosion phenomena and their impact on materials will be discussed, with a focus on uniform and localized corrosion as these two types are seen during EOR treatments and experiments of this thesis.

1.2.4.1 Uniform corrosion

This corrosion pattern is characterized by corrosion attack homogenously distributed across the metal surface, where instantaneously differences in the corrosion rate may occur but as the system changes continuously a uniform pattern is achieved. There are three possible states for metals: active, passive and immune.

Active:

The metal, mostly those with equilibrium potential not too far below hydrogen evolution potential, i.e. iron, copper, nickel, or low alloyed steels, must be in direct contact with its environment (electrolyte). In humid atmospheric conditions aqueous films can form on the

metal surface by adsorption acting as electrolyte, the critical humidity for corrosion decreases with salt and SO_2 contaminations. In a dry atmosphere, corrosion can take place at elevated temperatures, i.e. high temperature corrosion. For liquid electrolytes the composition has a major influence on half-cell reaction which take place (pH, dissolved components etc.). On a macroscopic scale anode and cathode changing their position continuously and corrosion rates are controlled by their kinetics. As most metals are polycrystalline or have different phases it's possible that slight differences occur, and the surface appears "bumpy". In an environment open to the air the corrosion rate depends on diffusion of oxygen to the metal surface for cathodic reduction. For example, in stagnant electrolytes the corrosion rate will be significant lower due to lower diffusion rates and therefore lower cathodic reaction rates. This active uniform corrosion has a low critical damage potential as corrosion rates may be estimated and therefore life time predictions are reliable[27, 30].

Passive:

In the passive region of Pourbaix diagrams the stable species are mostly oxides and hydroxides and corrosion rates are controlled by their properties, i.e. how dense and uniform the formed protective layer is (uniform metal oxide layer). In general, the corrosion rates are not significant if a uniform protecting oxide layer is built on the metal surface but the possibility for localized corrosion in specific environments increases due to possible defects in the passive layer[27].

Immune:

As described above, the metal is in a thermodynamically stable state (Figure 5) and corrosion rates diminish. In the case that the environment is free of metal ions low corrosion rates occur to reach the metal ion concentration required for equilibrium state[27].

1.2.4.2 Localized corrosion

There are various types of localized corrosion phenomena for metals, including pitting, crevice corrosion, intergranular attack, and stress corrosion cracking. Pitting and crevice corrosion are the major types, despite the different morphologies of these phenomena the mechanism behind is the same. Therefore, this chapter is focusing on pitting as localized phenomena. [22, 30].

A condition for localized corrosion is a heterogeneous surface with small areas where anodic processes are preferred and larger areas where the cathodic reaction occurs. This heterogeneous condition can be originating from multiphasic metals or due to the influence of electrolyte components on protective layers. During local corrosion there are possible potential, or pH differences and two types can occur. At Type I the pH regime shifts from the surrounding surface of the pit to the bottom of it, there a pH value remains constant. In combination with an occurring potential difference between pit bottom and metal surface and the resulting higher anodic current densities in the pit, cathodic reactions are suppressed. The cathodic reaction take place on the remaining metal surface, while anodic metal dissolution is more and more accelerated in the pit bottom.

Type II occurs in EVANS elements or locations where little or no exchange of corrosion products from the pit to the environment is possible, due to diffusion limitations. The rate

controlling reaction is therefore the oxygen reduction at the cathode on the metal surface. Due to the poor electrolyte exchange and diffusion limitation at the anode, anions of the electrolyte accumulate and acidify the pit as a result [30].

Despite these two types there can be a certain potential observed for pitting (E_{pit}) and a possible re-passivation potential (E_r). At potentials below E_{pit} (more negative) no localized corrosion is observed, no matter how long the metal is exposed to the environment otherwise, above (more positive) pitting starts almost immediately. The pitting potential is a function of temperature, composition of the metal and environmental composition. Measuring the E_{pit} potentiodynamically bears some errors as the pits need time to nucleate and therefore values measured at a certain potential scan rate may appear slightly higher than they are. Figure 8 shows schematically a potentiodynamic measurement for a passive metal in a chloride solution. The corrosion current density increases immediately after E_{pit} is reached and even if the potential is decreased afterwards, the current remains high till the re-passivation potential E_r is reached. This hysteresis is due to acidification of the pit bottoms and diffusion limitation of the electrolyte. At E_r passivating metals are able to re-passivate and corrosion attack is stopped.

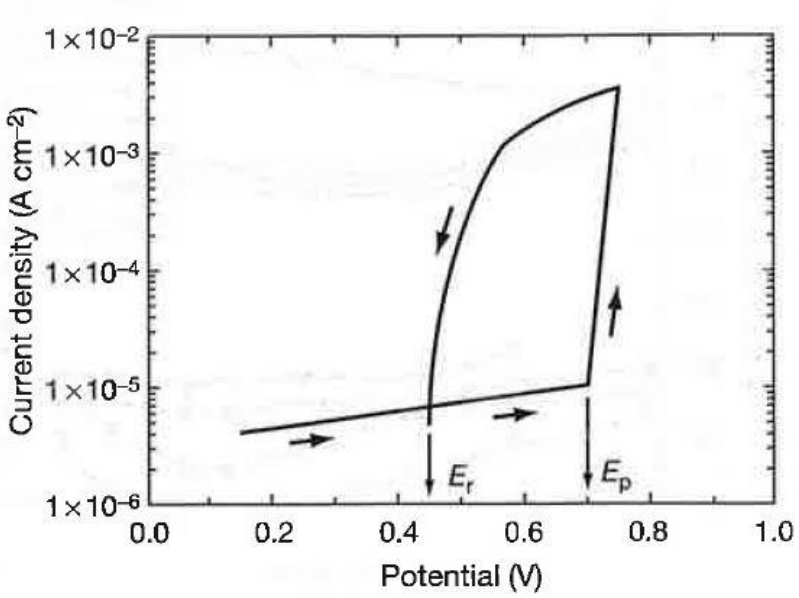

Figure 8: Polarization curve showing E_{pit} and E_r for a metal in a chloride solution[27].

1.2.5 CO_2 Corrosion

As described above the electrochemical corrosion reactions consist of two half-cell reactions. In case of CO_2 corrosion, the anodic reaction is the iron dissolution (oxidation) and the cathodic reaction is the reduction of certain species in the electrolyte for example, H_3O^+ or carbonate species from dissociation of H_2CO_3. The mechanism for corrosion in aqueous carbon dioxide saturated environment at elevated temperatures (up to 100°C) is well described by various publications [36-38], Equation 18 and Equation 19 show the dominating reactions in carbon dioxide saturated environment of mild steel [39]. The iron ions can form $FeCO_3$ in this environment when the saturation level for iron carbonate precipitation is exceeded.

$FeCO_3$ may precipitate on the steel surface forming a protective layer and reduce corrosion rates [36, 40]. The ratio between carbonate formation/precipitation to the corrosion rate defines the protectiveness of the built layer. To form a dense and protective layer the formation/precipitation rate has to be faster than the corrosion rate. Vice versa, if the corrosion rate is faster than the formation/precipitation ratio, the scaling tendency is reduced and only a porous iron carbonate layer is able to form [41-44].

Equation 18:Predominationg anodic reaction of carbon steel in CO_2 sat. environment.

$$Fe_{(s)} \rightarrow Fe^{2+}_{(aq)} + 2e^-$$

Equation 19: Predominating cathodic reactions of carbon steel in CO_2 sat. environment.

$$2H^+ + 2e^- \rightarrow H_{2(g)}$$
$$2H_2CO_{3(aq)} + 2e^- \rightarrow 2HCO_3^- + H_{2(g)}$$
$$2H_2O_{(l)} + 2e^- \rightarrow 2OH^-_{(aq)} + H_{2(g)}$$

Further parameters influencing the CO_2 corrosion are the pH, the temperature and partial pressure. Solubility of $FeCO_3$ depends on the pH, with increasing pH the solubility decreases leading to a higher scaling and precipitation rate [39, 41]. There are various studies concluding that with increasing temperature the corrosion rate of carbon dioxide corrosion increases due to kinetic effects of these electrochemical reactions[45]. Concluding the discussed literature formation of corrosion product, especially iron carbonate precipitation, strongly depends on prevailing temperature, pH and CO_2 partial pressure in ambient conditions.

As mentioned above there exists literature of effects for temperature and pH on CO_2 corrosion, Tanupabrungsun et al. [39] compiled various studies and developed potential-pH diagrams for the Fe-CO_2-H_2O system for various temperatures (range between 25°C to 250°C) and constant partial pressure of CO_2, i.e. constant activity of dissolved CO_2. The selected Fe^{2+} concentration for the developed Pourbaix diagrams is 10 ppm. The three Pourbaix diagrams Figure 9 to Figure 11 show the stable phases for Fe-CO_2-H_2O system at 25°C, 80°C and 100°C. Dashed lines indicate metastable phases ($Fe(OH)_2$ and Fe_3O_4), which have higher Gibbs free energy and are considered to transform into $FeCO_3$ (lowest Gibbs free energy). Tanupabrungsun et al. [39] conclude as follows:

- With increasing temperature, the $FeCO_3$ region shifts to the left therefore, formation and precipitation starts at lower pH.
- Below 80°C Fe^{2+} is stable in acidic conditions whereby $FeCO_3$ is stable in neutral and alkaline conditions. With increasing temperature (up to 250°C) additionally Fe_2O_3 becomes a stable phase in neutral and alkaline conditions (<80°C metastable Fe_2O_3).

Further, he was able to construct three-dimensional E-T-pH diagrams and T-pH diagrams and showed that with increasing Fe^{2+} concentration the stable phase area of $FeCO_3$ becomes larger, as well as with increasing CO_2 pressure.

Not only pH, temperature and CO_2 concentration are influencing this corrosion phenomenon, low-molecular-weight organic acids, especially acetic acid (HAc), can lead to corrosion of upstream facilities (tubing's, pipelines, separators etc.). Significant acceleration of corrosion rate is seen at temperatures >50°C and low pH <5. The formed iron acetate has a higher

solubility and therefore, impairs the protectiveness of iron carbonate[22].
Crude oil has as well effects on CO_2 corrosion, some inhibiting effects by providing naturally occurring chemicals acting as corrosion inhibitors and a wettability effect. Second effect is seen at low water cuts, where the crude oil phase is able to sweep away water from internal pipe walls. Naturally inhibiting components, containing oxygen, sulfur or nitrogen are surface active and get adsorbed on the steel surface[22].

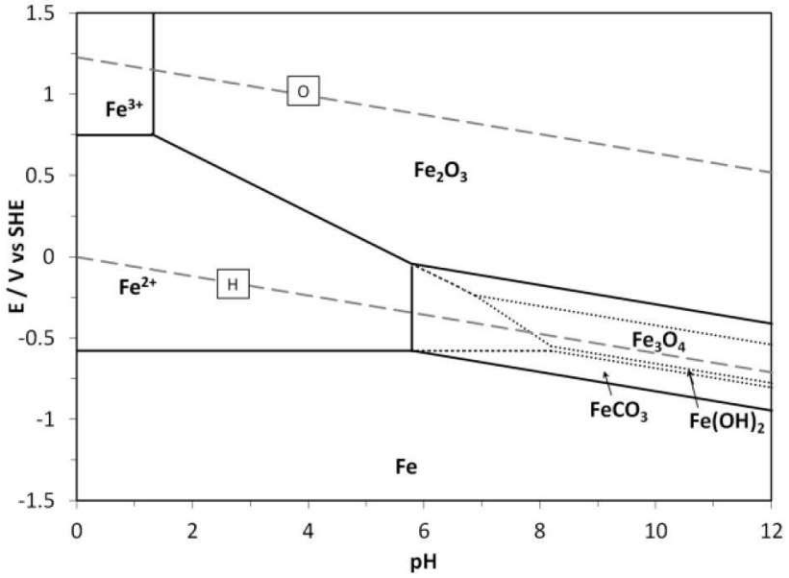

Figure 9: Pourbaix diagrams for Fe-CO2-H2O system; c(Fe^{2+})=10 ppm, c(Fe^{3+})=10 ppm at 25°C.

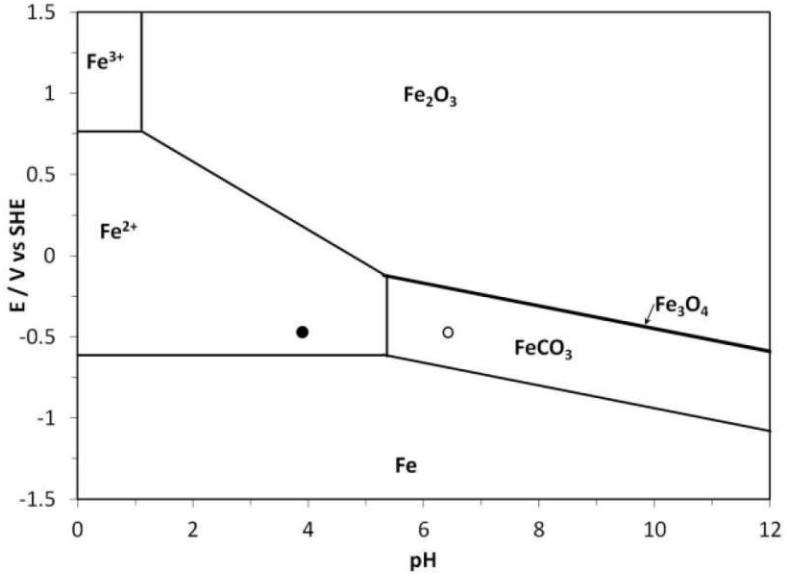

Figure 10:Pourbaix diagrams for Fe-CO2-H2O system; c(Fe^{2+})=10 ppm, c(Fe^{3+})=10 ppm at 80°C.

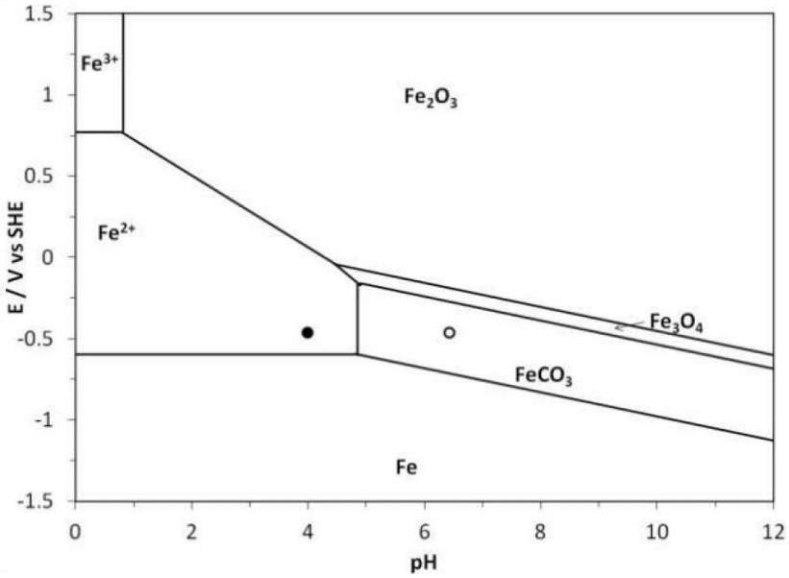

Figure 11:Pourbaix diagrams for Fe-CO2-H2O system; c(Fe^{2+})= 10 ppm, c(Fe^{3+})= 10 ppm at 100°C.

1.2.6 Corrosion protection

Corrosion protection starts with planning, design and construction of components which are exposed to a corrosive environment. Further, different aspects like costs and benefits, lifetime and safety have to be considered. These corrosion prevention methods are:

- Construction
- Material selection
- Modification of the interface metal/electrolyte
- Electrochemical corrosion protection
- Modification of the environment

For construction and material selection the ambient conditions, like salinity, temperature, pH etc. have to be well known. Also, materials combination must be chosen wisely to prevent galvanic corrosion. Considering all these parameters to select the right material for certain applications the environmental influence must not be neglected. As diffusion of reactants for corrosion reaction is a major influence, construction should be done properly to avoid dead ends or crevices.

The interface metal/electrolyte can be modified by organic or inorganic coatings therefore the adhesion to covering of metal surface is important to generate a new interface coating/electrolyte.

For cathodic corrosion protection there are two ways, using a sacrificial anode (Mg, Al, Zn) or the impressed current method [25, 30].

Depending on the area of application it's reasonable to modify the environment either by adding protective components (inhibitors) or removing corrosive agents (degassing, ion exchange). A definition for corrosion inhibitors is given by former National Association of Corrosion Engineers (NACE): "A substance which retards corrosion when added to an environment in small concentrations" [25]. Corrosion inhibitors (CI) have a wide spread application area, they are used for storage and transportation, in heating and cooling systems,

petroleum industry etc. and can be classified in environmental conditioners (scavengers) and interface inhibitors. Scavengers remove the corrosive species in the environment, for example oxygen scavengers are binding the oxygen in the electrolyte and therefore supressing the cathodic reaction. Interface inhibitors form a film at the interface metal/electrolyte and building a new interface: inhibitor film/electrolyte. These may be further subdivided into liquid phase inhibitors and vapor-phase inhibitors, for this thesis only liquid phase inhibitors are relevant [22].

Liquid phase inhibitors are classified into anodic, cathodic, or mixed type inhibitors depending which part of electrochemical reaction gets inhibited. Anodic or passivating inhibitors form or facilitate the formation of passivating films that inhibit the anodic metal dissolution. A major problem with this type is, with insufficient dosage, the CI will not adsorb homogeneously on the metal surface leaving uncovered sites leading to localized attack. The anodic area is relatively small compared to the cathodic area favouriting localised attack, where corrosion can be accelerated. Cathodic inhibitors can decrease the rate of reduction reaction or precipitate selectively at cathodic areas. Due to this precipitation a reduced reaction rate can be achieved by diffusion limitation of species used in cathodic reactions, i.e. oxygen. The most widely used corrosion inhibitors products are mixed type, which are acting in three possible ways [22, 25, 46]:

1. Physical adsorption
   Due to electrostatic attraction inhibitor components adsorb on the metal surface depending of its charge. These inhibitors interact rapidly but can be removed very easily again.
2. Chemisorption
   Compared to physical adsorption, chemisorption is a slow process but with increasing temperature adsorption and inhibition increases. The chemisorption involves charge sharing or charge transfer between inhibitor components and the metal surface. Therefore, it's possible that this phenomenon is not fully reversible.
3. Film formation
   By surface reaction adsorbed corrosion inhibitors can produce polymeric films. The formed inhibitor film blocks the electrolyte from the metal surface and can have conducting or non-conducting characteristics.

The corrosion inhibitor products can consist of either organic or inorganic components, which are influencing their solubility in hydrocarbon and water phases. Examples for inorganic components are chromates, molybdates, phosphates and polyphosphates, and zinc. Organic components include amines, amine salts, esters, ammonium derivates, mercaptans etc.

As the effectivity of an inhibitor is dependent on its adsorption on the metal surface, functional groups such as -NH, -N-N-, -CHO, R-OH and aromatic groups have a positive influence [25, 47].

1.2.7 Corrosion testing

There are different methods to asses corrosion rates and to test materials in certain environmental conditions to see their interaction and possible corrosion phenomena. The range is wide, from surface studies with X-ray diffraction and scanning electron microscopy (SEM), salt spray tests and weigh loss measurements to electrochemical methods. All these methods can be used to estimate the rate and the mechanism of corrosion.

Salt spray tests are used for evaluating the corrosion resistance of coatings used as a protective layer. The accelerated corrosion can be achieved by spraying a well-defined (pH, composition etc) salt solution on samples. Duration depending on the samples and requirements and can range up to 120 days, the performance of the samples is evaluated visually, following the DIN EN ISO 9227 [48].

Weight loss tests are a common and simple technique for corrosion rate assessment and they can be used for preliminary estimations about the corrosion pattern. Its expressed as the loss in weight per unit area or depth of metal ion per time. The specimen (the coupon) is exposed to a certain environment for a given duration, then analysing the specimens optically, removing corrosion products and determining the weight loss. The weight loss measurements are extremely versatile, since the coupons can be machined easily from any metal or alloy. A major advantage of this technique is the fact that it can be used in different environmental conditions (gases, liquids etc.), temperature can be controlled easily, the corrosion products can be analysed, and localized attack can be identified. But as the duration of this tests can extend from weeks up to month (usually 90 days), they are used for systems where the corrosion rates and phenomena do not significantly change over a long time period. Quick changes in corrosion processes may not be assessed [19, 25].

1.2.7.1 Electrochemical measurements

These methods are based on the measurement of potentials and current. While the measurement of the potential is rather simple there are some points to be considered, as the voltmeter should have a suitable high input impedance, and a reference electrode hast to be chosen. Without information about the system, interpretation of measured potential can be difficult [27]. In the following review three different electrochemical methods are discussed: polarisation curves, the linear polarisation resistance measurement and impedance spectroscopy.

1.2.7.1.1 Polarisation curves

This is the relation between current and potential over a wide range in the order of a volt. Measuring such curves should be normally under near steady-state conditions, to measure the resulting current from a long period at constant potential. However, this is practically not possible due to the change of surface conditions during corrosion reaction, especially during measurements in the anodic region. Thus, depending on the corrosion reaction rate such measurements are a compromise, in systems with low corrosion rates the electrodes will change slowly and currents will be more easily perturbed if the scan rate is high. At systems with a high corrosion rate, the electrode surface will change more quickly and therefore,

higher scan rates can be applied. Choosing the right sweep rate is an important parameter, as it controls the closeness with which a steady state is approached.
It does not matter whether the current is measured under potential control or the potential under current control. Since its more complicated to control current, especially in the active passive region, approaches almost invariably use controlled potential measurements. The potential can be held at any value and the current is measured, to extract a polarisation curve the potential is swept smoothly, leading to a potentiodynamic polarisation curve. Figure 6 is a schematic drawing of a potentiodynamic scan and Figure 7 is the Tafel plot of a scan. This are two examples of diagram are possible plots to present potentiodynamic scans. While in scans plotted as shown in Figure 6 it's possible to determine sections where specific reactions are dominating, a Tafel plot (Figure 7) can be used to calculate the Tafel slopes and therefore the corrosion rate. The equations for this calculation are provided in chapter 1.2.3, but there are some limitations for the Tafel extrapolation. The selection of Tafel lines and therefore, the calculation of Tafel slopes (βa and β_c) can be erroneous as there are some requirements for this calculation. To minimize these errors the anodic and cathodic extrapolation should be done 50-100 mV away from E_{oc} and both polarization curves should show a linear behaviour over a range of one decade of current density. Further the Tafel slope should not undercut the polarization curve between OCP and the start of the Tafel region [25, 27].

1.2.7.1.2 Linear polarisation resistance (LPR)

At the OCP, i.e. zero current, the polarization resistance Rp is the linear slope of the E-i relationship. There are different approaches to measure LPR, the potential can be swept through a narrow range either side of the OCP, ±10 mV respectively, and current is recorded. It's also possible to apply a sine wave of potential and measure the amplitude of corresponding current respectively. This would be equal to a single frequency impedance measurement, which is discussed in the following section. With the Stern-Geary equation Equation 9 and Equation 17 the measured Rp can be interpreted. The Stern Geary constant β is dependent on the metal and environment and must be generated from separate experiments, for examples by measuring the Tafel slopes. As this method makes a number of assumptions, errors may arise when interpreting the results. Anodic and cathodic reaction must obey Tafel's Law and the estimation for corrosion rates is an average assumption for uniform corrosion attack, localized phenomena will not be assessed [27].

1.2.7.1.3 Impedance spectroscopy

Electrochemical impedance spectroscopy has a minor influence on corrosion processes on the metal surface compared to potentiodynamic scans. During the measurement, the working electrode is excited with a sinusoidal potential signal that deviates only minimally from the OCP. The AC response signal oscillates at the same frequency but is shifted in phase (Figure 12). The frequency of the excitation potential is swept over a certain range, and the response current is measured[25, 49]. The impedance of a measured cell is determined by analysing the input and output signals, where Equation 20 is the input potential signal E_t and Equation 21 is the corresponding current signal I_t. The oscillating potential and current at time t have a

signal amplitude E_o and I_o and the angular frequency ω. The current signal I_t is shifted by the phase ϕ. The angular frequency ω and the frequency f are related to each other by Equation 22. Similar to Ohm´s law the impedance can by calculated by Equation 23 and is expressed by a complex function Equation 24.

Stability, linearity and causality are three requirements for impedance spectroscopy. Stability assumes that the measured system has stable conditions (steady state equilibrium), which is often difficult to achieve for corrosion reactions. The linearity is given, if measurements are made in a sufficiently small potential range (around the OCP) in which the relationship between current and voltage is approximately linear. Therefore, the amplitude (E_o) hast to be small enough to fulfil this condition. Finally, the causality must exist, the excitation of the system with AC-potential must trigger the response signal [49-51].

Plotting this complex impedance will lead to a Nyquist plot (Figure 14), where the negative imaginary and real impedance are on the y- and x-axis. The measured impedance refers to a particular frequency. The angle between the arrow of length $|Z|$ (impedance) and the real part (x-axis) is the phase angle ϕ [25].

As the polarisation resistance Rp or charge transfer resistance R_{ct} of a corrosion system is often of interest, the curve of the Nyquist diagram can be modelled with an electrical equivalent circuit for extrapolation of Rp values. With sufficiently complex circuits, it is possible to simulate many of the curve shapes that result from EIS measurements, but often these do not necessarily have anything to do with the physical reality of the processes in the measurement cell. Several different models can be fitted to one and the same curve by adjusting their parameters. This simplifying data evaluation in case where it is often not necessary to derive the individual physical and chemical processes in the cell from the equivalent circuit diagrams used. Figure 13 represents the simplest electrochemical equivalent circuit, the so-called Randel´s circuit, where the electrolyte resistance is an offset at the x-axis, and the R_{ct} (also Rp) with parallel C_{dl} define the semi-circle with only one time constant. The x-axis, real impedance, corresponds to the ohmic resistance and the imaginary impedance corresponds to capacitive phenomena (i.e. double layer etc.). As mentioned above there are different ways for interpretation and modelling EIS spectra, on the one side they can be used to simple extrapolate the Rp values. On the other hand, equivalent circuit diagrams can be used to determine the physical and chemical properties of the elements occurring at the electrochemical interface No matter which approach is used, the response current will flow either through the ohmic resistor or through the capacitor, depending on the frequency that is applied. Referring to the Randel's circuit, the AC-current signal at high frequency flows through the capacitance and at low frequency through the ohmic resistance. As real measurements are often no single semicircles, by adapting the equivalent circuit and its elements, it's possible to fit the data and calculate the Rp [25, 50, 52].

To modify equivalent circuits for real measurements it could be necessary to extend the circuits or adding more complex elements. A common phenomenon are depressed semi-circles, where the centre is not on the x-axis of Nyquist plot but rather below it. It’s not possible to fit these depressed semi-circles with an ideal capacitance (C_{dl}) accurately.

Therefore, a constant phase element (CPE) has to be used. The impedance of CPE is expressed in Equation 25 where A and ψ are parameters independent from frequency. For ψ=0 Equation 25 describes the behaviour as an ohmic resistance, vice versa at ψ=1 the behaviour of a capacitance [53-55].

Another example for equivalent circuits used for interpreting measured impedance spectra is given in Figure 27. It should be mentioned that such a circuit and its components (i.e. resistors and capacitors) do not represent real electrochemical reactions and phenomena on the electrode surface, it´s rather possible to use and modify values of the circuit components to fit and extrapolate the measured impedance data. In other words, the used equivalent circuit diagrams represent an electrical system which provides the same results in measurements.

Another phenomenon which possibly appears during impedance measurement of metal surfaces with adsorbed species is a pseudo-inductivity. This pseudo-inductivity can be seen in the Nyquist plot below the x-axis (Figure 15). It was shown that it is permitted to fit such phenomena with negative resistances and capacitances, the resulting Rp is shown in Figure 15[55, 56].

Equation 20: Input potential signal E_t.

$$E_t = E_o \sin(\omega t)$$

Equation 21: Output current signal I_t.

$$I_t = I_0 \sin(\omega t + \phi)$$

Equation 22: Correlation of angular frequency (radians/second) and frequency (Hz).

$$\omega = 2\pi f$$

Equation 23: Impedance expressed by Ohm´s Law.

$$Z = \frac{E_t}{I_t}$$

Equation 24: Impedance as a complex function.

$$Z(\omega) = |Z|(\cos\phi + j\sin\phi) = Z_r + jZ_i$$

Equation 25: Impedance of a constant phase element

$$Z_{CPE} = A(j\omega)^{-\psi}$$

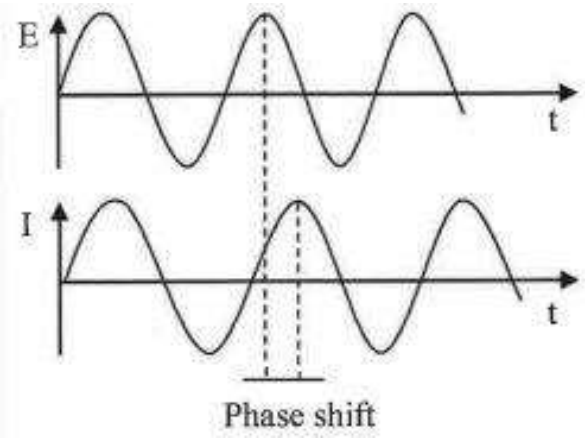

Figure 12: Phase shift of the sinusoidal current response[25].

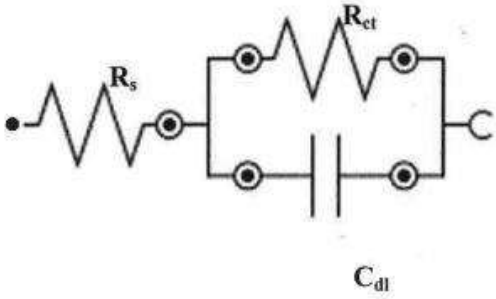

Figure 13: Randal circuit with elements: electrolyte resistance R_s, charge transfer resistance R_{ct} and double layer capacitance C_{dl}. [25]

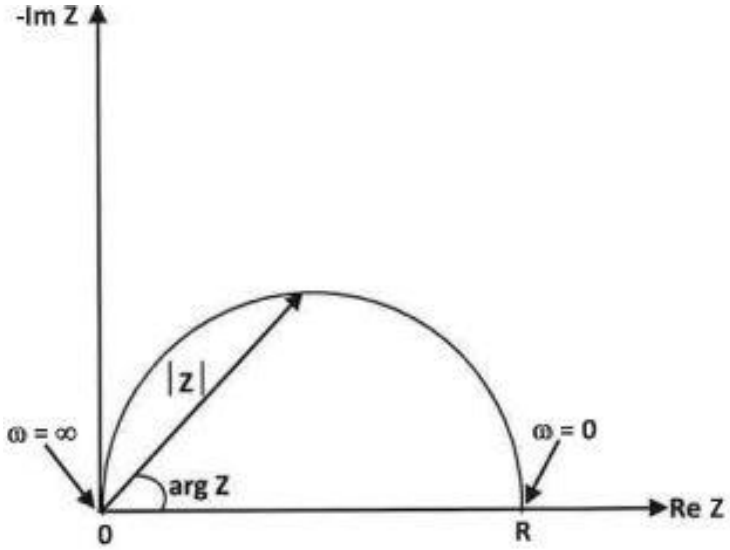

Figure 14: Example of a Nyquist plot[25].

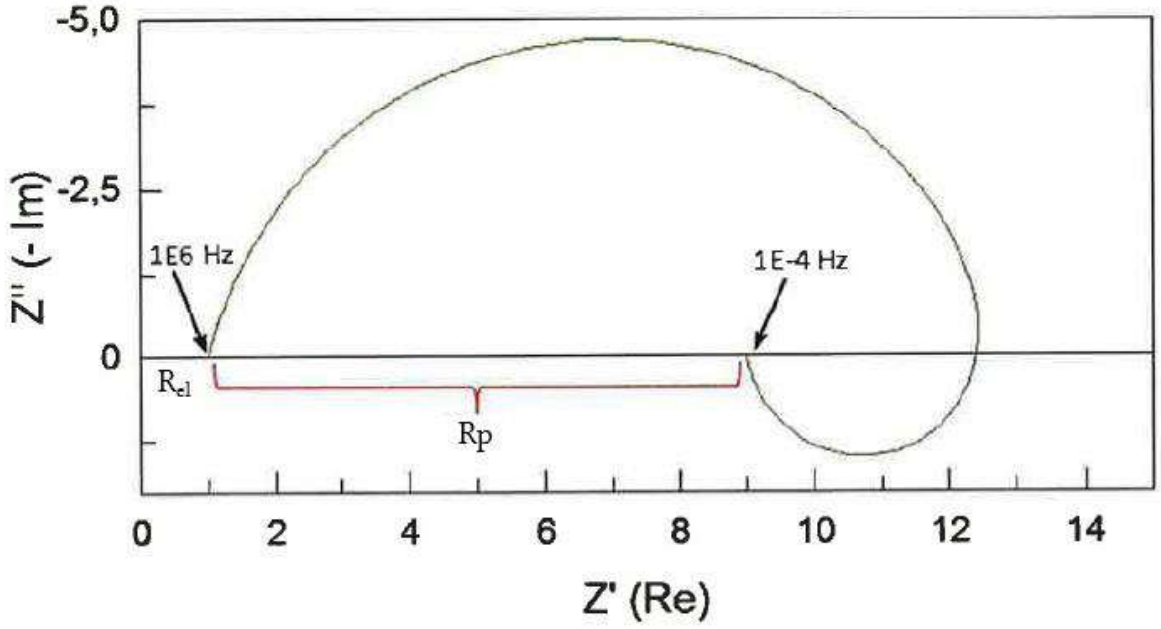

Figure 15: Simulated pseudo-inductivity (reproduced from [57]).

2 Subjects of investigation

As oil recovery rates in Austrians oil fields are running low, OMV started field trials with the enhanced oil recovery (EOR) method: polymer flooding, to increase the rates again. With this method a polymer, mostly hydrolysed polyacrylamides, or polysaccharides, were dissolved in the waterflood increasing its viscosity and therefore enhancing the displacement of crude oil in the reservoir. During this procedure, it is observed that the corrosion rates in oil production increases and corrosion phenomena change during Enhanced Oil Recovery (EOR) treatment. Especially during polymer flooding with hydrolysed polyacrylamide (HPAM) products (Polymer 1 field trial), the corrosion rate increased until field engineers scaled up the corrosion inhibitor concentration to about twice the normal (HPAM free) value. In Figure 16 and Figure 17 the corrosion rate in orange, the corrosion inhibitor dosage in green und the back produced polymer concentration in blue are plotted over months. Both diagrams indicate that with increasing polymer (P1, HPAM, blue) concentration the corrosion rate, which is monitored by corrosion coupon measurements increases drastically. Only by the described inhibitor concentration increase (green) it was possible to reduce these corrosion phenomena. Furthermore, corrosion monitoring with carbon steel coupons indicated a change in the corrosion pattern from uniform corrosion (Figure 18) to localized corrosion (Figure 19 and Figure 20). The coupons from Figure 18 originate from a period were no EOR treatment was used, they were installed after a wellhead for approximately three months. This corresponds to the left part (3 years, without back produced polymer) of Figure 16. Figure 19 and Figure 20 are coupons which were installed during a period of EOR treatment with P1 HPAM, which is indicated with the blue line, i.e.: polymer concentration increase (polymer back production). Increasing corrosion rates and severe localization of corrosion attack can be observed at these coupons, creating an even more problematic situation which has to be investigated. Therefore, there is a demand for identifying alterative corrosion inhibitors (CI) with higher corrosion protection efficiency and to find a polymer, which does not promote these negative effects, and to test such potential candidates of CI and polymer in a field trial afterwards. The autoclave wheel tests [58] so far used are time consuming and do not fully represent oil field conditions, especially the flow conditions. A robust and reproducible method is needed to asses corrosion rates, where the environment (electrolyte composition) and oil field conditions, (oxygen free, flow rates, temperature, CO_2 or H_2S environment etc.) can be varied easily. After literature studies the rotating cylinder electrode RCE was selected for controlling flow conditions, and due to a relatively simple test specimen geometry it allows easy preparation (grinding) of the electrode surface[59, 60]. To asses corrosion rates in varying electrolyte compositions, the electrochemical impedance spectroscopy (EIS) was chosen. Its low-amplitude potential variation minimizes the perturbation by the measurement on the corrosion processes, i.e. it operates close to non-invasive. Furthermore, its output, the impedance and the resulting polarisation resistance Rp from fitting the Nyquist plot, is straight forward related to the corrosion rate by the Stern-Geary equation [9].

A further aspect of investigation is the influence of EOR polymer itself on corrosion rates and corrosion processes in a carbon dioxide saturated and well inhibited environment which

should be studied. Therefore, potentiodynamic and potentiostatic measurements with RCE should give further information about phenomena at the electrode/electrolyte interface, especially the possible competition of polymer and corrosion inhibitor for adsorption on the carbon steel surface. Further analytical methods as, FTIR, rheological measurements and SEM should give additional information on polymer composition, viscosity and structural information on possible built up of a protective layer.

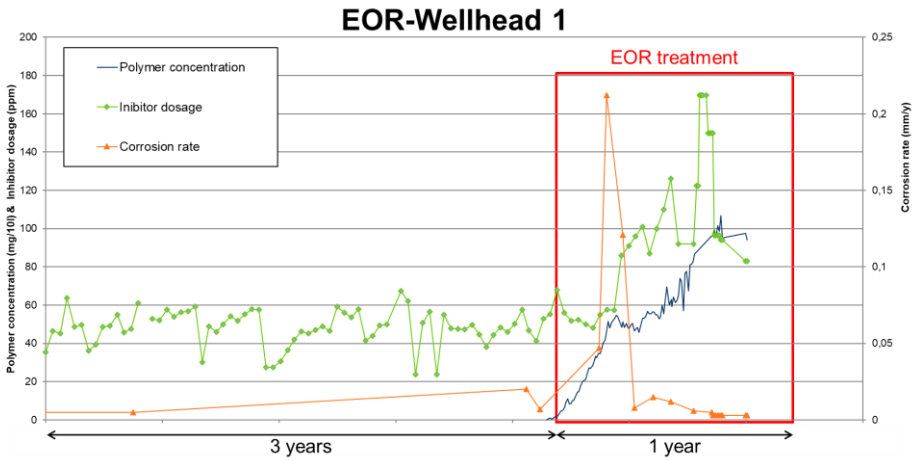

Figure 16: Example of corrosion monitoring for wellhead 1.

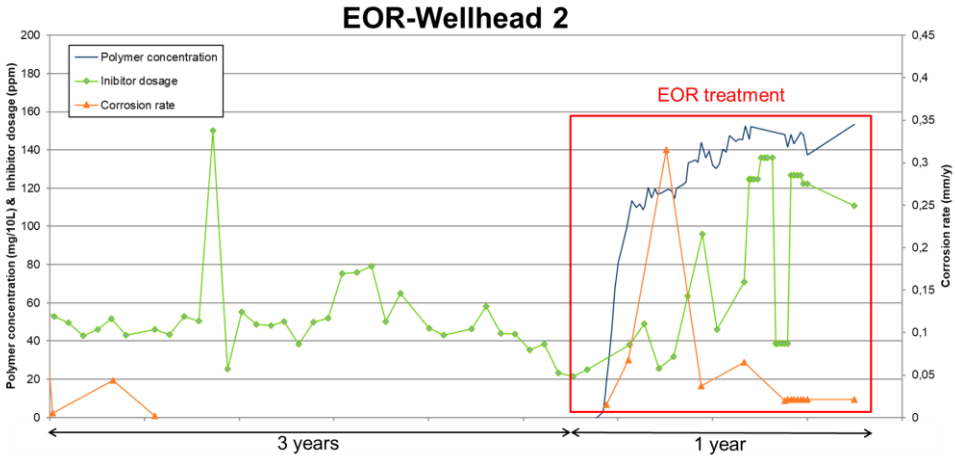

Figure 17: Example of corrosion monitoring for wellhead 2.

Figure 18: Corrosion coupon without HPAM (P1) and uniform corrosion attack at low corrosion rates.

Figure 19: Corrosion coupon with HPAM (P1) at wellhead 1 and localized corrosion attack.

Figure 20: Corrosion coupon with HPAM (P1) at wellhead 2 and localized corrosion attack

2.1 Considerations on the influence of polymer EOR on corrosion

After literature studies it was not possible to find any reference to the practical phenomena described in the section above. Possible reasons could be that in other oil productions higher alloyed steel grades are used or the applied standard inhibitor concentration is higher than concentrations used in OMV oil fields. Therefore, some considerations where made to complete the tasks which are requested, inhibitor and polymer selection with an alternative method compared to standard autoclave tests, and the investigation of changes in corrosion phenomena during EOR treatment. Figure 21 should give an overview of possible interactions between polymer, carbon steel surface and the environment in oil field facilities.

First, it has to be considered that the polymer HPAM may promote corrosion, either by its interaction with the environment or by degradation products[61, 62]. Second, does the polymer influence on the formation of a protective iron carbonate layer on a bare steel surface, and its influence on an already formed layer could be a factor. Third, the polymer may influence the mode of action of the corrosion inhibitor used. Corrosion inhibitors (CI) are multicomponent liquids, with ingredients like quaternary ammonium compounds, fatty acids, glycols, various alcohols and sulfuric compounds like mercaptoethanol etc. These substances may interact with the anionic hydrolysed side groups of HPAM or with amino side groups. Consequently, active components which contribute to the effect of a CI would not be available anymore. Further, it's possible that the partly neutral and partly anionic charged polymer chains may adsorb at the steel surface and compete with corrosion inhibitor

for adsorption sites [63]. Lastly, the polymer may support the growth of microorganisms (MO) by acting as nutrient or by providing a protective environment for formation of biofilm possibly resulting in corrosion (MIC).
During the treatment no biofilm was found in EOR oilfield facilities, therefore no further consideration in this part were made.

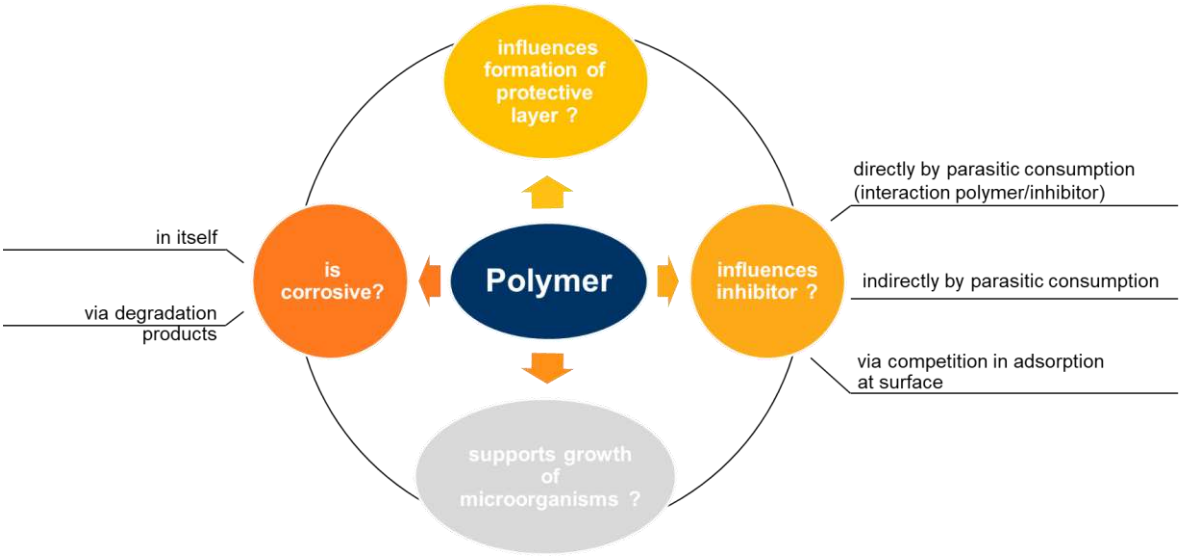

Figure 21: Considerations how a polymer (HPAM) could influence the system: carbon steel/corrosion inhibitor/polymer.

3 Experimental procedures

3.1 Polymer brine preparation

The solvent for polymer solution with a concentration of 1000 ppm polymer (PX-AfB, X for 1…5 see Table 2) is a field based artificial brine (AfB), which composition is provided in Table 1. The equipment for PX-AfB mixing is a rotor from EUROSTAR (IKA-WERKE) and a propeller stirrer (Figure 22 and Figure 23). The artificial brine (1000 or 1500 mL per batch) is placed in a 2 L beaker and the rotation speed for the stirrer is set to 500 rpm. The used weight of polymer includes 10% excess to compensate for the known moisture uptake during storage. It's important to add the polymer slowly and continuously to the stirred brine to prevent the polymer from agglomeration during dissolving. After addition it is necessary to stir for further 15 minutes to homogenize the swollen polymer particles. Then the speed is reduced to 300 rpm and the solution remains stirring overnight [64].

All polymers for polymer selection were basically hydrolysed polyacrylamides (HPAM) with different grades of hydrolysis and molecular weights. They are commercially available products from different producers who provided the related specifications in Table 2.
The samples P2 and P3 have a stabilizing agent as additive for the polymer. The supplier doesn't declare the type of the agent and the stabilizing mechanism, but literature indicates possible components as follows: oxygen scavengers and complexing agents[65]. Furthermore, P3 is a Ter-polymer with a sulfonic acid side group.

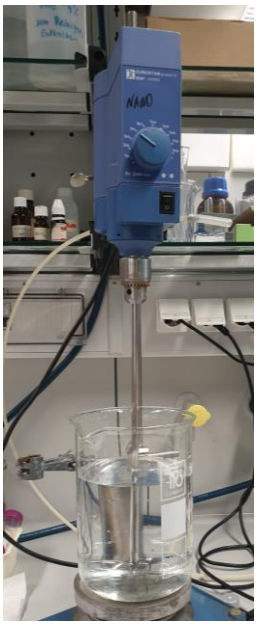

Figure 22: Stirring unit for polymer brine preparation.

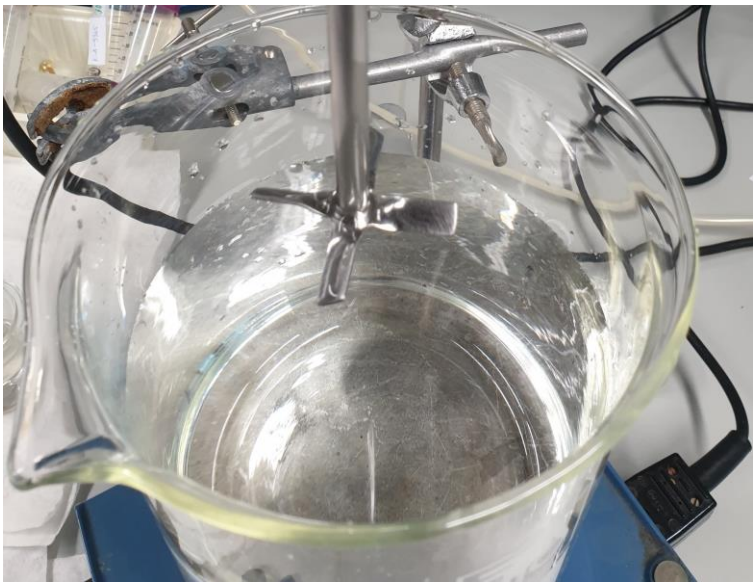

Figure 23: Propeller stirrer with diameter of 50 mm.

Table 1: Composition of artificial brine (AfB).

Salt	g/L	Calculated Base Brine - Elements (mg/L)	
NaCl	20,66	Na^+	8541
NH_4Cl	0,19	NH_4^+	64
KCl	0,14	K+	73
$MgCl_2*6H_20$	0,645	Mg^{2+}	77
$CaCl_2*2H_20$	0,65	Ca^{2+}	177
$NaHCO_3$	1,51	Cl^-	13264
		HCO_3^-	1097

Table 2: Tested polymer samples for polymer selection with data provided by the suppliers.

Polymer acronym	Polymer Type	Molecular weight (MDa)	Hydrolisis Degree (%)
P1	Co-polymer	18	25-30
P2	Co-polymer	20-25	25-30
P3	Ter-polymer	20-25	20-25
P4	Co-polymer	24	30
P5	Co-polymer	16	25

3.2 Corrosion inhibitors

A variety of corrosion inhibitors from a number of different suppliers have been used during this thesis and are listed in Table 3. Corrosion inhibitors are considered to be multi-component liquids, the composition of which is often unknown. Table 4 is intended to provide a summary of the components listed in the material safety data sheet (MSDS). Only the hazardous components are required to be listed in the MSDS and therefore there is a possibility of other components being present in the inhibitor, changing its interaction with the environment.

Table 3: Tested inhibitor samples.

Inhibitor	Acronym	Supplier
1	CI1	A
2	CI2	B
3	CI3	C
4	C4	D
5	CI5	A
6	CI6	A
Lab sample	CI7	L

Table 4: Composition of corrosion inhibitors used.

Inhibitor components	CI1	CI2	CI3	CI5	CI6
Ethylenglykol	10-<20,1	30-<50	<20	10-<25	10->24
Mercaptoethanol		3-<5	<5	<5	
Butoxyethanol		25-<30			
QAC	3-<4,53	5-<10			
Reaction mass of Amines		5-<10			
Mono-Coco Alkyl-Amine		2,5-<5			
Coconitriles		0,5-<1			
Amines (dicoco alkyl)		0,5-<1			
Diethylenglycol monoethyl ether		5-<10			
Diethylenglykol		0,25-<0,5			
Isopropylalcohol	1-<3				
Aminoethanol	1-<1,008				<1,2
Polyethers	10-<25			<10	10-<25
Dodecenylsuccinic acid, with nitrilotriethanol (1:1)	3-<5				<10
Imidazole-1-ethanol, 4,5-dihydro-, 2-nortall-oil alkyl derivs			<5		
Decanaminium, Ndecyl- N,N-dimethyl-, carbonate (3:2)			<15		
Ammoniumchloride			<2		
Polyehter, phosphates				10-<25	

3.3 Rheological measurements

Rheology tests of Polymer brines were conducted on a modular compact rheometer MCR 300 by Physica Anton Paar. The viscosity of the formulations was measured at 30°C (5 min acclimatization of the rheometer before measurement) with a CP-25 or CP-50 measuring system (diameter 25 mm and 50 mm) at a gap of 48 µm. The two systems are used for different viscosity ranges, for very low viscosities (<2 cP) the CP-50 is recommended to use[66]. The measurements were taken as follows:

1) 20 s temperature holding for equilibration.
2) Measurement of a linear ramp divided into 10 measured points, each measured for 5 s with a shear rate range of $\tau = 1 - 100\ s^{-1}$
3) Measurement of 5 points, each for 10 s at a shear rate of $\tau = 7{,}36\ s^{-1}$, which are averaged.

3.4 Specimen preparation

To assure reproducible surface conditions of the carbon steel specimen, with a diameter of 13 mm and height of 13,3 mm (S235JR [67], provided by OMV E&P, Figure 25), it must be grinded accurately before each measurement. The cylindric specimen was mounted on a screw and fixed on a drill. For cooling and removal of abrasive products the grinding of the cylinder specimen is done under flowing deionised water, using SiC paper with following grit sequence: #320, #500, #800 and #1200. Afterwards, the specimen is rinsed with deionised water, dried with acetone and put in isopropanol

into an ultrasonic bath for approximately five minutes. To dry the sample after the cleaning process, compressed air is used. Then it is mounted between two equal sized rubber (thickness: 1 mm EV600 Viton) sealings with a diameter of 14 mm (to minimize the risk of crevice corrosion) on the electrode adapter (Figure 24).

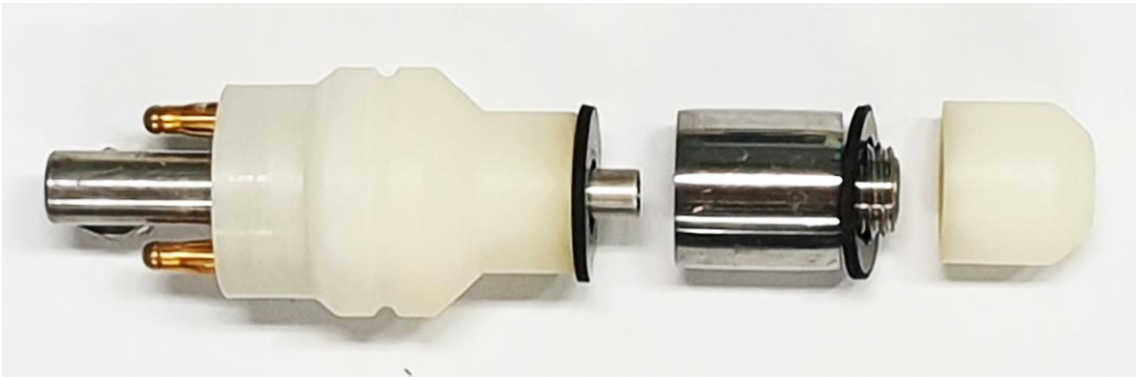

Figure 24: Specimen holder with seals and carbon steel sample.

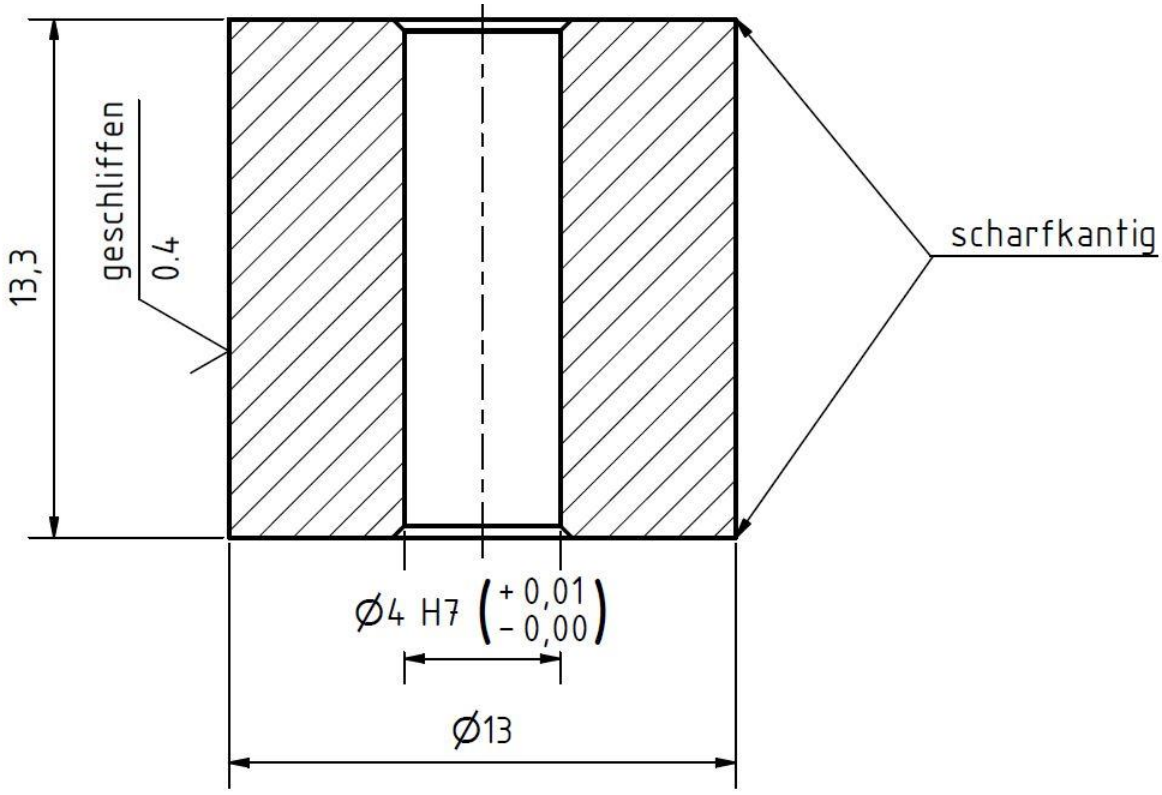

Figure 25: Blueprint of the used cylinder specimen with dimensions and tolerances.

3.5 Metallographic preparation

For the investigation of cylindric samples with a carbonate layer by optical methods or scanning electron microscopy (SEM), the cylinder specimen is rinsed with deionized water, immediately after artificial corrosion experiments, and dried with acetone and placed centrically in an embedding mold. STRUERS Epo Fix Resin and Epo Fix Hardener with a ratio 25:3 is used. To fix the sample and the grown carbonate layer for further preparation steps the embedded sample is put into a desiccator and degassed with a vacuum pump for at least three times (p <150 mbar) immediately after introducing the resin. Thenr 24 hours of curing, the sample is cut radially with a STRUERS Accutom-50 and an aluminium oxide cutting blade (STRUERS, 30A13, 125x0,5x12,7 mm) at 3500 rpm and a feed of 0,1 mm/s. After this process the upper part of the embedded sample has to be prepared as follows with a STRUERS Tegramin-30:

1. Grind: 220 µm, MD Piano, 3 min with water
2. Polish: 9 µm, MD Allegro, 4 min with DiaPro Allegro diamond suspension
3. Polish: 3 µm, MD Dac, 6 min with DiaPro-Dac3 diamond suspension
4. Polish: 1 µm, MD Nap, 4 min with DiaDuo-2 diamond suspension

Between each step the samples were rinsed with deionized water and cleaned in isopropanol in an ultrasonic bath for minimum 5 minutes to ensure that no diamonds or steel residues were carried to another polishing plate.

3.6 Scanning electron microscopy

A Fei Quanta 200 was used for collecting of SEM pictures. For this purpose, the embedded samples were placed unetched but polished in the sample holder. To prevent the sample from becoming charged, it was contacted to the metallic sample holder using copper tape. If samples charge despite copper tape they must be sputtered with gold or the Low Vacuum mode of the SEM has to be used. Images were taken using backscattered and secondary electron detectors at an operating voltage of 20 kV with different magnifications. A spot size between 2 and 4 was selected for these images.
To differentiate between the built corrosion product layer and the specimen an energy dispersive X-ray detector is used to perform mappings, point- and line scans. The spot size is set to 6-7 for increasing the count rate of the detector. The analysis was performed at magnifications between 1000x and 2500x depending on the investigated layer.

3.7 Pickling of carbon steel specimen

If necessary, the carbon steel specimens are pickled to remove corrosion products from the surface. As reference standard serves the DIN EN ISO 8407 [68]. The pickling solution is prepared as follows: 500 ml conc. HCl and 3,5 g Hexamethylentetramin are filled into a volumetric flask and diluted to 1000 mL with deionized water.
Depending on the thickness of the carbonate layer, the specimens must remain in the pickling solution for 2 to 10 minutes at room temperature. After this process the samples were washed with deionized water and dried with acetone.

3.8 Fourier-transform infrared spectroscopy (FTIR)

To identify impurities and differences of polymer samples FTIR was chosen. The polymer powder was milled in a ball mill (Retsch, MM400) for 10 seconds at a frequency of 35 s^{-1}. The equipment for this ball mill was made from tungsten.

The measurements were performed using a Tensor 37 FTIR spectrometer (Bruker Corp., Ettlingen, Germany) equipped with a Platinum ATR unit. The sample compartment of the spectrometer was continuously flushed with dry air during IR measurements. IR spectra were acquired with a spectral resolution of 1 cm−1 and a total of 32 scans were averaged per spectrum. Spectra analysis was performed using the software package OPUS 7.5 (Bruker Corp., Ettlingen, Germany).

3.9 Rotating cylinder electrode (RCE)- with Electrochemical Impedance spectroscopy (EIS)

This procedure is the result of the methodical development as reported in section 4.2. It is mandatory to follow this experimental sequence to ensure reproducibility of the EIS results, see section 4.2.1.

3.9.1 Test cell setup

The test cells for all further measurements are double walled glass cells (400 mL) attached to a thermostat. Through the sealed lid, the RCE-electrode adapter, the reference electrode, the counter electrode, and the CO_2 purge in- and outlet extend into the cell, a schematic drawing is given in Figure 26. Three different types of test cells are available. At TU Wien there are a prototype cell and a Model 2 cell (Figure 37) and at OMV there are two Model 2 cells and a Model 1 cell and each is equipped as follows:

- **Temperature control**

The double walled EIS cells were constantly heated up to 60°C by pumping thermostats (VWR International), filled with deionized water. Depending on the conducted tests and required conditions more than one cell could be attached to a thermostat. The temperature loss should not exceed 1°C for cells connected in series.

- **Rotor**

Electrode rotator and speed controller are from Jaissle Elektronik GmbH/Ingenieurbüro Schrems, Münster, Germany. TU-A (prototype) cell manufactured in 2008, all other cells manufactured in 2021 (Model 1 and 2). They have an adapter for cylinder electrodes with a diameter of 13 mm and height of 13,3 mm. Rotation speed range is from 0-4000 rpm, the speed used for experiments is 1500 rpm, corresponding to a flow rate of 1,04 m/s.

- **Gas supply**

For a CO_2 saturated environment 4.5 CO_2 from Messer (<10 ppmv O_2) is used. The connection between gas flask and test cell depends on constructional conditions at the laboratories, it's important to use gas tight tubing, to prevent oxygen intake. To ensure CO_2 saturation the flow must be high enough to generate a CO_2 stream through the exhaust pipe. During purging the flow should be approximately 2 L/h and during measurement it could be reduced to 1 L/h.

- **Electrochemical Impedance Instruments**

For impedance and potentiodynamic scans two electrochemical workstations from Zahner Elektrik (Germany) are used. Zahner IM6 for the TU Wien equipment and a Zahner Zennium XC for OMV equipment.

- **Reference electrode**

A saturated Ag/AgCl sat. KCl electrode with NS 7 glass cone from Sensortechnik Meinsberg (SE11 NSK7) is used for all EIS cells.

- **Counter electrode**

OMV cells used a platinized rod electrode with ca. 1375 mm² wetted surface. TU-A has also a platinized rod electrode with ca. 622 mm² wetted surface. The TU-N cell used a flexible round platinum sheet electrode with a surface of ca. 1187 mm².

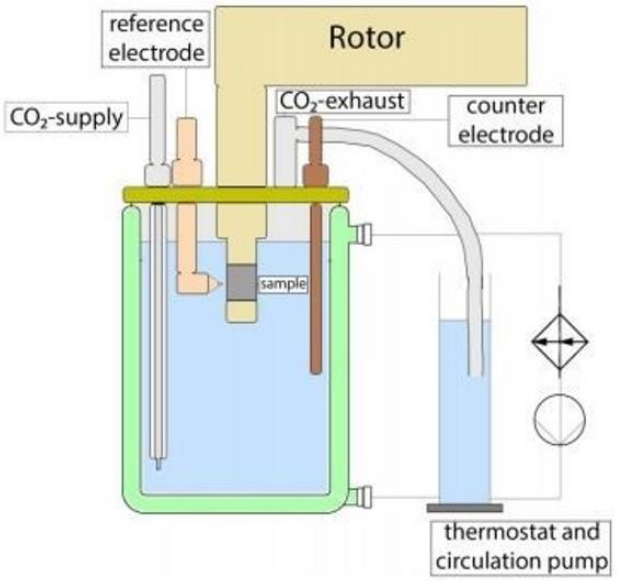

Figure 26: Schematic drawing of RCE cell.

3.9.2 RCE and EIS Setup

To simulate the flow conditions seen in oil field facilities the RCE was chosen with an operating speed of 1500 rpm which corresponds to a flow rate of 1,04 m/s at the cylinder surface. Further, the cylindric specimen allows to secure a reproducible and recyclable surface state by the procedure described in section 3.4.

For impedance spectra, instruments and settings in Table 5 were used resulting in the total time for recording a spectrum of approximately 20 minutes. During this time the system has to be in a stable concentration of inhibitor and there should be at least three measured impedance spectra to verify a stable steady state of the investigated system. The validity of collected impedance data was verified by using the Z-Hit procedure implemented in the instrument's software (IM6 and Zennium XC, Zahner Elektrik, Germany) to check for the reproducible conditions during measurement.[69].

Table 5: EIS instruments and settings.

Instruments	IM 6 (TU Wien) and Zennium XC (OMV)
DC potential	open circuit potential (OCP) at start
Frequency range	200 kHz down to 6,3 mHz
Points per decade	4-10, selected automatically
Amplitude	10 mV_{pp}
Transition cycles	≥ 1.5, selected automatically
Integration cycles	1-10, selected automatically

To determine the corrosion rate, the polarisation resistance Rp is used, which is indirectly proportional to the corrosion rate. This means the higher Rp, the lower is the corrosion rate. Rp is the impedance of the electrode/electrolyte interface estimated for DC (i.e. frequency f = 0 Hz), which cannot be measured directly. Rp is calculated by extrapolation from the impedance spectra by fitting with a suitable impedance model which is not required to be related to physical and chemical processes at the electrode surface. A mathematical model which is consistent with the spectra is sufficient for determination of Rp [70-72]. It is represented by the so-called ladder circuits, Figure 27 provides the model structure used where R_{el} corresponds to the electrolyte resistance of the test cell. The three- time constants R1/CPE1…R3/CPE3 were individually chosen and adapted to the impedance data, while R4/CPE4 was only used if no sufficient fit accuracy could be achieved with three time constants (software provided error value <15%). For data fitting the software ZView-2 (Scribner Associates, USA) was used. After fitting the value for Rp can be calculated by:

$Rp(f \longrightarrow 0) = R1 + R2 + R3 (+ R4)$.

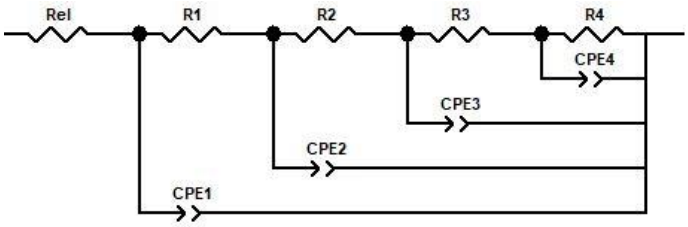

Figure 27: impedance model used for data fitting, four stage ladder circuit.

3.9.3 Setting up the electrochemical experiments

A strict workflow was followed in setting up the experiments as this was found decisive for reproducibility of the tests: The cell is filled with electrolyte (AfB or AfB+polymer, 300 mL) and all connection components, gas in-/outlet, counter electrode, and salt bridge with reference electrode, are put in position, while the feedthrough for the RCE- adapter just gets plugged with a Teflon plug. The cell is purged with CO_2 (ca. 2 L/h) for at least two hours, to remove the oxygen in the electrolyte, while it is heating up to 60°C. Before inserting the RCE- adapter carrying the freshly prepared specimen (Figure 24), a corrosion inhibitor (CI) is dosed if required by the experiment, in order to ensure its homogeneous distribution. For removing the air (oxygen) unavoidably introduced during this procedure or by small arbitrary leaks, CO_2 purging is continued throughout the experiments at 1-1,5 L/h.

3.10 Potentiodynamic scans

These are performed with a potentiostat IM6 from Zahner in a three-electrode setup, typically after EIS measurements in the same test cell. The conditions for the measurement are as follows:

Rotation speed: 1500 rpm ≙ 1 m/s at the specimen's surface
Scan rate: 500 µV/s
Scan definition: OCP-100 mV →1200 $mV_{Ag/AgCl}$ →OCP-100 mV
Current limit of scan: ± 5,6 mA (corresponds to 100 µA/cm²), scan direction changed when current limits are reached.

3.11 Potentiostatically accelerated corrosion (PAC)

PAC tests were carried out as separate experiments using an either the IM6 (Zahner) potentiostat or a Bank (Germany) potentiostat hooked to a Keysight 37492A data acquisition instrument. After setting up the cell as described in section 4.2, OCP was monitored for at least 1 hour until a steady value was reached (<±2 mV over 5 min. [73]). Then, the desired potential, either OCP+50 mV or OCP+100 mV, was applied and the resulting current was monitored for up to 75 hours.

Immediately after PAC experiments the complete sample holder including the sample, is washed with deionized water and dried with acetone to stop corrosion processes, due to influences of oxygen, outside of the RCE-EIS cell. Depending on the built carbonate layer on the steel specimen further preparation is done. If the specimen is free from any corrosion products, the dried sample is photographed and stored. If there is localized corrosion, distinct spots with iron carbonate, while the rest of the specimen is unattacked, the sample should be photographed before and after pickling (described in 3.7). When there is a uniform carbonate layer built on the specimen's surface, it is embedded as described in 0 for further investigations by SEM or light microscope.

As a pre-test for potentiostatically accelerated corrosion, potentiodynamic scans were recorded. If the desired anodic potential shift lies in the regime of the anodic TAFEL lines no change in the corrosion mechanism during the PAC test is expected. Nevertheless, due to the considerable speed of potentiodynamic scans, possible changes in the mechanism in the potentiostatic mode by time, must not be neglected but may be reflected in the trend of current.

4 Results

4.1 Characterisation of carbon steel specimen

The used steel grad for RCE specimen are manufactured from S235JR rods. To validate the composition of them, 3 samples were embedded and metallographically checked. The specimens are embedded, cut, ground and polished as described in section 3.4, cleaned and dried with isopropanol and etched with 1% Nital etching solution. Each etching step consists of 2 seconds etching with the reagent, washing with deionized water and cleaning and drying with isopropanol. After each step the sample was studied with a light microscope (LOM). If necessary, the steps were repeated several times to obtain a sufficiently etched carbon steel surface showing the alloys microstructure.

Figure 28 and Figure 29 are LOM pictures from specimens etched for 4 and 6 seconds, respectively. They indicate a structure with composition below the eutectoid point in the Fe/C phase diagram [74]. The grey to brownish etched areas are pearlite, which is a lamellar microstructure, the ferritic grain structure remains unetched. This observation corresponds to the carbon amount of <0,17 % for this steel, and therefore the area in iron-carbon phase diagram, which is expected from the composition given from the manufacturer. Black dots appear to be residuals from polishing diamonds, as the size of them is between 1-3 µm [75]. SEM measurements with backscattered electron detector confirm above mentioned microstructure. Pearlite (P) is the lamellar structure seen in Figure 30, while the plane grains are the ferritic structure.

Further, in order to measure the macro hardness of the specimen, the device Test-M4U-025 from the company "Emco" was used and the hardness was determined according to Vickers (HV10) [76]. Five hardness indentations were made in the embedded carbon steel specimens. These were obtained with a diamond pyramid, and a force of 100 N for 10 seconds. Afterwards the diagonals of the indentations can be measured with the LOM at a magnification of 200x (Figure 31). The calculation of the hardness values is done according to following Equation 26, where F is the force used for indention and $d_{1/2}$ where the length of the indentation diagonals. The measured and calculated values of approximately 140 HV10 are confirmed by literature [75].

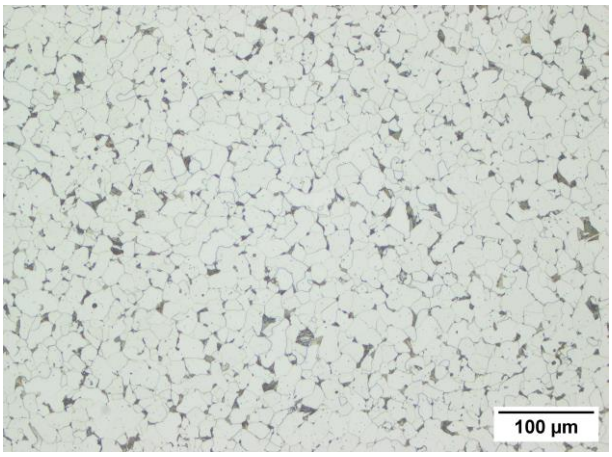

Figure 28: Carbon steel specimen, etched with 1% Nital for 6 sec., 200x.

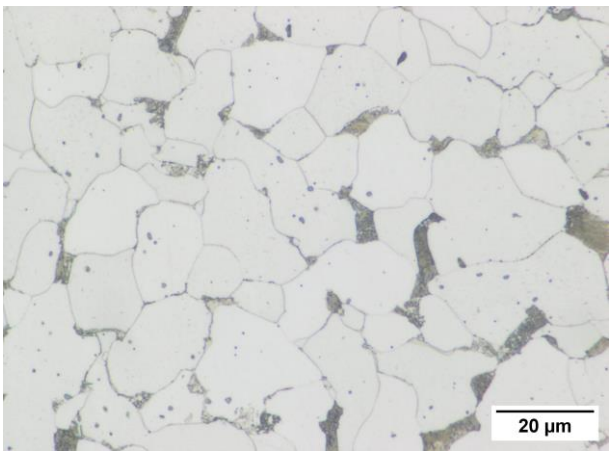

Figure 29: Carbon steel specimen, etched with 1% Nital for 6 sec., 1000x.

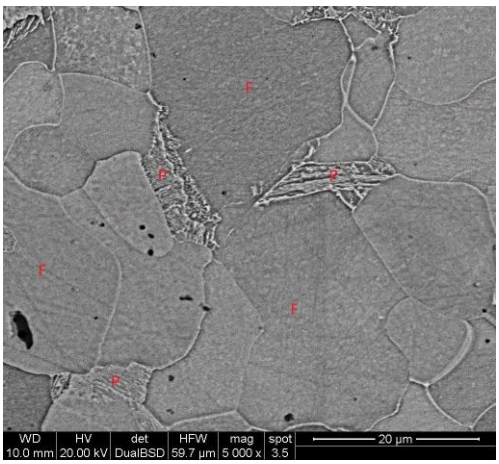

Figure 30: SEM BSE image of carbon steel specimen at magnification 5000x.

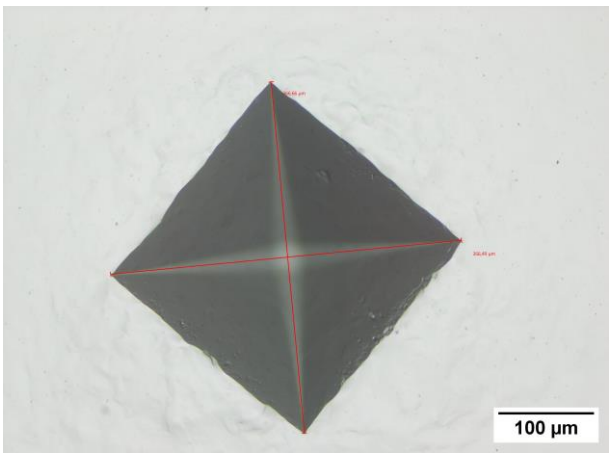

Figure 31: Dimensioning of hardness indentation at 200x magnification.

Table 6: Data for calculation of HV10.

HV10	d_1 (µm)	d_2 (µm)	HV
1	366,66	366,49	141
2	366,69	366,05	141
3	368,24	368,02	140
4	368,03	366,05	140
5	367,46	368,09	140

Equation 26: Calculation of Vickers Hardness.

$$HV = 0{,}1891 * \frac{F}{d^2}$$

$$d = \frac{d_1 + d_2}{2}$$

4.2 Methodology development of EIS experiments

A focus of this thesis was the development of an electrochemical method which fits the standards of OMV E&P and provides primary the possibility of a fast and simple screening for corrosion inhibitor, different electrolyte compositions (different polymer brines) and provides the opportunity for material selection (different cylinder specimen). Further, this newly introduced procedure should help to understand phenomena appearing in the oil field due to a change in the environmental composition, especially electrolyte composition during EOR polymer treatment.

The currently used method for corrosion testing are autoclave tests with carbon steel coupons where the material loss during corrosion processes is observed. However, due to the intrinsic technical limitations it is not possible to recreate the same conditions as are in the oilfield, especially flow conditions. Thus, there was a demand for a test system providing control on flow velocity. Ohaba and Kuroda did numerical analysis of flow around a rotating cylinder[60] which leads to the method of rotating electrodes.[77] The rotating disc electrode (RDE) is one of the best-known geometries used but a number of further geometries such as the rotating cylinder electrode (RCE) were explored and described.[77, 78] While the RDE provides controlled mass transfer on laminar flows, there is normally turbulent flow in oil field flow lines and the RCE is the method of choice. With the RCE it should be possible to control mass transport rates to/from the cylindrical surface and assure uniform current- and potential distribution at turbulent flow. Moreover, the RCE requires a relatively simple test specimen geometry at required flow conditions[59]. It was previously used in several studies to assess the efficiency of corrosion inhibitors for oil and gas lines.[79, 80]

There are various electrochemical techniques that can be combined with RCE. Electrochemical

impedance spectroscopy (EIS) was chosen because of it is non-invasive character, due to its low potential variation. After some data processing the final output, the polarization resistance Rp, is directly related to the corrosion rate.[81]

4.2.1 Setting up a new method

The first approach for the RCE-EIS procedure was a continuous measurement to asses polarization resistances and the efficiency of the corrosion inhibitor respectively. The procedure of this approach was as follows.

Continuous procedure:

1. Preparing of the electrolyte (AfB or PX-AfB) and assembly of the electrochemical cell.
2. 2 hours of CO_2 purging.
   2.1. Steel sample preparation and cleaning.
   2.2. Cutting of ring seal.
3. Mounting of specimen and inserting the RCE.
4. Equilibration of OCP
5. Starting three consecutive EIS measurements.
6. Dosage of corrosion inhibitor (additional dosage Table 7) and repetition of step 4 to 6 for increasing the inhibitor concentration stepwise in one experiment.

2 hours of CO_2 purging is sufficient to remove oxygen from the electrolyte, which was previously experienced during an internal project. The open circuit potential (OCP) is measured till it reaches a constant value, i.e. ±1 mV shift in 10 minutes. If this criterion was fulfilled, the first of three consecutive impedance measurements could be started. During these three measurements (approx. 1h; 20 minutes for each impedance spectra) the OCP should not shift more than ±1 mV and to check the validity of the measured spectra, it was evaluated with the Z-Hit algorithm, provided by the Zahner instrument (Kramer-Kronig variant). Step 4 to 6 are repeated as often as needed to measure the required corrosion inhibitor concentrations in ascending order. During the whole procedure (step 2-6) the electrolyte was continuously purged with CO_2, approx. 1 L/h during OCP tracking and EIS measurement and 2 L/h during CI dosing to prevent oxygen contamination. For each concentration step data from OCP and Rp are collected, during one EIS experiment (≙ two days) it's possible to gain data for concentrations between 0 to 80 ppm corrosion inhibitor.

In Figure 33 there are Rp values of AfB and P1-AfB with different corrosion inhibitor concentrations fitted from related continuous procedure measurements. At least three repetitive tests were carried out.

First, the observations from oil field trials (section 2), an increase in corrosion rate if P1 is present in the electrolyte, can be confirmed by this approach and resulting data. For a critical point of view, the standard deviation and scattering for each of the fitted Rp, i.e. each measured impedance spectra, is high for a reliable interpretation of this data. Therefore, there is a need for adapting the previous described procedure to improve the reproducibility of measured EIS data. After literature study a possible point of improvment is the time for equilibration of a steady state, which is required for

valid electrochemical impedance spectra [50, 51]. The time for equilibration of the corrosion system was extended to 20-24 hours (overnight) and the experiments have been adapted as follows.
Single measurement procedure:

1. Preparing of the electrolyte (AfB or PX-AfB) and assembling of the test electrochemical cell.
2. 2 hours of CO_2 purging.
   2.1. Steel sample preparation and cleaning.
   2.2. Cutting of ring seal.
3. Dosing of corrosion inhibitor if necessary (single dosage Table 7).
   3.1. 5minutes to homogenize.
4. Mounting of specimen and inserting the RCE.
5. Equilibration of corrosion system over night (>20 h)
6. Starting three consecutive EIS measurements and validating with Z-Hit algorithm.
7. Additionally, a potentiodynamic scan was done after the last EIS measurement.
8. Cleaning of the whole RCE-EIS equipment before the next inhibitor concentration can be measured and the procedure is started again at step 1.

To prove the theory of a developing steady state after equilibration overnight, Figure 32 shows a Nyquist plot for an inhibited (20 ppm CI1) polymer 1 brine. The impedance was measured every two hours to observe the development of the equilibrium of the corrosion system. Between the measured data for 12 and 14 hours an abrupt rise can be detected reaching a stable steady state for EIS measurements. Therefore, we were able to proof that an equilibration time of the corrosion system for at least 20 hours will ensure steady state conditions to a high degree.
Figure 34 are the fitted Rp values for inhibited (CI1) and uninhibited AfB and P1-AfB gained with the adapted procedure. First thing to mention, oil field trial observation, i.e. increased corrosion rates with polymer present in the electrolyte while corrosion inhibitor concentration stays constant, can be confirmed with RCE EIS based on Rp the difference in both procedures were able to show this phenomenon. However, with the adapted procedure it was possible to decrease significantly the scattering of impedance data, i.e. Rp values. Further, compared with Figure 33 polarization resistances are by an order of magnitude higher within the single measurement procedure, especially at low concentrations. As the used corrosion inhibitor CI1 is a mixed type inhibitor, supressing cathodic and anodic reaction, a stable open circuit potential does not reflect a stable steady state condition, which was wrongly considered to be sufficient when developing continuous procedure. It's possible that the OCP stays constant while both, anodic and cathodic reaction have not yet reached their equilibrium states and change uniformly till they reach it. The full effect of corrosion inhibitor, i.e. the actual Rp of the system, will be seen after the corrosion system is in a steady state. Therefore, the equilibration time of >20 h and the adapted procedure is required to ensure the reproducibility and reliability of EIS data.
Bode plots, from single measurement procedure, showing uninhibited AfB and P1-AfB

measurements (Figure 35) indicate a heterogeneity of the corroding carbon steel surface represented by a slope <45° of the curves. A slope of 45° corresponds to an ideal capacitor, as the measured system follows non-ideal condition, and this is also reflected in slight depressed semi circles in Nyquist plots (not shown here). Consequently, the method described above must be followed precisely from sample preparation to sample installation to ensure reproducibility of measurements.

Table 7: Inhibitor dosage rates.

Corrosion inhibitor concentration (ppm)	Single dosage (µL)	Additional dosage (µL)
0	0	0
5	1,5	1,5
10	3	1,5
20	6	3
40	12	6
80	24	12

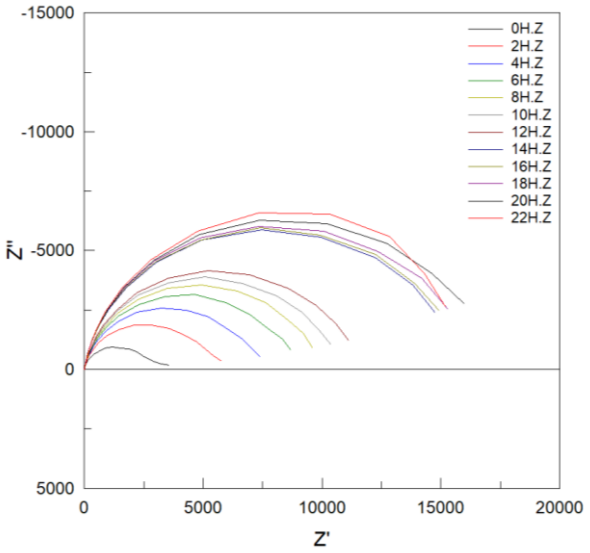

Figure 32: Nyquist plot of continuous EIS measurement for P1-AfB with 20 ppm CI1.

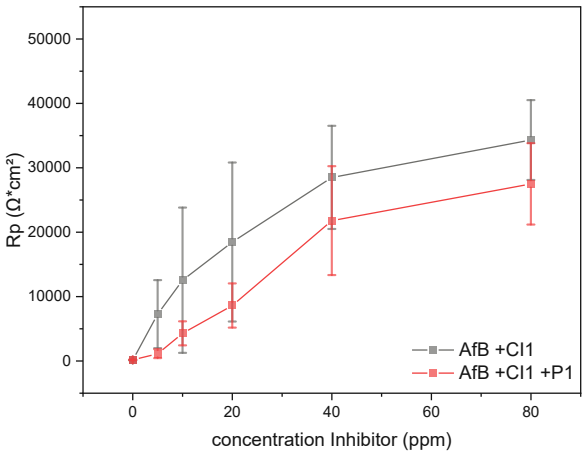

Figure 33: Comparison of Rp for AfB and P1-AfB with different concentrations of CI1 during continuous procedure.

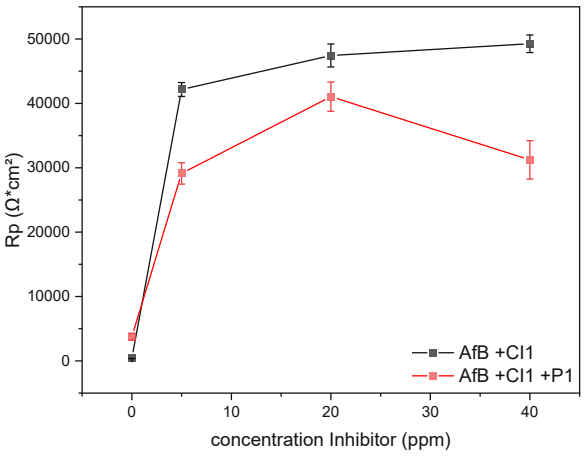

Figure 34: Comparison of RP for AfB and P1-AfB with different concentrations of CRW85579 during single measurement procedure.

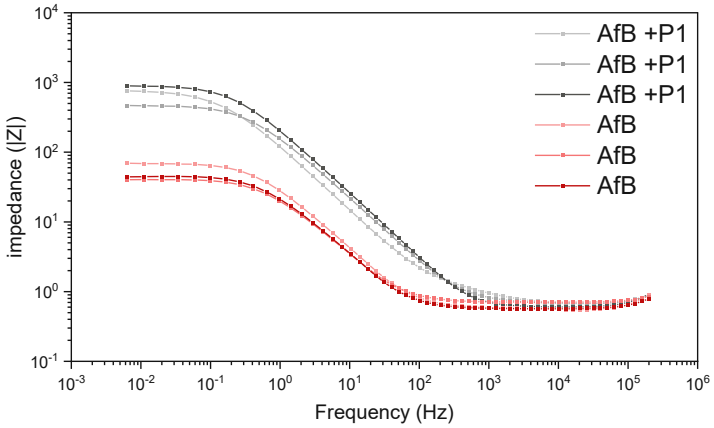

Figure 35: Bode plot for uninhibited AfB and P1-AfB during single measurment procedure.

4.2.2 Round robin test with different EIS equipment and single measurement procedure

The aim of this round robin test was to verify the robustness and reproducibility of the above elaborated EIS procedure. Therefore, an interlaboratory test at OMV Gänserndorf and TU Wien laboratory was performed to uncover possible weaknesses of the procedure and differences between RCE-EIS equipment from OMV and TU Wien. A test schedule (Table 8) was established and performed for one week at OMV laboratory, afterwards tests A and B were repeated at the laboratory of TU Wien only with the TU equipment.

For this round robin test, equipment from TU Wien and OMV Gänserndorf was set up as follows. Two TU Wien cells were connected with one thermostat (Figure 37) and three OMV cells are connected with a second thermostat (Figure 36). The temperature loss for both setups was smaller than 1°C. Each group (OMV and TU) had separate CO_2 gas supply (Messer, 4.5 CO_2). For all connections, during this round robin test, a flexible silicone hose was used, and flow rate was controlled with hose squeezers.

By contrast, the gas supply line at TU Wien laboratory consists of a Swagelok steel tube and a Swagelok hose (Flame Resistant Hose WP 350 Push-On ¼") with a pin valve, to control the gas flow. Further components of used test cells and the general setup were identical to those in section 3.9.1.

To minimize the errors and to ensure an exact and reproducible round robin test the set up procedure for RCE-EIS in section 3.9.3 and the timetable (Table 9) was strictly followed for all tests. Impedance spectra should be measured five minutes after specimen insertion to ensure the cell connection, especially for "model 1" RCE electrode adapter. Afterwards the system is given an equilibration time of 22 hours until the first of three consecutive impedance spectra was measured and validated with Z-Hit algorithm. Finally, a potentiodynamic scan was performed as described in section 3.10.

For all tests described in Table 8 an inhibitor concentration of 20 ppm CI2 was agreed which is equivalent to a dosage of 6 µL per 300 mL test solution.

Table 8: Test schedule for round robin test.

Test	Day	Brine	P1 conc. (ppm)	Cl2 conc. (ppm)
A	Monday/Thuesday	AfB	-	20
B	Thuesday/Wednesday	AfB	1000	20
C	Wednesday/Thursday	AfB	1000	20
D	Thursday/Friday	AfB	-	20

Table 9: Strict time table for round robin test.

Cell	Gas start	Inhibitor dosage	Electrode insertion	EIS Test	Equilibration	EIS 1	EIS 2	EIS 3	I/U
OMV N1	09:00	11:00	09:05	09:10	over night	07:00	07:20	07:40	open end
OMV A	11:30	13:30	13:35	13:40	over night	09:30	09:50	10:10	open end
OMV N2	13:00	15:00	15:05	15:10	over night	11:00	11:20	11:40	open end
TU N1	10:00	12:00	12:05	12:10	over night	08:00	08:20	08:40	open end
TU A	12:00	14:00	14:05	14:10	over night	10:00	10:20	10:40	open end

Figure 36: OMV cell setup, l.t.r.: OMV-A (model 1), OMV-N1 (model 2), OMV-N2 (model 2).

Figure 37: TU Wien cell setup, l.t.r.: TU-A (prototype), TU-N (model 2).

4.2.2.1 Test A & D

During Test A, all three OMV cells had a slight rusty brown coloured electrolyte after the equilibration overnight, iron ions in the electrolyte could have reacted with oxygen contaminations (Figure 38) and form iron oxide which are dissolved in the bulk electrolyte. These contaminations may possibly result from a too small cell lid seal (given by the manufacturer´s design). Therefore, an extra rubber seal was used for the next experiments with the OMV cells. The cylinder specimens, however, developed a dark grey layer on the surface which might be iron carbonate (Figure 39). The TU cells (prototype and model 2) seemed to be more airtight (Figure 40).

In test D, OMV-N2 and OMV-A showed again a contamination with oxygen indicated by the brownish coloured electrolyte, all other cells were airtight and were not influenced by oxygen intake.

Figure 38: OMV-N1, Test A, rusty brown electrolyte due oxygen contamination.

Figure 39: OMV-N1, Test A, corrosion layer on specimen after 24h EIS.

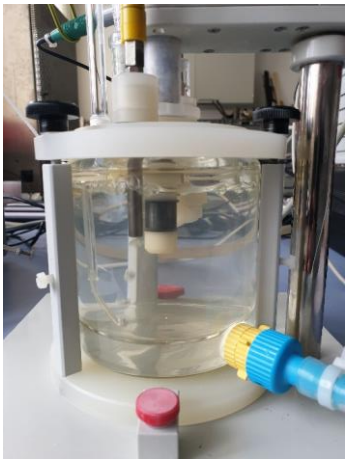

Figure 40: TU-A, Test A, electrolyte without O_2 contamination

The results of EIS tests A and D with AfB in the OMV Lab are shown in Figure 41. A scattering in Rp was found during the round robin test at OMV laboratory, between Test A and D. Within one test series differences between all cells were in a range of the calculated standard deviation but compared with the tests three days later the measured resistances differ up to 50%.

Figure 42 shows that the tests at TU Wien laboratory had slight variations too, including one outlier but the polarisation resistance is ten times higher than at measurements in the OMV Lab. This reveals a large discrepancy, during the repetition of test A and D in TU Wien laboratory, compared to tests performed in OMV Gänserndorf laboratory.

Potentiodynamic scans (Figure 43 and Figure 44) measured at the OMV Lab, exhibited a shift to a more negative potential and higher current densities compared with those measured at TU Lab (black and red line). This corresponds with Rp values, samples at OMV Lab where in a more active state of corrosion (higher corrosion current and lower Rp values). Compared with TU Wien laboratory measurements, the measurements conducted at OMV laboratory are closer to the Blank curve (uninhibited polymer-free AfB) which could be an indicator that the inhibitor had low efficiency in these experiments.

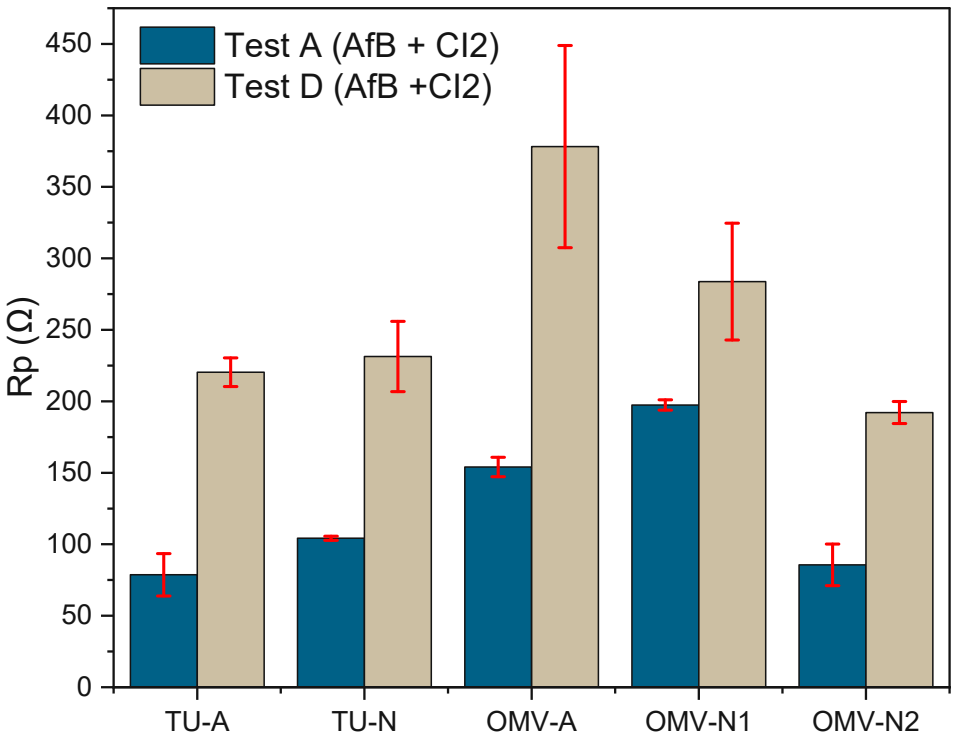

Figure 41: Test A&D, Results from EIS measurements @ OMV Lab.

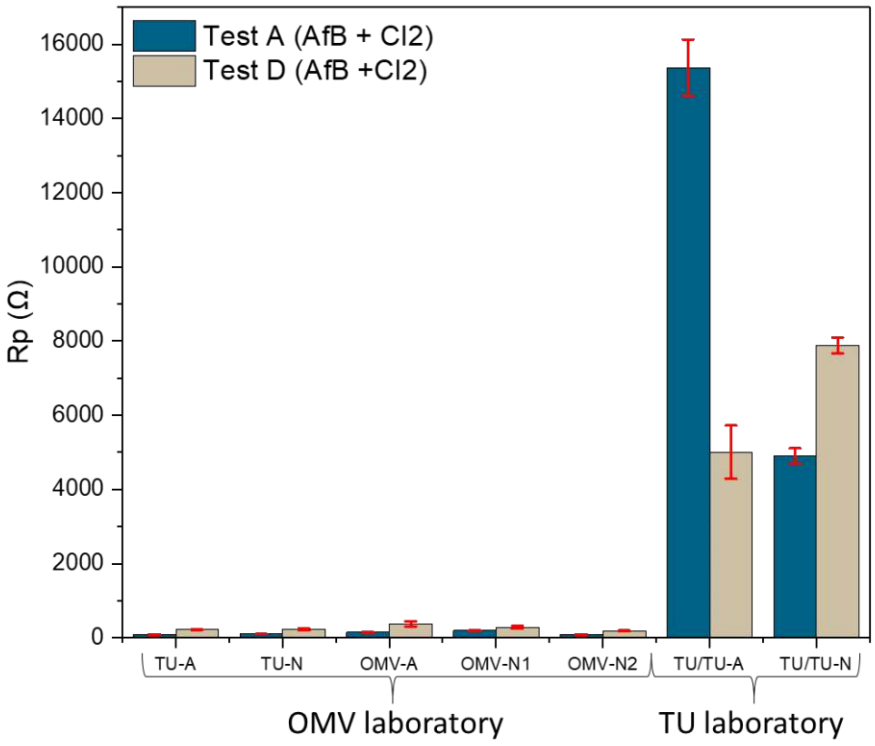

Figure 42: Test A&D, Results from EIS measurements @ OMV and TU Lab.

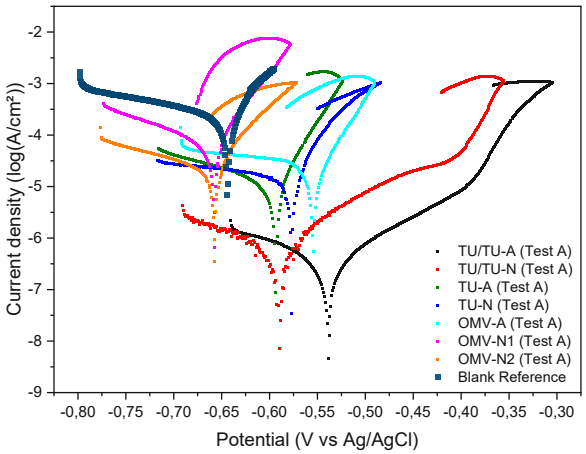

Figure 43: Test A, potentiodynamic scans.

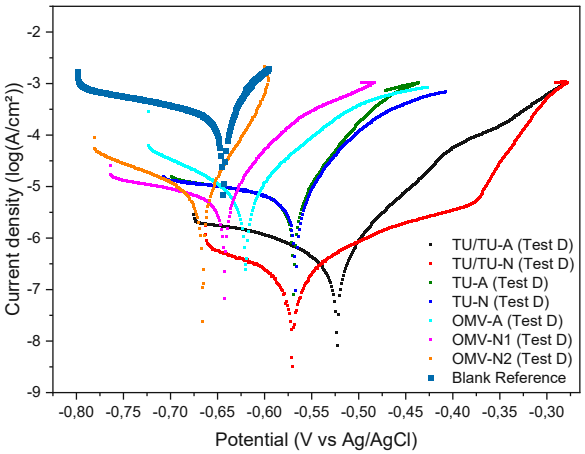

Figure 44: Test D, potentiodynamic scans.

4.2.2.2 Test B&C

All test cells had a clear electrolyte.

During test B, a problem with the pumping thermostat for TU cells occurred over night, because of water evaporation it switched off, preventing it from overheating and the temperature dropped to 40 °C. Before EIS measurements were started the cells were reheated to 60 °C. Therefore, EIS measurements of TU Wien equipment were possibly corrupted, and they will not be considered for further analysis of test C. Furthermore, OMV-A test cell lost the electric contact to the specimen and could not be used for measurements.

It was not possible to fit any data from Test B of cell OMV-N2, Z-Hit algorithm indicates an invalidity of measured data, therefore no data will be plotted. As mentioned above during Test B problems with the thermostat occurred with the TU Wien equipment, the fitted Rp values were plotted in the results, but were not considered for evaluation. The only valid polarization resistance from Test B in Figure 46 is from OMV-N1.

Rp values for Test C are plotted in Figure 45. A high scattering in Rp between the five tested cells could be determined. Compared to the measurements of test C in the TU Vienna laboratory, the polarisation resistances were again significantly lower during measurements at the OMV Lab. A possibility for the scattering may be the viscosity of the polymer electrolyte (Table 2), which is significantly higher (approx. 13 cP) than the normal AfB electrolyte (<1 cP), therefore the homogeneous distribution of the corrosion inhibitor is possibly hindered, and the CI cannot adsorb on the metal surface.

To compare the potentiodynamic scans the dark blue line represents a P1-AfB as reference. Figure 47 shows a high varying of scans and OCP. For further discussion Figure 48 of Test C is used. As described in Test A&D, scans at the OMV Lab shift further to the Blank reference except TU Alt and OMV Alt which are shifted to more negative potential and show a steeper slope of the anodic branch. All other curves have a flatter ascent of anodic current till they reach a certain potential where the current density increases abrupt and corrosion processes are accelerated.

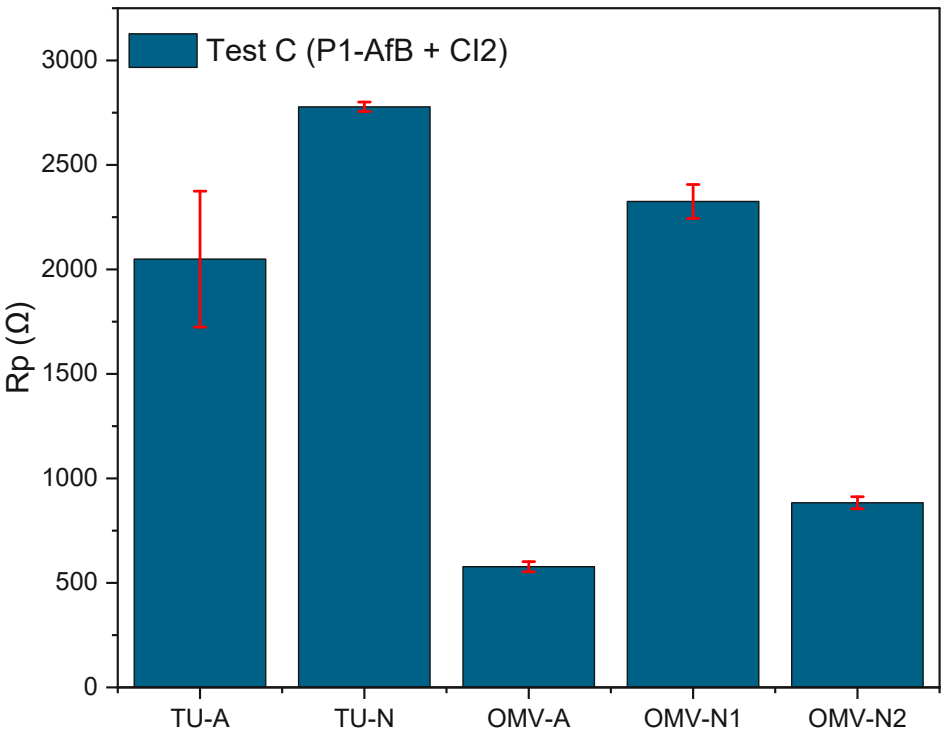

Figure 45: Test C, Results from EIS measurement @ OMV Lab.

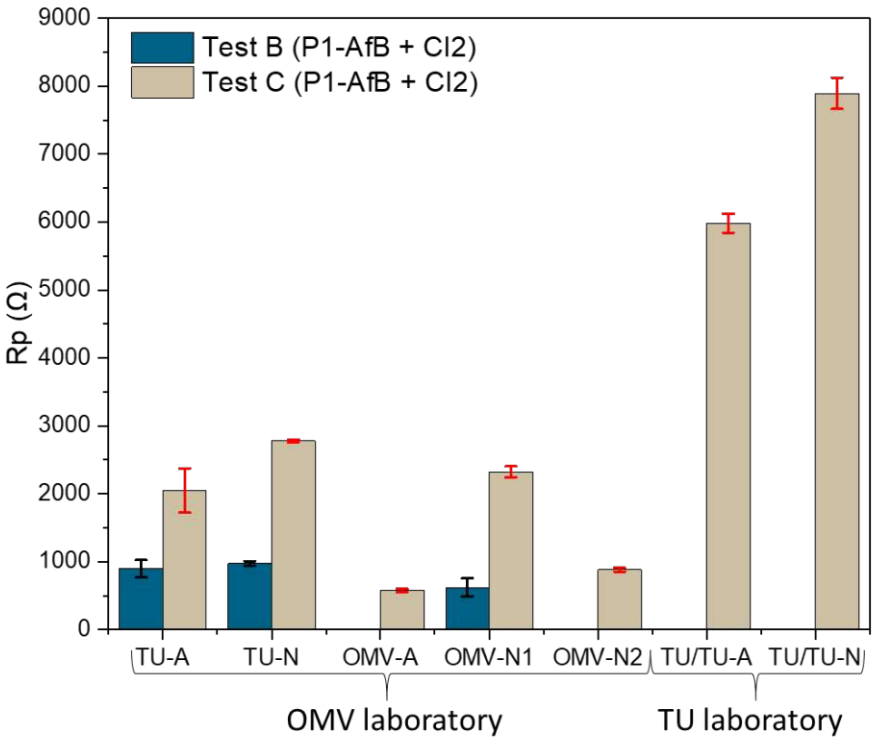

Figure 46: Test B&C, Results from EIS measurements @ OMV and TU Lab.

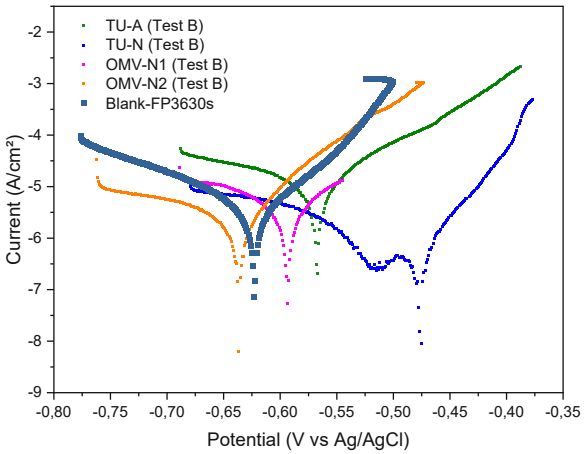

Figure 47: Test B, potentiodynamic scans.

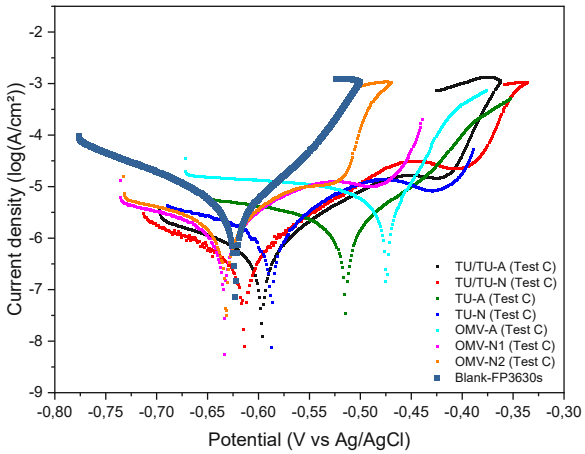

Figure 48: Test C, potentiodynamic scans.

4.2.2.3 Setup review

The data and results gained by EIS measurements and potentiodynamic scans mentioned above, concludes that there was a discrepancy between measurements at OMV Lab and TU Wien Lab. Therefore, the experimental setup was subjected to a comprehensive review. The only difference in experiments A to D was found in the type of CO_2 supply line. In OMV laboratory, it was a flexible silicone line, in the laboratory of the TU Wien the CO_2 line was permanently installed and consists of a stainless-steel Swagelok and a Swagelok hose line to the cell entrance.

Silicone elastomers have a high amount of free volume and a high degree of chain mobility due its low intermolecular forces and single bonds which link the Si and O atoms. Further, the type of gas affects solubility and diffusivity depending on the gas molecule size and the polarity. Pressure, temperature, and thickness of the silicon rubber also have an influence on the permeability and diffusivity of gas through the silicone hose. For a dimethylsilicone rubber the permeability is $62*10^9$ $cm^3(STP)*cm/(s*cm^2*cmHg)$ and the diffusivity is $16*10^6$ cm^2/s for oxygen [82].

Consequently, the CO_2 supply at OMV Lab was changed to a Swagelok steel line and for proof of concept at TU Wien Lab a silicone hose of approx. 30 cm was inserted into the CO_2 supply line short bevor RCE cell entrance. Test C with 20 ppm of corrosion inhibitor 2 and 1000 ppm polymer AfB was repeated.

Figure 49 shows the different measurements at OMV Lab and TU Lab with and without silicone hose inserted in the CO_2 supply line. The green bar is an EIS measurement at OMV Lab with a Swagelok steel tube and as seen in the diagram the Rp increases without assumed oxygen contamination. The brown bar on the right side of the diagram is an EIS measurement at TU Lab with a silicone hose as gas supply line. The value drops due to the oxygen contamination and the electrolyte turned rusty brown during the 24 hours of EIS procedure.

We can conclude that oxygen influences the measured system by either reaction with the corrosion inhibitor or by influencing the corrosion process itself. Further, it's possible that the oxygen in the electrolyte reacts with free Fe^{2+} ions, forms Fe^{3+} and colours the electrolyte brownish, i.e. iron oxide precipitation. Further discussion to the influence of oxygen see section 4.9.5.

To conclude it´ s important to be aware of a possible oxygen contamination via leaking seals at the

EIS-RCE cell and contaminations through the gas supply. All cell connections must be sealed with Teflon tape and if necessary, an additional rubber seal for the lid can be used. Experiments lasting longer than 24 hours have to be carefully prepared to prevent ingress and accumulation of oxygen over time. For construction of gas supply lines, the air tightness of tubing and valves must be selected to minimize oxygen contaminations.

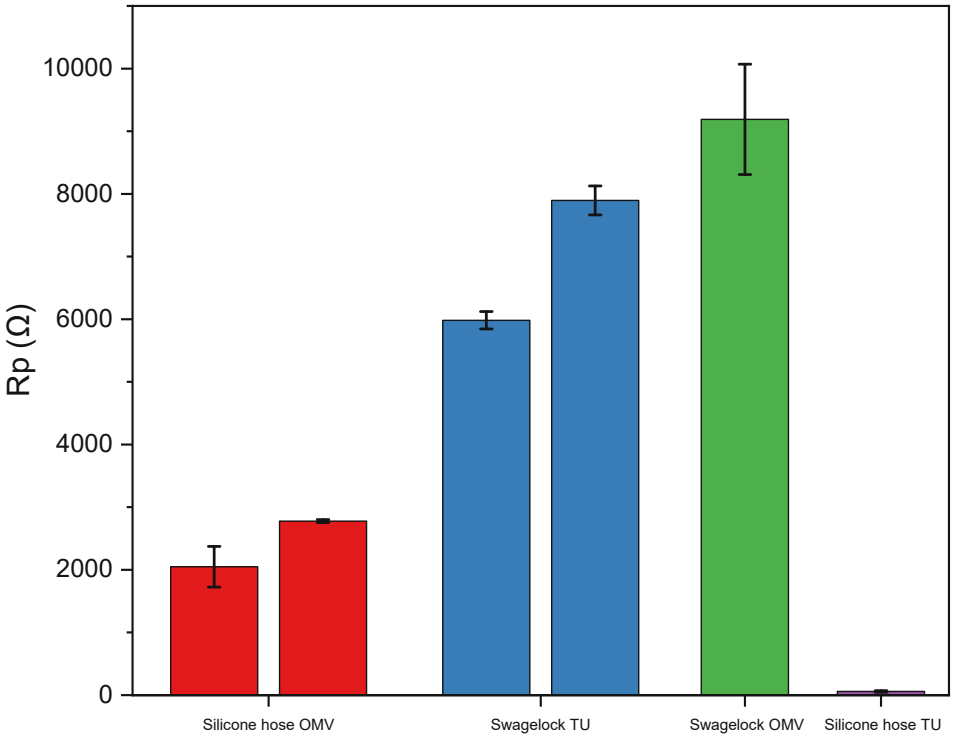

Figure 49: Test C, different CO_2 supply lines.

4.3 Influence of polymer 1 in laboratory tests

As mentioned above in section 4.2.1 with the established RCE-EIS method we attempted to replicate the practical phenomenon observed during EOR treatment: This is based on the experienced increase of corrosion rates of oil field facilities (Steel grade J55) where P1 (HPAM) is re-produced and with higher inhibitor concentration it's possible to compensate for it. With the newly elaborated experimental approach, we can replicate the corrosion rate increase observed in the field by laboratory measurements, with polymer 1 used. Figure 50, where the polarization resistance, Rp, is plotted against the corrosion inhibitor concentration, points out the phenomenon described above. The efficiency of the used corrosion inhibitor (CI1) decreases, if P1 is present in the electrolyte. We can conclude that the established RCE-EIS procedure is suitable to investigate phenomena appearing due to different electrolyte compositions, i.e. corrosion inhibitor or polymer addition.

Comparing the Bode plots (Figure 52 and Figure 53) for uninhibited and inhibited AfB electrolytes we observe a shift to more heterogeneous surface conditions when CI1 adsorbs on the carbon steel surface. Inhibitor-free electrolytes show well-defined reactions and non-dispersive time constants based on the information from Figure 52. With the addition of CI1 the phase angle in the high frequency area (10^1-10^5 Hz) shifts, see Figure 53. The corrosion inhibitor adsorbs at the metal surface,

forming an additional interface between electrolyte and steel with a very low capacitance influencing the phase angle in the measured frequency area.

With polymer 1 present in the electrolyte Bode plots (Figure 54 to Figure 55) indicate a reduction in phase angle shift, due to the adsorption of polymer on the metal surface and its slight inhibitive effect and interaction with the corrosion inhibitor.

A possible explanation for this phenomenon is that the CI, which is considered a multicomponent liquid, may interact physically (adsorption) or chemically (reaction) with the polymer. This could mean that one or more inhibiting components would be missing for adsorption at the metal surface and thus the overall CI efficiency would decrease. Moshtaghi et al. [83] measured by FTIR a possible formation of hydrogen bonds between polymer and corrosion inhibitors containing quaternary ammonium salts (QAC), due to the peak broadening of O-H peaks. Another effect could be the competition of polymer and inhibitor in adsorption at the metal surface. As a result, some spots on the surface are protected by the inhibitor while the rest of surface is covered by adsorbed polymer (or vice versa). Consequently, corrosion attack would be localized to the non-inhibited areas. The protected surface with adsorbed CI might even enhance the corrosion processes at unprotected zones by acting as cathode. Depending on the interaction between CI and polymer or the competition for adsorption sites combinations of both can lead to synergistic or antagonistic effects. To gain more information on this, tests with different corrosion inhibitors (section4.4) were performed, to evaluate the influence on different CI compositions.

In addition to this, an inhibiting effect of polymer P1 can be seen without corrosion inhibitor in Figure 50. The higher polarization resistance measured in uninhibited P1-AfB compared to AfB electrolyte, as plotted in Figure 51, indicates a moderate inhibitive effect of a P1 containing electrolyte. The black curve in Figure 55 representing an uninhibited P1-AfB, showing a similar phase angle shift at higher frequency's (10^1-10^5 Hz) as seen with inhibited AfB electrolytes, when polymer 1 is present, indicating the slight inhibitive effect of the polymer.

The reasons for this effect can be manifold, long polymer chains may adsorb on the iron surface and build a stationary, diffusion-controlled interface. Therefore, corrosion processes on polymer covered parts of the surface are weakened or possibly stopped. Furthermore, the P1-AfB shows higher viscosity than an AfB electrolyte. The diffusion of reactants from the bulk electrolyte to the metal surface or vice versa may be slower and corrosion processes get reduced, as is indicated in the sketch in Figure 56. A briefer discussion of the influence of polymer type on corrosion behaviour will be given in section 4.5.1.

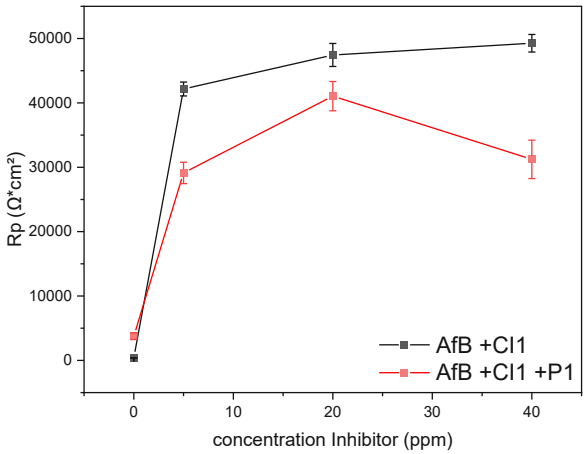

Figure 50: Rp values of different electrolyte brines (AfB and P1) with Cl1.

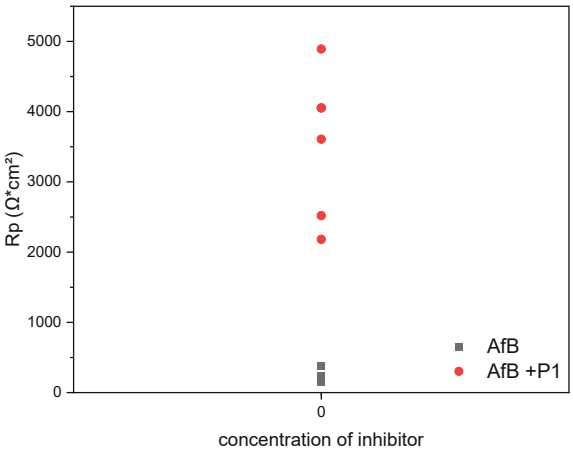

Figure 51: Inhibitor free Rp values of AfB and P1-AfB.

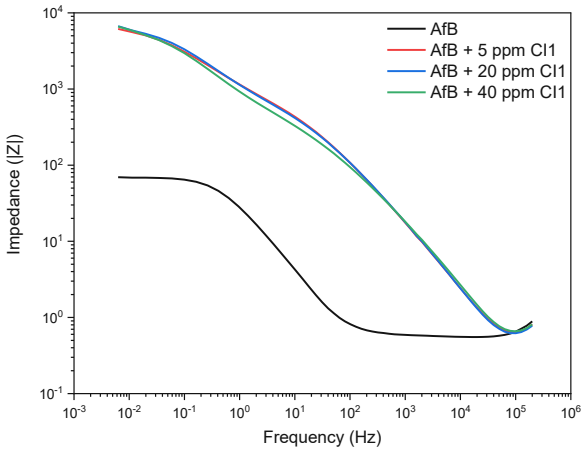

Figure 52: Bode plot, Impedance vs frequency for inhibited and uninhibited artificial brine with Cl1.

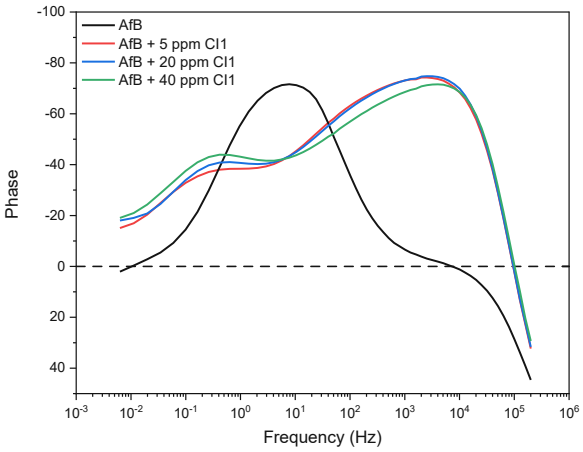

Figure 53: Bode plot, phase vs. frequency for inhibited and uninhibited artificial brine with Cl1.

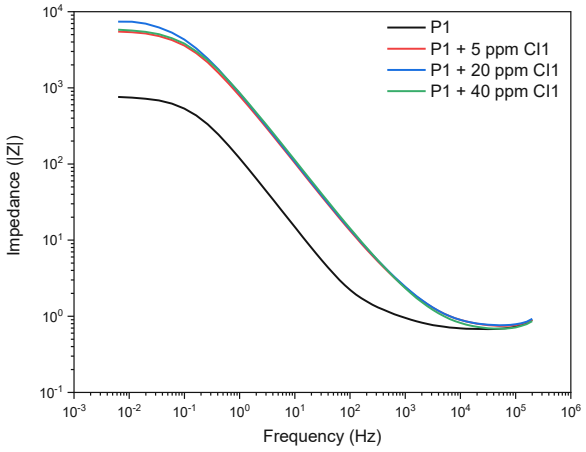

Figure 54: Bode plot, Impedance vs frequency for inhibited and uninhibited P1-AfB with Cl1.

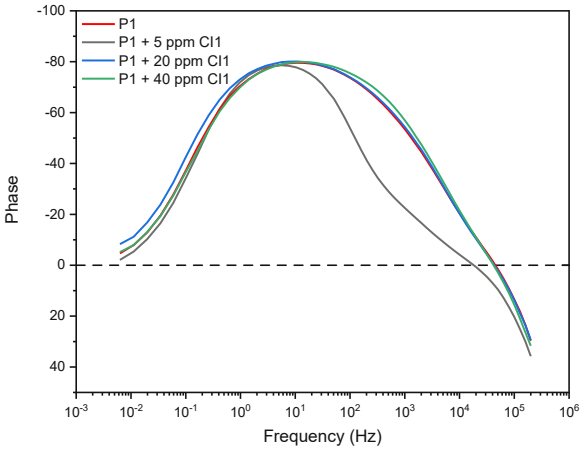

Figure 55: Bode plot, phase vs frequency for inhibited and uninhibited P1-AfB with Cl1.

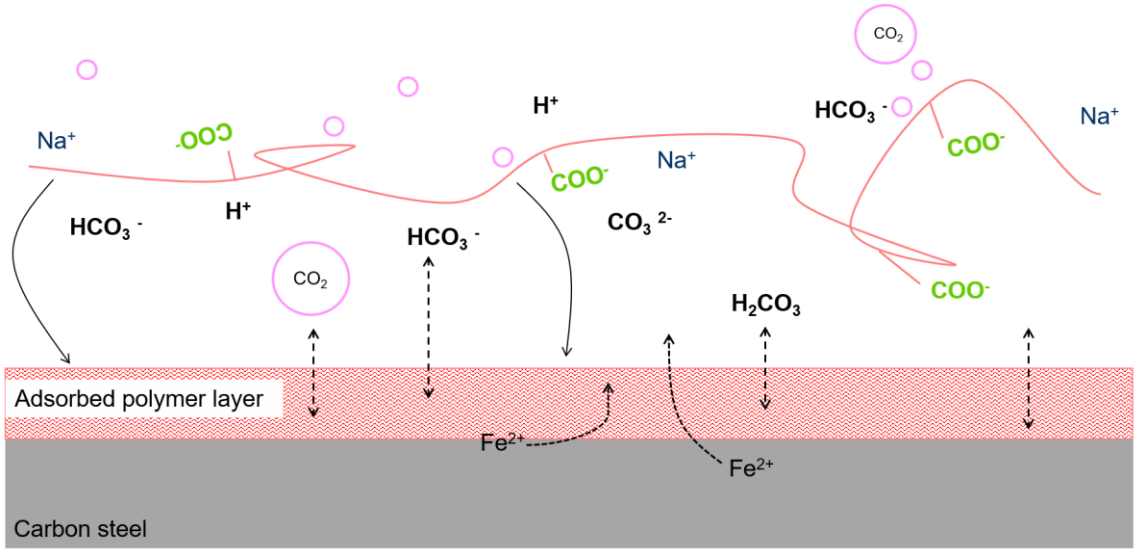

Figure 56: schematic sketch of adsorbed polymer and the diffusion limitation.

4.4 Comparison of different corrosion inhibitors and their influence

To determine the influence of the corrosion inhibitor composition on P1-AfB, it was necessary to screen several inhibitors, provided from different suppliers. Finding potential candidates, compared to standard used CI1, to reduce the corrosion rate in oil fields and at the same time reduce the concentration of used corrosion inhibitor may give information of the interaction between polymer and CI. To be as near as possible at oil field conditions, the tests were performed in a solution consisting of: 1000 ppm Polymer (hydrolysed Polyacrylamide HPAM, P1) dissolved in artificial brine (P1-AfB), which equals an average concentration of back produced EOR polymer, shown in Figure 16 and Figure 17.

Seven CIs were tested in polymer AfB (P1-AfB) electrolyte, including CI1 (OMV standard). Six are from commercial source and on is an experimental composition (Lab-sample) (see Table 3). The corrosion inhibitor samples were preselected and provided by different chemicals suppliers. By pre-tests and after agreement with OMV, inhibitor concentration should be between 5 to 40 ppm, which represents an average inhibitor dosage in Austrians oilfields.

Table 4 presents the ratios of components used in the corrosion inhibitors as far as were provided by the suppliers as these are proprietary formulations. The major component is the solvent, for example ethylene glycol or Butoxyethanol. Surface active substances which contribute to the inhibition effect are quaternary ammonia compounds (QAC), aromatic carbon compounds, amides and amines, mercaptan groups etc. These could interact with the metal surface, for example by adsorption, forming a film and contributing to the inhibitive effect.[83-85] Khamaysa et al. [84] showed with XPS, that there a two main types of interaction between iron atoms from the metal surface and inhibitor molecules (all inhibitor parts), electrostatic and chemical interactions.

As Figure 57 shows, some of the tested CIs will head into a saturation of protection at higher concentration (40ppm) under the tested laboratory conditions.

Compared to the standard CI, the CI7 (light blue) and CI6 (brown) are the ones with very poor performance. Since there is hardly any information to the composition of CI7 it will be not included

into further analysis.
Supplier D provided CI4, which is specially adapted to environmental requirements during polymer EOR. The dark blue line indicates low corrosion protection at a concentration below 20 ppm, but above its performance is significantly better. After consultation with the supplier, their specialists claim that it's possible to improve the efficiency via small modifications in the formulation. It should be noted that this corrosion inhibitor is yet not commercially available.
CI5 (violet) and CI3 (green) performed a little, but not significantly, better than OMV standard inhibitor (CI1). The major difference appears at low CI concentrations. The corrosion protection of these two products is on a constant high level from low to high concentrations. Which leads to the assumption, that with both CI it may be possible for field engineers to decrease the CI concentration at constant corrosion rates. Both CI have no QAC components, CI5 is based on polyether's and derivates, whereas CI3 consists mainly of imidazoline and other heterocyclic N-derivates. Therefore, it is reasonable that these corrosion inhibitors have different mechanism of adsorption on carbon steel surfaces and were not as strongly influenced by the polymer as CI´s with QAC.
The best performance was found with CI2 (red). This CI provides high corrosion protection from low to high dosages in a P1-AfB electrolyte. With linear polarization resistance (LPR) measurement under laboratory test conditions supplier B was able to confirm that CI2 is the best performing corrosion inhibitor of their own product portfolio. Further, it appears that this product is not heading into saturation at the tested concentrations, but in fact shows an increasing effect in corrosion protection. Compared to the other corrosion inhibitors used, CI2 consists of a higher number of N-containing compounds (up to 30%), thus are active components adsorbing on the carbon steel surface forming a protective film and are considered to possible displace adsorbed polymer molecules [85].
To conclude, EIS data reveal differences in corrosion inhibitor products compared to the Benchmark of CI1 inhibited AfB electrolyte. Their different composition causes changes in the interaction behaviour with the iron surface and the polymer. As described above, some of the contacted suppliers can confirm our measurements or were able to improve their CI compositions, but for an end user of these products it's hardly possible to interpret the different performance of multicomponent liquids without detailed information about their composition. Material safety data sheets (MSDS) give only a small view of components used, i.e. labelling obligated, thus the real compositions of different CI products were not provided by the supplier and therefore, no qualitative conclusion can be provided which component of CI will enhance or decrease the performance with EOR polymer in the environment. Since CI2 showed a significantly better effectiveness during these tests, it was used for further tests and the analysis of the differences in comparison with CI1.

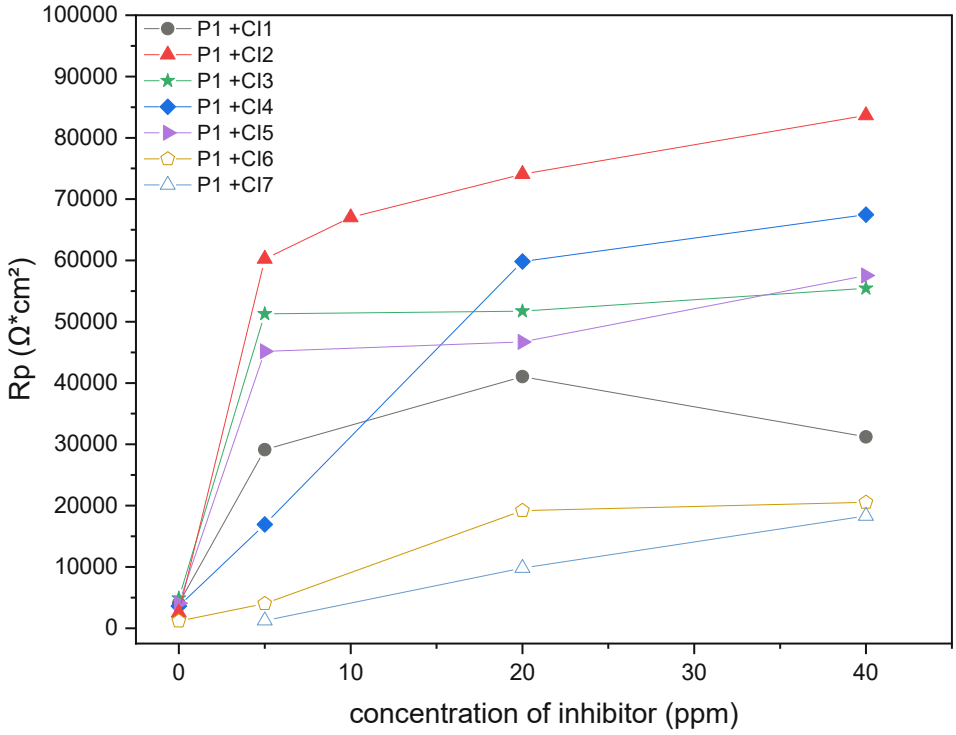

Figure 57: Fitted Rp values of different corrosion inhibitor samples in P1-AfB.

4.4.1 Comparison of CI1 and CI2

Comparison of the best performing inhibitor CI2 with the standard product CI1 should show differences in the interaction with polymer 1 and the carbon steel surface.

The first major difference of the inhibitors can be seen in Table 4: CI1 has a low amount of QAC and amines, polyethers with the highest concentration in CI1 were considered to be the surface-active components. CI2, on the other hand, is based on higher concentration of QAC, amines and mercaptan components. That difference is seen in EIS experiments in AfB, plotted in Figure 58. Both AfB +CI1 (black) and AfB +CI2 (blue) show similar Rp at low inhibitor concentrations (5 ppm) but Bode plots (Figure 59 and Figure 60) reveal a difference already at low inhibitor concentrations. For low frequencies (10^{-1} to 10^{1}) the phase angle for AfB with 5 ppm CI1 is closer to zero compared to CI2, indicating a difference in adsorption at the metal surface. At concentrations higher than 20 ppm CI2 causes by an order of magnitude higher Rp values, described in Figure 58. As described above nitrogenous inhibitor components have a good adsorption on steel surfaces which corresponds to the higher Rp values due to stronger adsorption. The Bode plots show higher negative phase angle values over a wider frequency range (10^{0} – 10^{4} Hz) indicating a more uniform adsorption and therefore a high efficiency of the corrosion inhibitor.

For both corrosion inhibitors Figure 58 shows an antagonistic effect with the polymer, i.e. a decrease in Rp compared to polymer-free electrolytes. The phase angle at high frequencies (10^{1} to 10^{4} Hz) in Figure 61 and Figure 62 for both CI show more negative values and approaches the value of uninhibited P1-AfB (black curve). The CI may not be able to replace the polymer from the adsorption sites and therefore some sites remain occupied by P1 chains, and the two CIs won't be able to form

a uniform CI layer. Due to its composition, this effect influences CI2 less, which shows a higher ability to penetrate the polymer layer and adsorb on the metal surface, which can be confirmed by Rp data in Figure 58 and Bode plots in Figure 62.

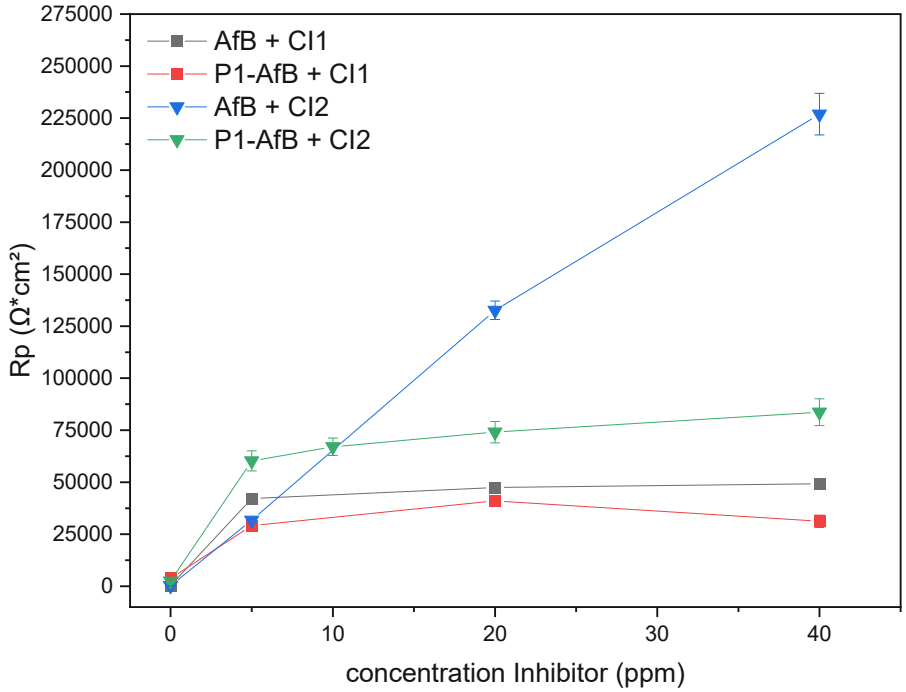

Figure 58: Rp comparison of AfB and P1-AfB with CI1 and CI2.

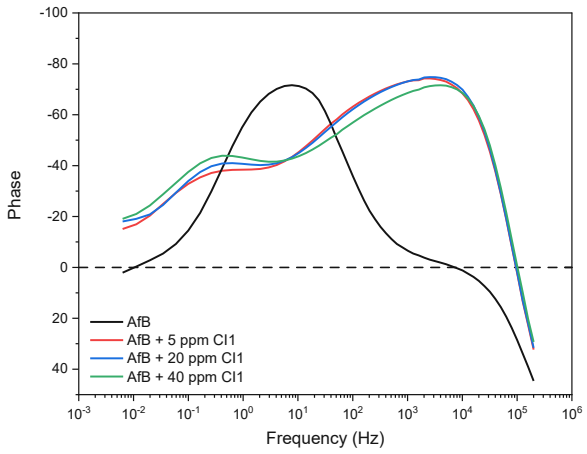

Figure 59: Bode plot, frequency vs. phase for uninhibited and inhibited AfB with CI1.

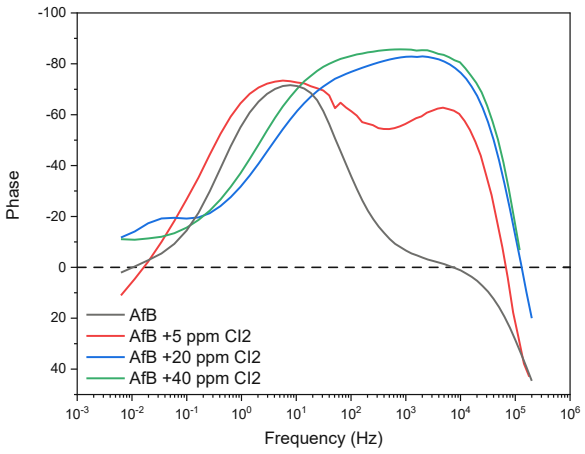

Figure 60: Bode plot, frequency vs. phase for uninhibited and inhibited AfB with CI2.

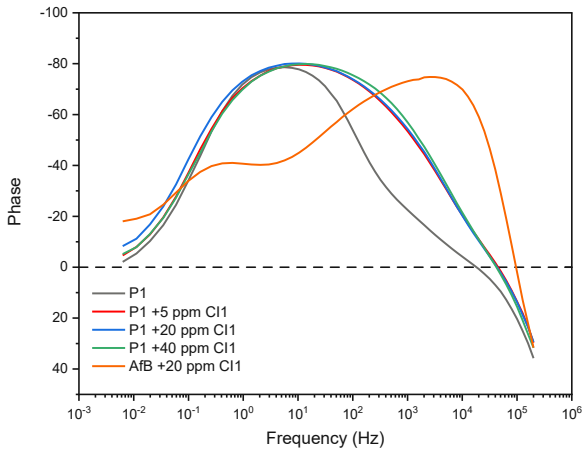

Figure 61: Bode plot, frequency vs. phase for uninhibited and inhibited P1-AfB with CI1.

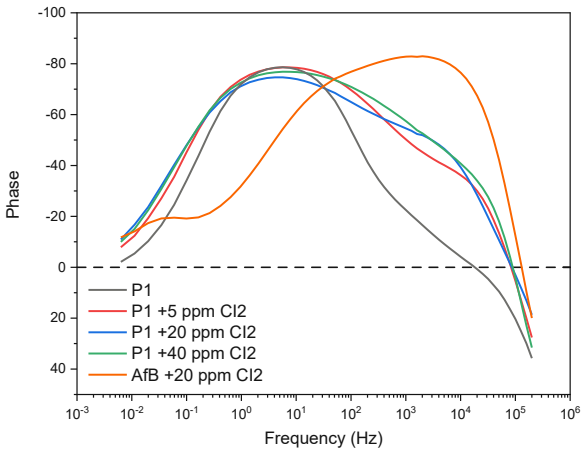

Figure 62: Bode plot, frequency vs. phase for uninhibited and inhibited P1-AfB with CI2.

4.5 Influence of the polymer type and chain length on corrosion behaviour

During this test series, it was detected visually that problems can occur with mixing when dosing the inhibitor into the highly viscous polymer solutions. After adding the inhibitor, threads of dosed CI can be visually detected for some (limited) time. Consequently, this phenomenon leaves some doubts on the homogeneity of distribution. This is very different from a polymer free brine, where the inhibitor is quickly dispersed. Therefore, it the specimen was mounted after 5 minutes, to ensure a homogeneous distribution in polymer brines with higher viscosity. Table 10 provides a list of tested polymer samples, including the type, molecular weight (MW), degree of hydrolysis as provided by the supplier and viscosity measured at a concentration of 1000 ppm.

Table 10: Tested polymer types.

Acronym	Polymer Type	shear Viscosity (mPas)	Molecular weight (Mda)	Hydrolysis Degree (%)
P1	Co-polymer	13,06	18	25-30
P2	Co-polymer	14,28	20-25	25-30
P3	Ter-polymer	16,47	20-25	20-25
P4	Co-polymer	15,21	24	30
P5	Co-polymer	10,23	18-20	25

4.5.1 Influence of different polymer samples on the carbon steel surface

Figure 63 presents the major difference between the tested polymer samples without CI, the polarization resistance Rp of PX-AfB, i.e. at CI concentration 0. All polymers with stabilizing agent or a Ter-polymer (P3) show higher Rp values and therefore a higher degree of corrosion inhibition compared to P1. Considering the replicate data contained in Figure 63 (i.e. at concentration 0) we see that some of these polymer AfB blank Rp values have a higher standard deviation, especially for polymer P3. This may be attributed to scattering in adsorption of polymer, due to its composition and possible additives. Therefore, the extent of polymer coverage at the specimen can vary easily

from experiment to experiment and consequently the values for the polarisation resistance vary accordingly.

Possible explanations for the higher Rp values at PX-AfB are:

- The viscosity difference of the used polymer samples. With higher viscosity the diffusion processes of reactants to or from the surface may be slower and thereby corrosion processes may get retarded. P3 and P4 with the high viscosities shows the higher Rp with higher standard deviations due to adsorption processes mentioned above. Despite the lowest viscosity P5 shows higher Rp compared to P1 and P2 (higher viscosity measured) which may result from a better adsorption behaviour (see explanations below).
- Stabilizing agents like oxygen scavengers can bind spurious oxygen from the electrolyte and complexing agents can interfere with dissolved iron ions. The resulting chelate may precipitate and possibly form a protective layer on the carbon steel surface. Moreover, various additives in P2-P3 may change the interaction between polymer and carbon steel surface, especially surface-active components which may interact by physisorption or chemisorption with the carbon steel surface. [84, 85]
- Different side groups and hydrolysation grades modify the adsorption and desorption behaviour of the polymer chains and corrosion processes on covered parts may get inhibited to some degree. Especially amine-, amid-, and sulphide (sulfonic acid group in P3) groups show a favoured adsorption behaviour on surfaces, as was seen by XPS [86].
-

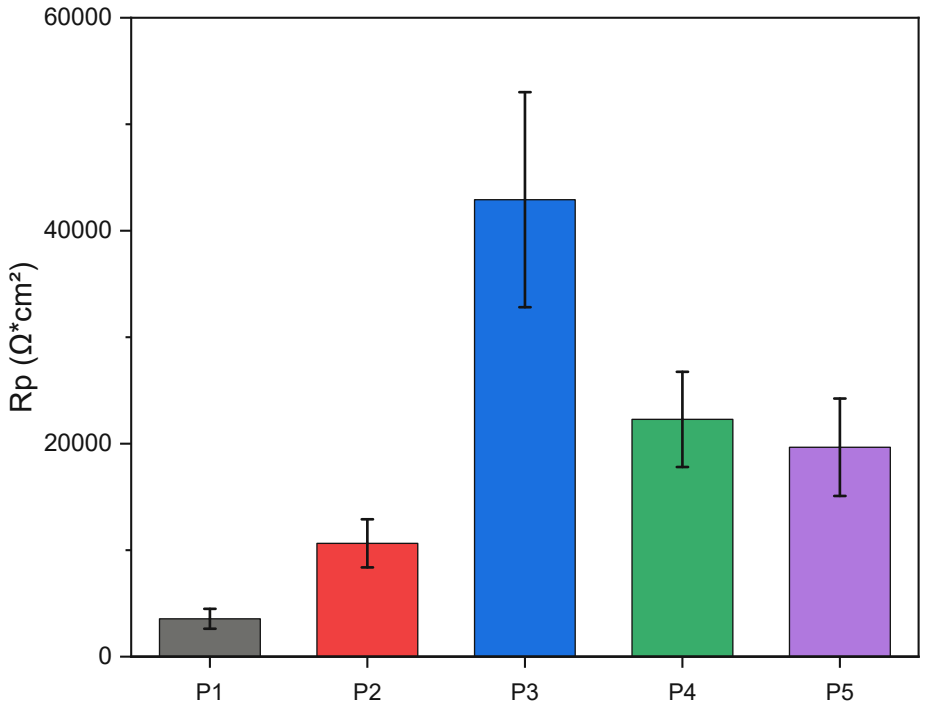

Figure 63: Rp values of different polymer samples at inhibitor concentration 0.

4.5.2 Polymer type influence on CI1

Results for Rp of PX-AfB + CI1 at varied inhibitor concentrations in Figure 64 show severe scattering indicating some interaction between inhibitor CI1 components and polymer. These measurements represent the average condition of the cylindric sample surface and may not represent systematically the behaviour of CI and polymer due to the scattering in measured data and scattering in adsorption of polymer and CI at the metal surface. The orange line marks the average Rp value of inhibited (20 ppm CI1) AfB electrolyte without polymer, to demonstrate enhancement or decrease in corrosion resistances with polymer and CI1 combinations used. To describe this unexpected phenomenon (sometimes increasing corrosion rate despite increasing inhibitor concentration) as seen in Figure 64, various assumptions can be made:

- Assuming homogeneous distribution of the corrosion inhibitor in the fluid, it is possible that inhibitor and polymer compete for adsorption on the steel surface. If the polymer, has relatively strong adsorption interaction with the steel it might block the inhibitor from adsorbing or even replace adsorbed inhibitor to some degree and the establishment of a concentration-governed adsorption equilibrium for CI by time may not occur due to poor reversibility of the adsorption/desorption processes. Consequently, an increase in inhibitor concentration has no systematic influence, the values for the polarisation resistance would rather scatter arbitrarily.
- Another hypothesis is that the polymer addition forms a highly viscous but inhomogeneous layer around the rotating specimen. Even homogenously distributed inhibitor in the bulk electrolyte will be hindered to diffuse uniformly towards the surface, leaving poorly inhibited areas. An increase in inhibitor concentration will not necessarily be reflected in an increase in the polarisation resistance as the polymer will adsorb as an inhomogeneous layer on the surface and this structure will change from experiment to experiment.

P1 (HPAM), P2 (stabilized HPAM) and P5 (may contain stabilizers) are the polymers reaching a relatively stable saturation state of polarisation resistance with increasing inhibitor concentration. These three polymers have lower viscosity compared to the other polymer samples (P3 and P4). The difference in the polymers is the stabilizing agents used in P2, which may contribute by an inhibiting effect, and the slightly higher viscosity of P2 compared to P1. A more detailed discussion of the influence of stabilisers is not possible as the suppliers do not provide any further information on the agents used.

The stabilized ter-polymer P3 (additional sulphonic acid side grouped) showed already high polarisation resistances without inhibitor, i.e. strong adsorption of the polymer on metal surface, while at lower CI concentrations (<20 ppm) Rp did not change. Only at elevated concentrations we see an increase in Rp i.e. the corrosion inhibition effect is enhanced, which may be due to a higher degree of adsorption of corrosion inhibitor components and a possible synergistic effect of the adsorbed polymer and inhibitor combination.

P4 in combination with low inhibitor concentrations exhibits improved corrosion protection. At higher inhibitor concentrations the efficiency of the inhibitor decreases which may be the consequence of the above-mentioned synergistic effects for polymer and CI1.

The best performance of standard inhibitor CI1 was seen with the polymer P5 at the CI concentration of 20 ppm and above, leading to a synergistic effect and enhancing the corrosion resistance of carbon steel combined with P5 and CI1.

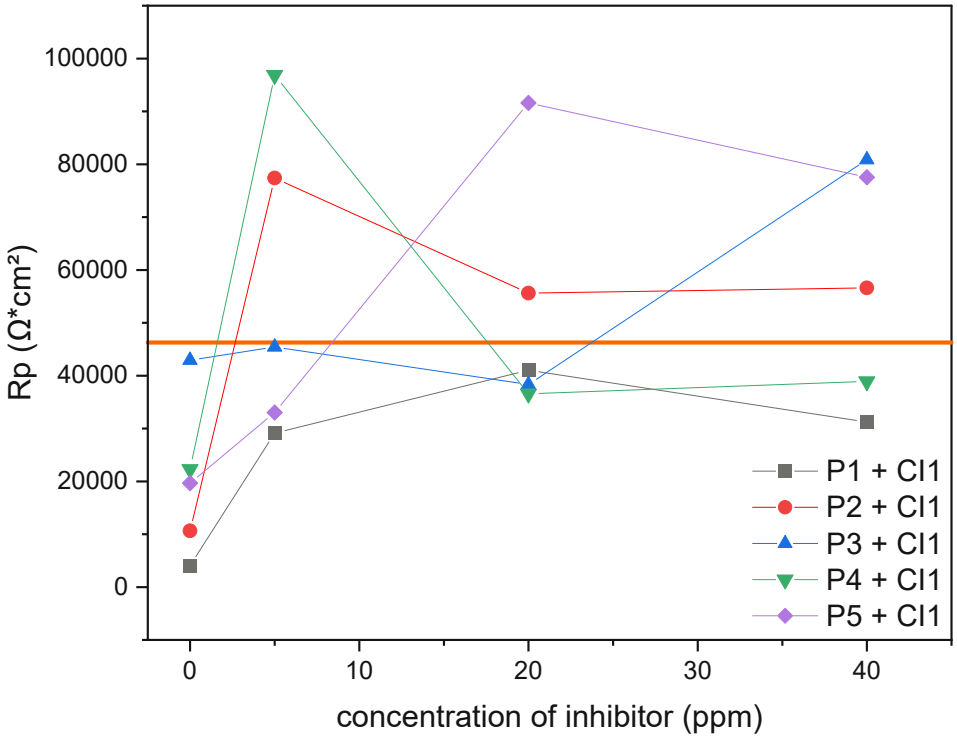

Figure 64: Comparison of Rp for different polymer samples and CI1.

4.5.3 Polymer type influence on CI2

Figure 65 shows the Rp values for PX-AfB + CI2 at varied inhibitor concentrations. The orange line at approx. 132000 Ωcm² marks the average value for 20 ppm CI2 concentration in AfB without polymer. The combination of inhibitor CI2 and various polymer samples show a decrease in Rp, leading to a decreased efficiency of corrosion inhibitor respectively. Moreover, this inhibitor shows a completely different interaction with the tested polymer samples and the carbon steel surface. The polarisation resistances plotted in Figure 65 suggest that CI2 may have a higher ability to penetrate through the polymer, but for some polymers a lower affinity to adsorb at the specimen´s surface compared to CI1 (Figure 64), i.e. the inhibitor and its components are not subjected to the distribution and/or diffusion limitations by the polymers as seen with CI1.

The chemical composition of CI2, as outlined in Table 4, is characterized by a higher proportion of nitrogen-containing components, predominantly comprising of Quaternary Ammonium Compounds (QAC) and amines. These components are recognized for their surface-active properties, which can promote adsorption onto the iron surface, which was shown by EIS experiments in section 4.4.1.

With all polymers except P3 (blue line) the inhibitor is able to diffuse to the surface, adsorb and or replace polymer from adsorption sites and forms a corrosion inhibitor layer increasing the Rp value.

The ter-polymer (P3, blue) shows higher Rp value at CI2 concentration 0, and a decrease in Rp when CI2 concentration increases.

For the other polymer samples, higher concentration of inhibitor does not improve the inhibition as the area fraction free for the inhibitor does not change. The type of used polymer (except the ter-polymer 3, blue) within this experiment had no major influence, possibly due to the positive influence on inhibitor diffusion and adsorption of above-mentioned inhibitor components.

Polymer sample P1 and corrosion inhibitor CI2 (black line) is the combination with highest polarisation resistances. This polymer has low molecular weight (Table 10) and the lowest complexity in composition compared to other polymer samples (no additives and additional functional groups). Combined with effects due the CI2 composition this may lead to a higher affinity of adsorption on the metal surface of CI2 and may be higher than that of the polymer. In consequence, the well penetrating CI2 is able to replace adsorbed polymer P1, and, with increasing CI2 concentration, more area of the specimen is covered by the inhibitor and the polarisation resistance Rp increases accordingly, i.e. the corrosion rate decreases. CI2 concentration above 20 ppm approaches the average Rp for AfB without polymer.

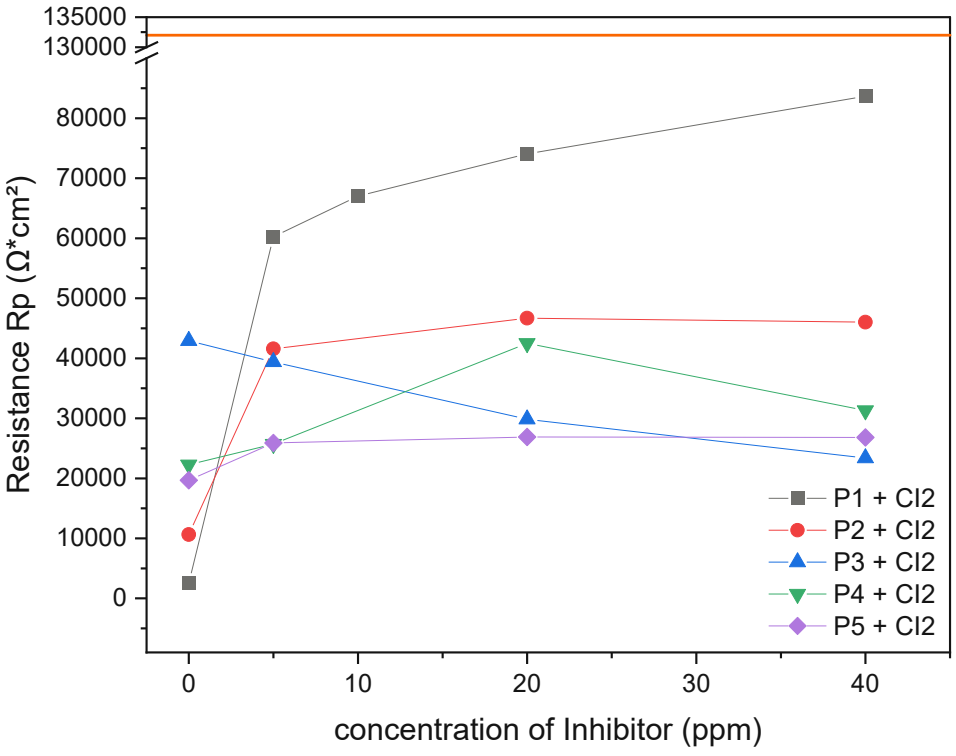

Figure 65: Comparison of Rp for different polymer samples and CI2.

4.6 Difference in polymer batches and their influence on corrosion behaviour

During this thesis different polymer batches were used to prepare the P-AfB electrolytes, in particular four different batches were used for P1 without differences found during experiments. Also, with P2 to P4 samples no differences between the batches were observed during the EIS measurements whereas P5 shows a significant discrepancy between two batches, see Figure 66. Batch 1 was provided from OMV and batch 2 was received directly from the supplier, together with samples of different molecular weights.

Differences were found in the viscosity, P5 Batch 1 has 10,23 cP and Batch 2 12,56 cP at 1 g/L.

The Rp values in Figure 66 of the uninhibited and inhibited P5 batches show a difference of one order of magnitude. Figure 68 indicates that uninhibited Batch 2 has twice the Rp of uninhibited Batch 1. The combination of P5 Batch 2 and CI1 seems to lead to an effect enhancing the corrosion resistance, compared to the lower Rp measured with P5 batch 1. Moreover, Rp values of Batch 1 compared to EIS measurements of P5 molecular weight standards (Figure 74) were lower than samples with molecular weights > 8-10 MDa. This may lead to the assumption that there is a greater adsorption of polymer from Batch 2. Despite this suggestion, i.e. the weaker adsorption of Batch 1, the Bode plot in Figure 67 show similar curves for both Batches. This would contradict the previous assumption.

Comparing the FTIR spectra, Figure 69 shows a difference in two bands between 3100-3400 cm^{-1} for both batches. The character of a polyacrylamide polymer structure is confirmed by the broadening of the bands compared to those shown by acrylamide monomer at 3350 and 3190 cm^{-1}, which are assigned to NH_2 stretching antisymmetric and symmetric modes, respectively [87].

With the data from the EIS, viscosity and FTIR measurements, a difference between the two batches could indicate a possible degradation of Batch 1 leading to lower Rp and viscosity. With the Bode plot and FTIR, a possible mix-up of polymer samples could be ruled out. As the composition of the batches is not fully known, some doubts remain as to the conclusion of possible degradation for HPAM. Nevertheless, FTIR could be a method to distinguish and control different polymer batches following degradation during storage.

It should be noted that Batch 1 was used for the EIS measurements, reported in section 4.4 and section 4.4.1, P5 Batch 2 was used for all other experiments.

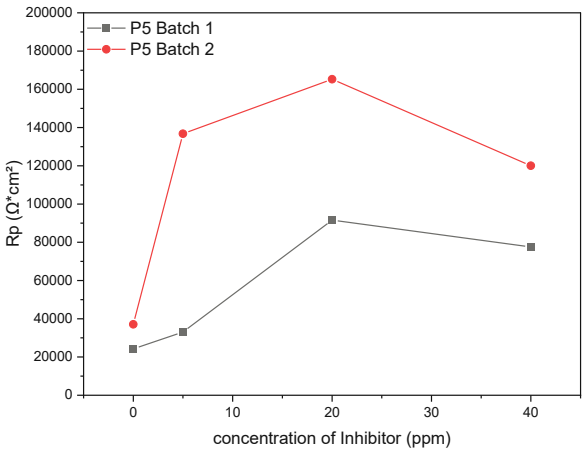

Figure 66: Rp for different P5 batches.

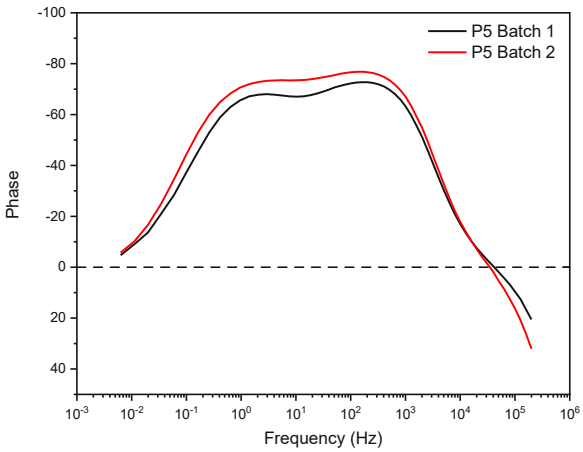

Figure 67: Bode plot, phase vs. frequency for P5 batches.

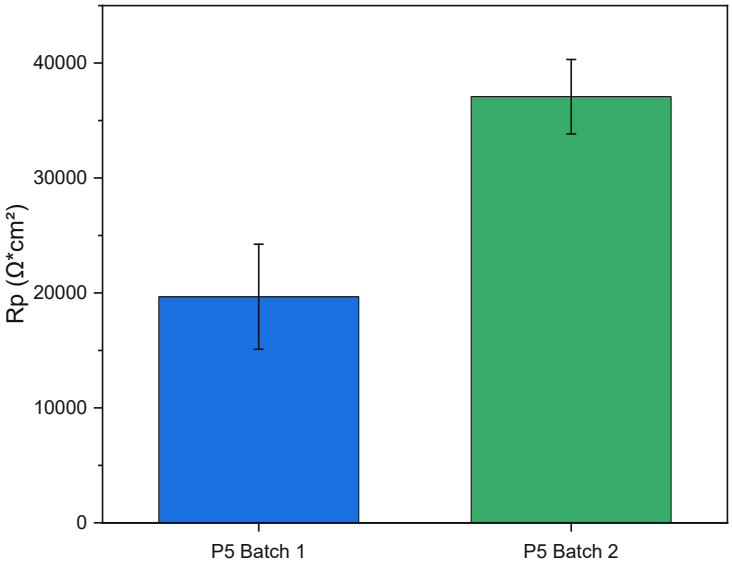

Figure 68: Differences for uninhibited P5 batches.

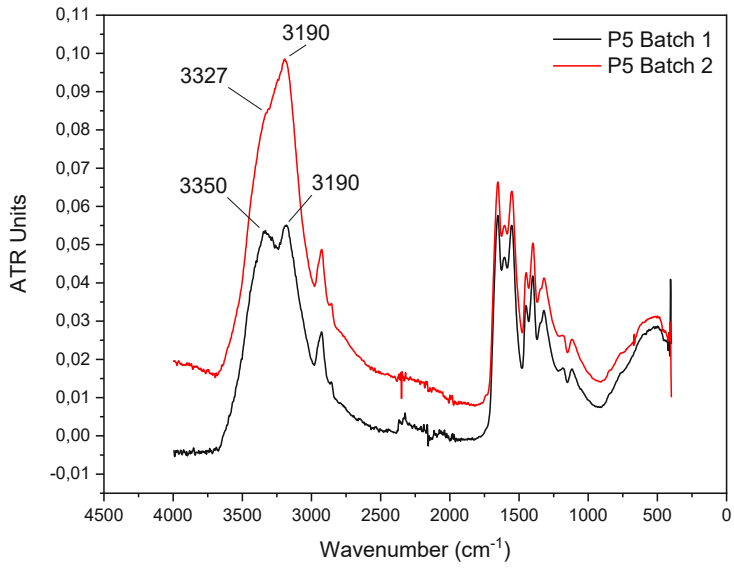

Figure 69: FTIR measurement of P5 Batch 1 and Batch 2.

4.7 Influence of the chain length of EOR polymer

In chapter 0 we proved that different polymer types influence the polarization resistance and therefore the corrosion behaviour due to their interaction with metal surface, mainly adsorption processes, and corrosion inhibitor. Even a possible degradation may influence the interaction between metal and polymer which was discussed in section 4.3 above. In order to obtain a deeper understanding of this interaction between polymer/metal surface and corrosion inhibitor, two polymers were tested with different chain lengths. The specifications of the two polymers and their variants (SLMW, VLMW, LMW, and MMW, referring to super low, very low, low, and medium molecular weight, respectively) used in this study are provided in Table 11. Both polymers P1 und P5 are HAPM co-polymers and commercially available products from different suppliers who also provided the variants and the related specifications except shear viscosity which was determined using a rheometer. P5 has a lower shear viscosity despite its slightly higher molecular weight and lower degree of hydrolysis. During dissolving of the polymer, the degree of hydrolysis may change to higher values by shear forces from stirring, and decrease the viscosity enhancing effect of the sample used [62]. Moreover, the supplier of P5 mentioned a possible addition of non-declared additive to prevent the polymer samples from degradation, which may influence corrosion processes. Thus, there are a few uncertainties which must be considered in data interpretation.

Table 11: Supplier specifications of polymers used and measured shear viscosity.

Polymer	Shear Viscosity (mPas) @ 1000 ppm	Molecular weight (MDa)	Hydrolysis Degree (%)
P1	13,06	18	25-30
P1 SLMW	1,63	1	25-30
P1 VLMW	4,15	6	25-30
P5	12,56	18-20	25
P5 VLMW	4,74	4-6	25
P5 LMW	6,51	8-10	25
P5 MMW	7,44	12-14	25

4.7.1 Polymer without inhibitor

Data on Rp determined without and with P1 and P5 at various inhibitor concentrations (CI1) are provided in Figure 70 were the orange line marks the average Rp of uninhibited AfB electrolyte (black squares). It should be noted that P5 in this experiment was a sample from a lot, provided directly from the supplier while the previously used one was provided by OMV. Discussed in section 4.5 EIS measurements reveal a difference between these two different batches of P5 polymer.

Without inhibitor, i.e. CI concentration 0 in Figure 70, both polymers exhibit some inhibitive effect indicating a kind of adsorption to the metal surface modifying its interface to the electrolyte. This inhibiting effect of the polymers appears dependant on the chain length (molecular weight respectively) shown in Figure 71.

For P1 (Figure 71) we find a minimum for Rp with the P1 VLMW variant (6 MDa), while both, P1

SLMW and the standard product P1, yield similar high Rp. This may be explained by different interactions between polymer and metal: While short chains (P1 SLMW, 1 MDa) adsorb more easily on the surface due to their greater flexibility in aligning properly, the much longer molecule chains of P1 adsorb less densely but at a high number of sites, resulting in a well attached, highly viscous polymer layer. At medium chain length (P1 VLMW), however, neither flexibility for alignment nor number of adsorption sites (amid groups) is sufficient for formation of a somehow protective layer. Bode plot in Figure 72 support, this theory, P1 VLMW show similar behaviour in the frequency range of 10^1 to 10^3 Hz as AfB electrolytes compared to the measurements where polymer adsorbs at the carbon steel surface.

By contrast, polymer P5 seems losing its inhibiting effect with lower molecular weight, as we derive from Figure 73 at first sight. However, when taking into account the molecular weights in Table 11, we find P1 VLMW and P5 VLMW with similar molecular weight ranges (VLMW≈4-6 MDa) show a similar decrease in protectiveness. With decreasing chain length P5 (< VLMW) may follow the same explanation as for P1. Nevertheless, Rp values of P5 and its variants are by an order of magnitude higher than those of P1, indicating a denser adsorption layer, i.e. an improved ability to adsorb at the steel for P5. However, mentioned above, possible additives may also improve the adsorption of P5 by providing surface active components (quaternary ammonium compounds etc.). For P5, the Bode plot for VLMW (Figure 74, dark blue) indicates a difference in adsorption behaviour of the polymer chains compared to the higher molecular weights. Furthermore, the difference to P1 is pointed out, by a shift in phase angle to higher values in the frequency range from 10^1 to 10^4 for P5, which supports also to the assumption that P5 has higher ability to adsorb at carbon steel surfaces compared to P1.

In summary, the extent of polymer coverage on the sample can vary depending on polymer chain length, and polymer type and the values for Rp vary accordingly. Since such polymer products are chemically not exactly defined substances, variations in anionic side groups and hydrolysation grades of different polymer products may influence the adsorption/desorption behaviour, i.e. the number of active adsorption sites like amides, amines, and QACs vary respectively. Moreover, the differences in viscosity of the used polymer samples (Table 11) may play a role. Viscosity is expected to influence the diffusion processes of reactants to or from the surface through a stationary interface layer built up by the polymer, thus affecting corrosion processes. Finally, as to repeat here, that polymer suppliers may use some additives like oxygen scavengers, stabilizing agents, and others to protect the polymer from degradation which may also change the interaction between polymer and metal surface, influencing the inhibitive effect. The resulting interaction and the phenomena observed during different experiments correspond with EIS results and their discussion in section 4.5.

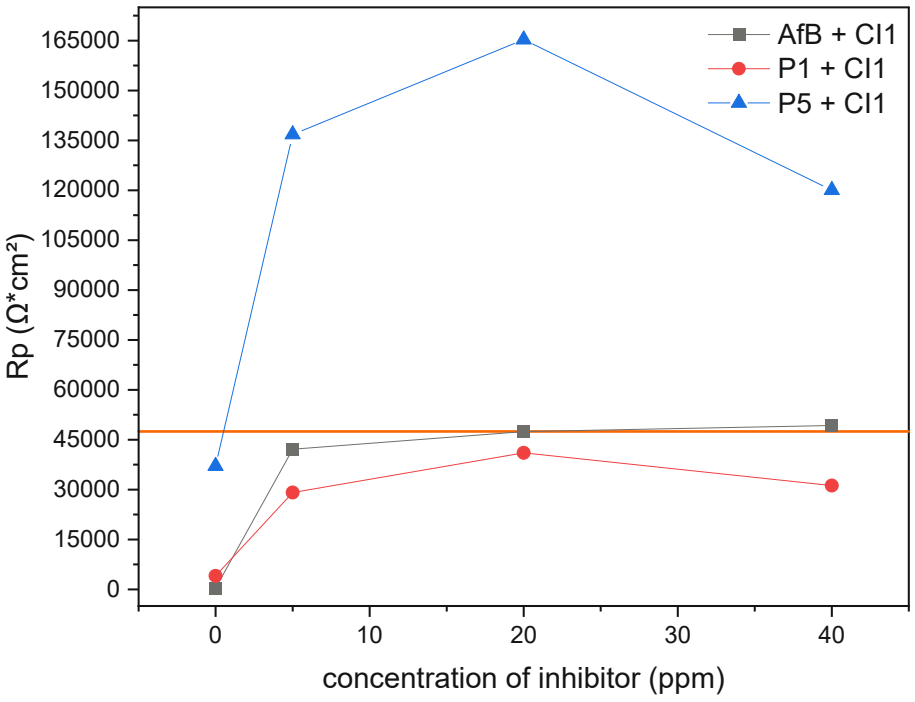

Figure 70: Rp values of AfB, P1 and P5 with different CI1 concentration

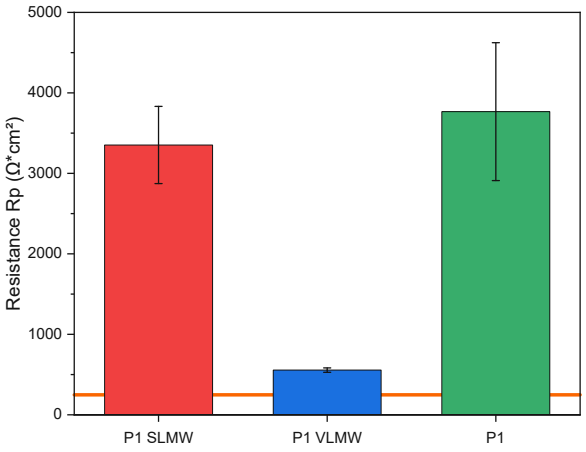

Figure 71: Rp values of uninhibited P1.

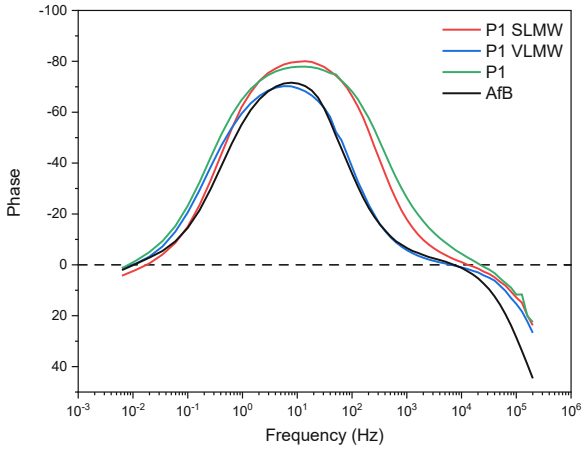

Figure 72: Bode plot, phase vs. frequency of uninhibited P1 and AfB.

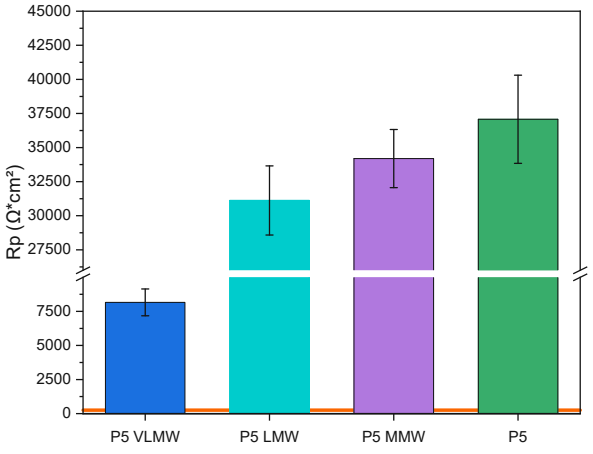

Figure 73: Rp values of uninhibited P5.

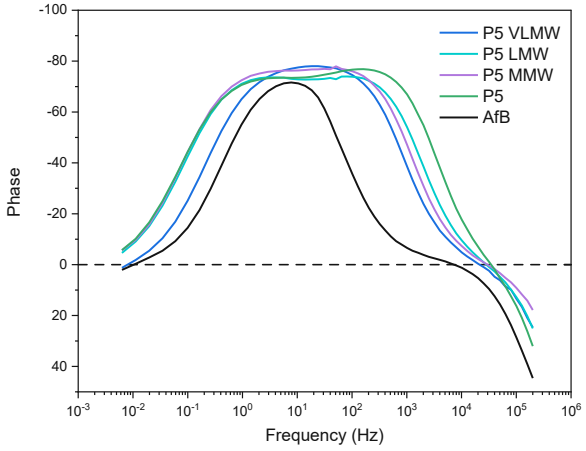

Figure 74: Bode plot, phase vs. frequency of uninhibited P5 and AfB.

4.7.2 Polymer with inhibitor

When inhibitor CI1 is added to the polymer solution, we find also different effects on the inhibition for P1 and P5 in Figure 70. The average Rp for 20 ppm CI1 in AfB is marked by the orange line. Polymer P1 seems to counteract the inhibition by CI1 to some degree, whereas P5 exhibits even a synergistic effect. For interpretation of these phenomena some assumptions on possible effects can be made. While inhibition in polymer free artificial brine is almost independent of the concentration of the inhibitor at the levels applied here, there appears a maximum in Rp for both polymers.

One consideration is that the polymer adsorbs and builds up a highly viscous but inhomogeneous layer around the rotating specimen. The inhibitor will be hindered to diffuse uniformly towards the surface, leaving poorly inhibited areas. An increase in inhibitor concentration will not necessarily be reflected in an increase in the polarisation resistance which will be lower than that of the corresponding polymer-free experiment but higher than the inhibitor free experiment with polymer. Since the structure of such an inhomogeneous polymer layer is assumed to vary significantly from experiment to experiment, rather poor reproducibility, and no clear correlation with inhibitor concentration of Rp values within these limits must be expected. In combination with a competition for adsorption sites at the metal surface this model conception seems to apply to the observations made with P1. Figure 75 underlines this consideration, uninhibited P1-SLMW and P1 both showed higher Rp values than P1-VLMW but with 20 ppm CI1 present, P1-VLMW shows an increasing Rp and therefore better corrosion protection than P1-SLMW and P1 where an antagonistic effect can be seen. As considered in section 4.7.1 there are less adsorption sites occupied by P1-VLMW, compared to P1-SLMW and P1, thus CI1 will be able to adsorb more uniformly and in combination with diffusive effects due to the polymer viscosity it leads to synergistic effect with the 6 MDa polymer sample. Moreover, this can be also seen in the Bode plot (Figure 76) where phase angle of the dark blue line shifts more towards the inhibited AfB curve (black), which indicates a different adsorption of inhibitor and polymer molecules on the metal surface.

Another effect to be considered is the competition in adsorption of polymer and inhibitor. If the polymer binds similarly strong to the steel, it might block the inhibitor from adsorbing. This effect may even be different at different kinds of adsorption sites. While at some such active sites the inhibitor binds and thus inhibits better than the polymer, other sites may offer preferential binding to the polymer which inhibits there better than the inhibitor would do. As a result, the combined action of inhibitor and polymer may yield some synergistic effect. Furthermore, the Bode plot in Figure 78 shows that P5 samples with increasing molecular weight shift the phase angle at higher frequencies more towards the inhibited AfB curve. This model may be considered suitable for the behaviour of P5, and it offers also an explanation for the appearance of a maximum in Rp with increasing concentration of CI1. The maximum may be attributed to the state where polymer and inhibitor bind to their respective adsorption sites, while at higher corrosion inhibitor concentrations the polymer gets replaced by inhibitor, resulting in loss of synergistic protection with Rp tending to the values found for the inhibitor without polymer. This synergistic effect can also be seen in Figure 77 and Figure 78, where with higher molecular weight, more polymer adsorbs at the metal surface, P5 is able to enhance the corrosion protection in combination with CI1 at a concentration of 20 ppm.

The effect of weaker adsorption with VLMW polymer, will lead to more adsorption sites for corrosion inhibitor and a loss of synergistic effect.

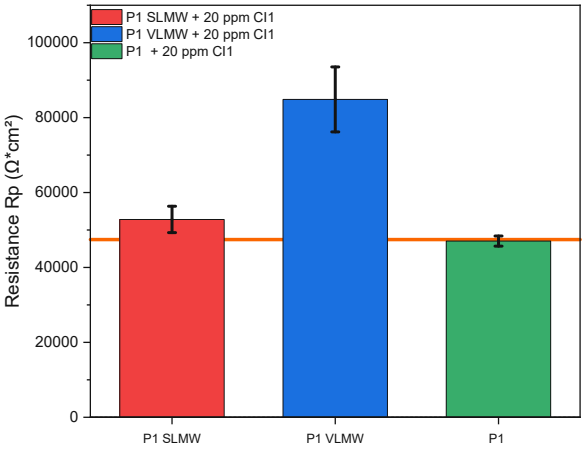

Figure 75: Rp values of polymer 1 with 20 ppm CI1.

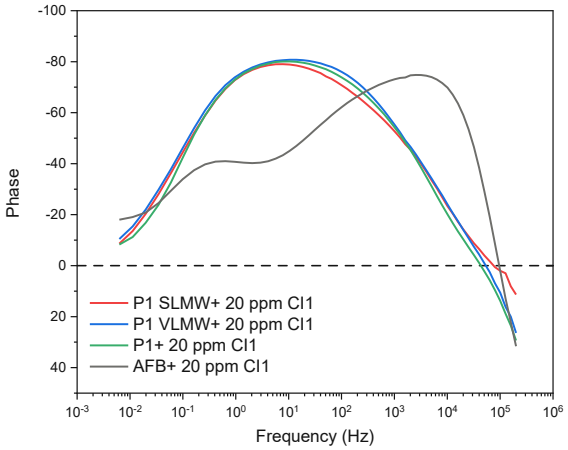

Figure 76: Bode plot, frequency vs phase for inhibited P1 and Standards with CI1.

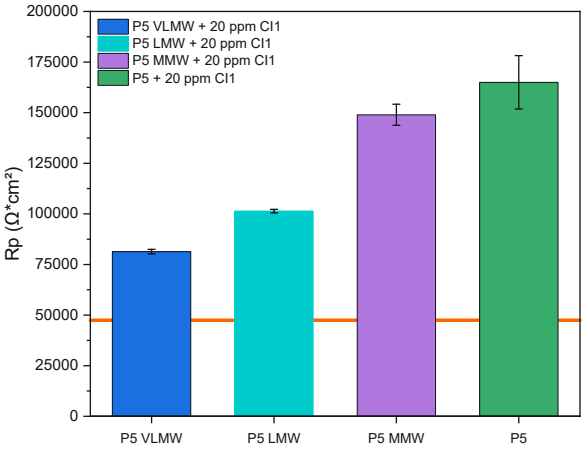

Figure 77: Rp values of polymer 5 with 20 ppm CI1.

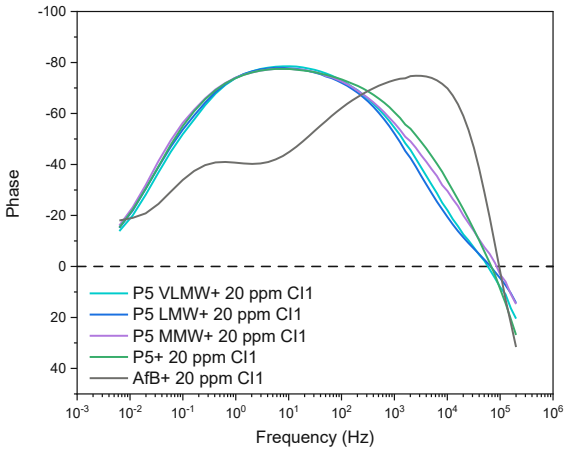

Figure 78: Bode plot, frequency vs phase for inhibited P5 and Standards with CI1.

4.8 Potentiodynamic scans

As described in chapter 3.10 potentiodynamic scans of inhibited AfB and its combination with P1 and P5, respectively, where carried out and plotted in Figure 79 and Figure 80, were the return measurement is not presented. OCP of uninhibited P1-AfB (Figure 79) is shifted to a more anodic potential (by 10 mV) compared to P5-AfB (Figure 80), but the current density of P5 is a magnitude lower than seen with P1. This corresponds with EIS experiments before (section 4.7.1, Figure 71 and Figure 73), where uninhibited P5-AfB shows higher Rp, i.e. lower corrosion rates.

OCP of inhibited P1-AfB is shifted to a more cathodic potential (by 25 mV) compared to the inhibited AfB, while no significant influence on OCP was observed with P5 (< 5 mV). It was noted that, after scanning through the initial cathodic branch, the potential of zero current occurred more anodic than OCP for the polymer-free and the P1 electrolytes. Compared to inhibited AfB (black for both figures), P1 suppresses the cathodic activity near OCP but allows for somewhat increased anodic current, which, in total, yields a small additional inhibiting effect, corresponding with the Rp values in Figure 70. P5 exhibits a different effect: both, anodic and cathodic Tafel branches are significantly shifted to lower currents, which corresponds with the synergistic effect of P5 with CI1 as indicated by Rp in Figure 70.

The anodic branches of inhibited electrolytes indicate that a potential shift of +50 mV to +100 mV from OCP. This is important for the potentiostatically accelerated corrosion (PAC) measurements reported below since such anodic polarization will only accelerate the corrosion processes. At first sight, this should not cause a new phenomenon changing the corrosion mechanism as there is a linear Tafel regime.

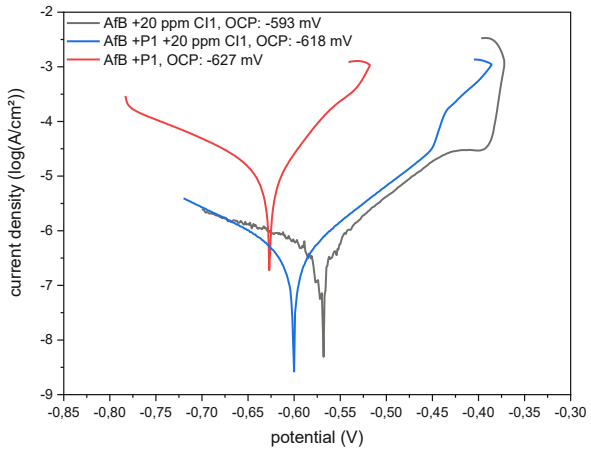

Figure 79: Potentiodynamic scan of uninhibited P1-AfB and inhibited AfB and P1-AfB. Only scans in anodic direction are displayed.

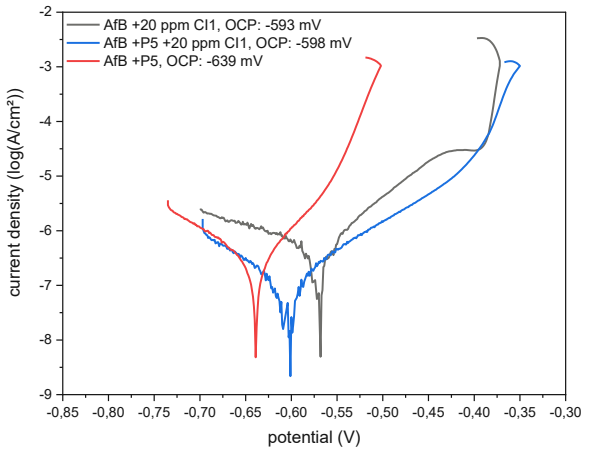

Figure 80: Potentiodynamic scan of uninhibited P5-AfB and inhibited AfB and P5-AfB. Only scans in anodic direction are displayed.

4.9 Potentiostatically accelerated corrosion PAC

Autoclave tests with steel coupons under free corrosion conditions need a long time, up to three weeks for one test series. Therefore, there is a demand for a faster method which represents phenomena as seen in the oil field during corrosion monitoring by weight loss coupons. Moreover, no corrosion attack was observed after EIS measurements: as they are considered to be non-invasive, the immersion time of test specimen is too short (24 hours compared to approx. 90 days). However, in order to accelerate the corrosion processes an anodic potential shift could be applied to speed up the tests, provided the mechanism is not changed.

4.9.1 Localized corrosion patterns in P1-AfB electrolyte

Corrosion at OCP during the EIS experiments caused hardly any visible effect on the steel surface, particularly in the inhibited cases. To drive corrosion until detectable attack occurs, experiments under potentiostatic control were carried out by applying a potential more anodic to OCP for extended time, while the evolution of current would provide further information. The anodic potential shift was chosen, on the basis of the results of the potentiodynamic scans in the respective test solution. By the shift, the applied potential should remain in the linear regime of the anodic Tafel-branches (Figure 79 and Figure 80) and acceleration of the anodic corrosion process without change of the reaction/mechanism may be assumed in the first approximation. On the other hand, due to the considerable speed of potentiodynamic scans, possible changes in the mechanism by time in the potentiostatic mode must not be neglected but may be reflected in the trend of current.

4.9.1.1 Anodic potential shift by +100 mV

In Figure 81, the red curve represents data gained from 20 ppm CI1 inhibited AfB without polymer, blue and violet are inhibited PX-AfB and the black and green curves were obtained with uninhibited PX-AfB containing polymer (P1 and P5, respectively).

The anodic potential hardly affects the inhibited steel (red curve), and the current remains stably low throughout the test, which results in a metallic blank steel specimen after the test (Figure 86) and the mode of CI1 action is schematically shown in Figure 90.

With the CI free polymers solutions (black for P1-AfB and green for P5-AfB), and their moderately inhibitive effect seen from Rp data (section 4.5), a certain corrosion current is established when applying the polarization, driving the dissolution of iron (Figure 81). This promotes the formation of a protective iron carbonate layer on the specimen's surface in the carbonate saturated environment (Figure 82 and Figure 84), supposedly supported by the diffusion limitation for iron ions by the adhering polymer layer. With the corrosion product layer getting thicker and denser, the current decreases over time, reaching the level of the inhibited AfB, finally. The current decay for P1 (black) appears slightly slower than that of P5 (green), while the initial current of P5 was considerably higher, owing to the 24 mV more anodic potential as consequence of its OCP. Figure 82 and Figure 84 present the steel specimens after the test, indicating uniform formation of the protective iron carbonate layer. Tanupabrungsun et al. [39] used thermodynamic calculations and the resulting Pourbaix diagrams to show that iron carbonate formation is promoted at elevated temperatures (60 °C) and pH> 5.5, the corresponding pH values for tested electrolyte solutions are given in Table 12.

The PAC tests with uninhibited PX-AfB (both P1 and P5) could demonstrate that the investigated polymers do not protect the steel by inhibition, but rather promote the formation of a protective layer by limiting the diffusion of iron ions. Figure 91 represents a sketch for this theory and the diffusion limitation of species through the absorbed polymer layer. SEM pictures of the embedded samples after PAC underline the measured data, Figure 87 shows the picture of uninhibited P1-AfB electrolyte with a carbonate layer of approximately 18 µm compared to P5-AfB where the layer is 28 µm thick (Figure 88). This corresponds with the corrosion current measured before, P5 had initially a higher current which leads to an acceleration of corrosion processes and a slightly thicker layer. To compare Figure 89 shows a specimen after PAC test with uninhibited AfB, which current density curve is not plotted in Figure 81. The formed iron carbonate layer in Figure 89 with a thickness of 68 µm, shows typical cubic crystals of iron carbonate [88]. Both polymers affect the formation of the carbonate layer, which becomes less thick and dense, due to the adsorption of polymer on the carbon steel surface and the resulting diffusion limitation effect. These observations confirm the EIS measurements in section 4.7.1 where it was shown that P5 has higher Rp values and therefore a better adsorption on the surface than P1, reducing diffusion and promoting the formation of a protective layer. A comparison of the PAC results with the corresponding Rp data from the uninhibited PX-AfB EIS experiments (Figure 70) must take into account the additional 22 hours more of equilibration time before EIS, which allows for formation of somehow protective layer. This is reflected in the relatively high values of Rp for uninhibited PX-AfB leading to the suggesting of a stronger inhibitive effect of the polymer on carbon steel.

PAC with inhibited AfB containing polymer, represented by the blue (P1) and violet (P5) curves in Figure 81, starts off at very low current, reflecting a well inhibited state. However, both exhibit a steadily increasing current trend over time. While the current for P1 reaches a maximum after 40 h followed by a slow decay, P5 continues to increase throughout the experiment (Figure 81). Such increasing current trend in potentiostatic experiments is characteristic for localized corrosion, due to the progressing acidification at the anodic local spots, and indeed, the steel specimen from the test with P1 presents localized attack: pits appear on the blank surface, shown for 20 ppm CI1 inhibited P1-AfB in Figure 83. The decrease in current trend of P1 after 40 hours may be related to the formation of corrosion products above the corroding spots, providing some degree of protection which can be seen in Figure 83 where the uncleaned specimen is shown. A schematic sketch of this theory is given in Figure 92 showing the adsorbed polymer blocking corrosion inhibitor from adsorption sites on the carbon steel surface.

With P5, the current increase appears less steep compared to P1 and the specimen looks very different after the test, Figure 85. Only two distinct pits appear on the free surface (just one is visible in Figure 85), while most corrosion had occurred at the edges of the cylinder. These edges are considered most critical as the 3-phase boundary steel/rubber-gasket/electrolyte in the edge configuration provides poor access for corrosion inhibitor to the steel. Furthermore, accumulated polymer along this line may form a diffusion barrier for the inhibitor. This effect is also visible on the specimen of P1, though to a lesser degree. Besides this, inhibition by CI1 and P5 was obviously better and more uniformly compared to the inhibition of P1, despite the test potential was 20 mV more positive. This indicates much better access of CI1 through the adsorbed, viscous layer of P5

and does not exclude an additional inhibitive effect of P5 as was considered in view of the synergistic effect derived from Rp data in Figure 70.

In summary, polymers P1 and P5 were found to negatively influence uniform access of corrosion inhibitor CI1 to the surface, although to a different degree: P1 appears more critical than P5 in respect to the degree of localization. In consequence distinct areas on the steel surface are lacking full inhibition, making them prone to localized corrosion which is shown in the schematic sketch in Figure 92. Moreover, the potentiostatic experiments have demonstrated that potentiodynamic measurements alone, due to their inherent speed, may miss important features of corrosion systems: The potentiodynamicaly acquired results gained here indicated straight, Tafel-like anodic branches over a wide potential range and did not yield any indication for the possible onset of localized corrosion in that range.

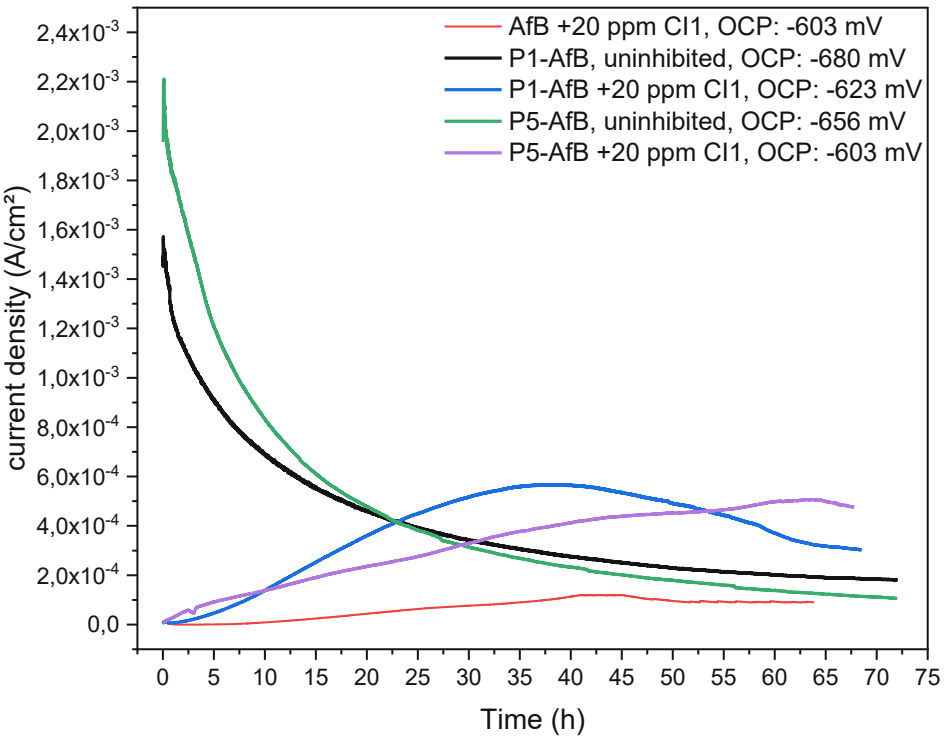

Figure 81: PAC tests at OCP+100 mV, in different solutions.

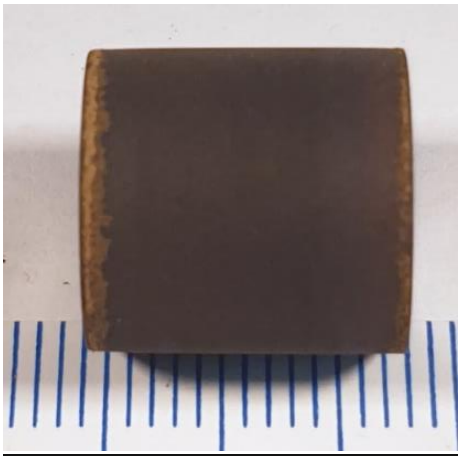

Figure 82: Carbon steel specimen after PAC with uninhibited P1-AfB, uncleaned.

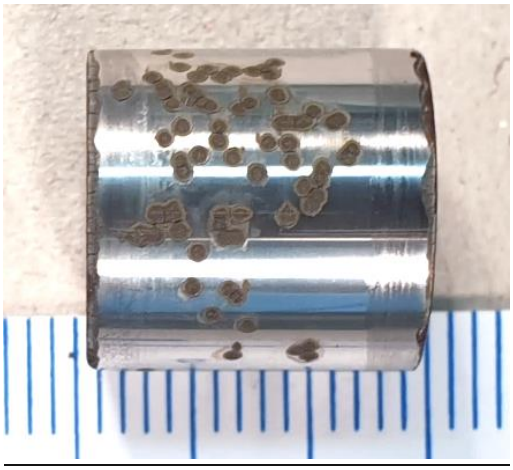

Figure 83: Carbon steel specimen after PAC with 20 ppm CI1 inhibited P1-AfB, uncleaned.

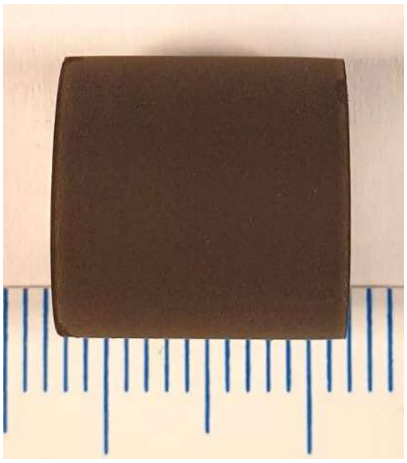

Figure 84: Carbon steel specimen after PAC with uninhibited P5-AfB, uncleaned.

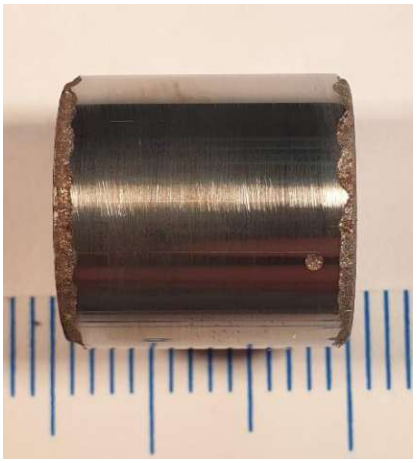

Figure 85: Carbon steel specimen after PAC with 20 ppm CI1 inhibited P5-AfB, cleaned.

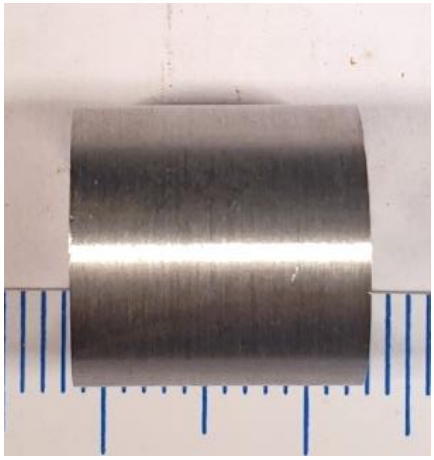

Figure 86: Carbon steel specimen after PAC with 20 ppm CI1 inhibited AfB, uncleaned.

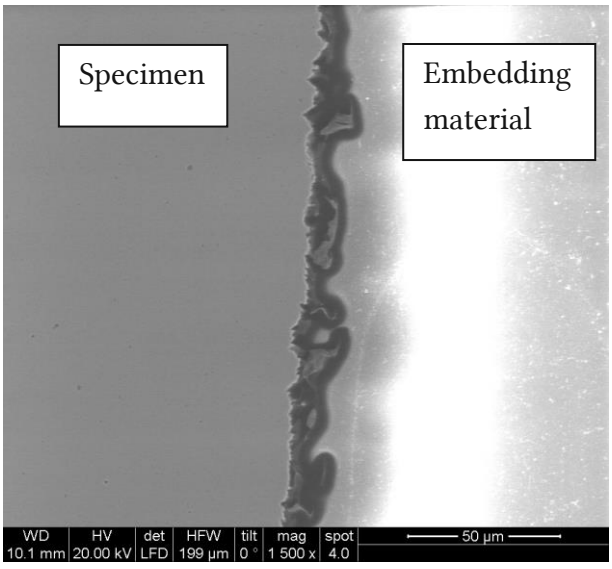

Figure 87: SEM picture of P1-AfB uninhibited, 20 kV, SE, 1500x.

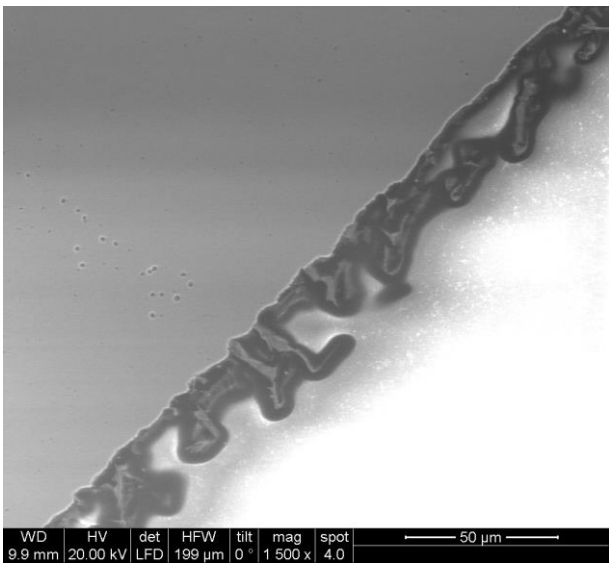

Figure 88: SEM picture of P5-AfB uninhibited, 20 kV, SE, 1500x.

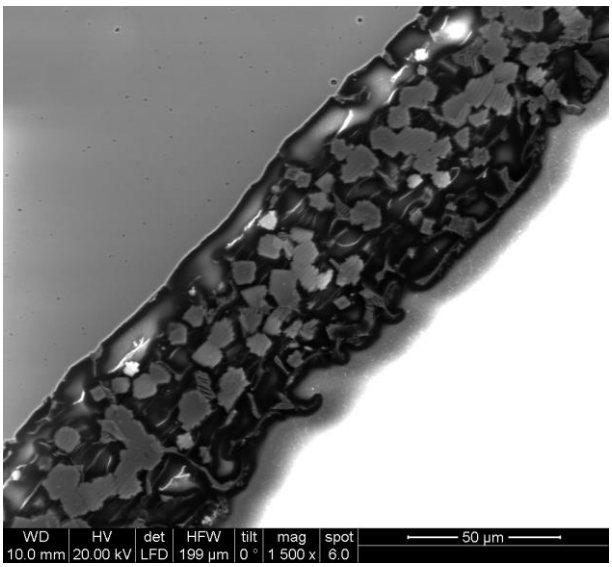

Figure 89 SEM picture of AfB uninhibited, 20 kV, SE, 1500x.

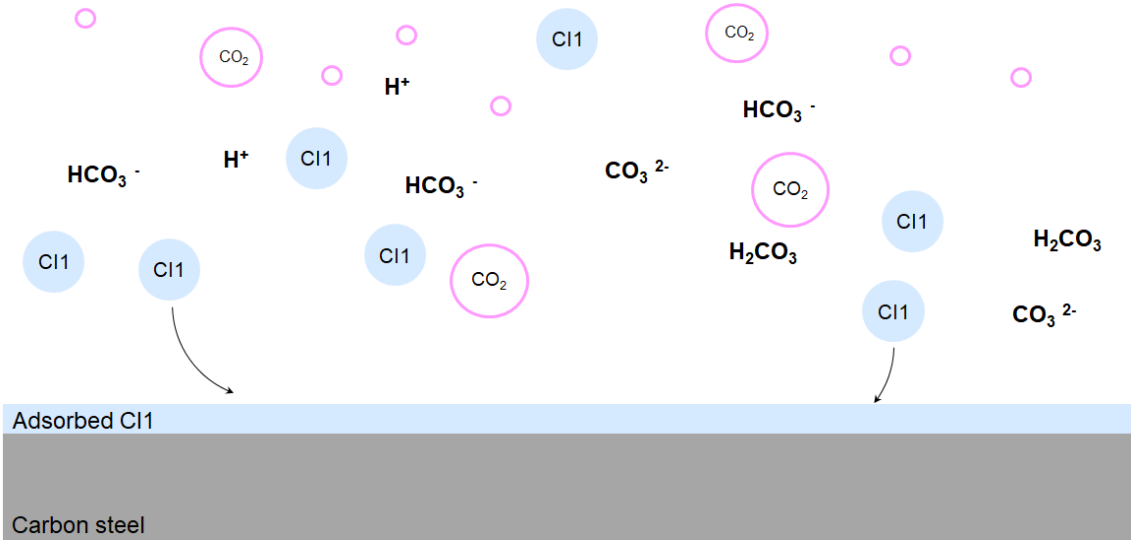

Figure 90: Adsorption of corrosion inhibitor on carbon steel surface.

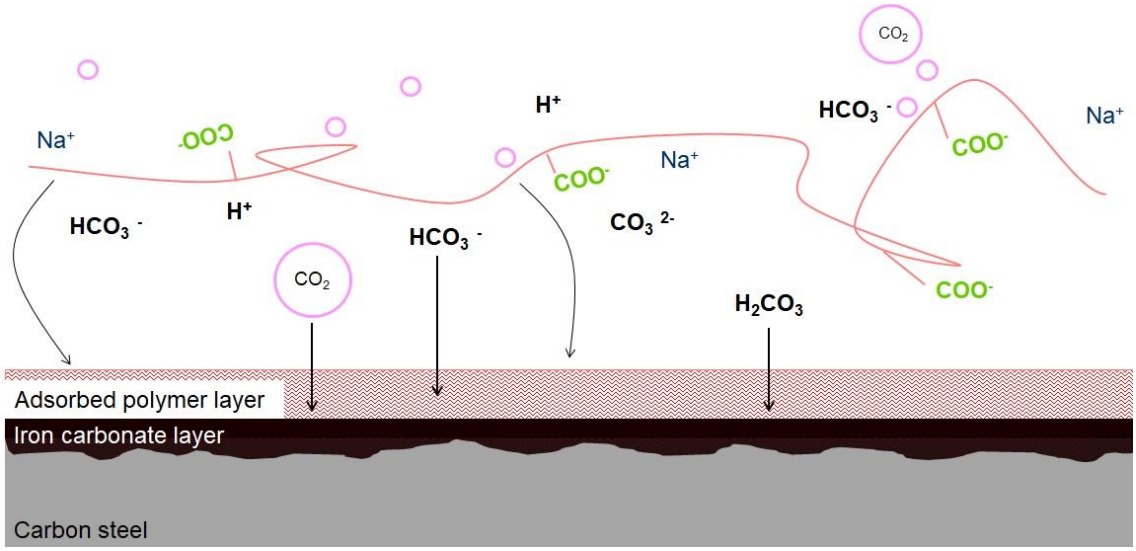

Figure 91: Adsorption of polymer on carbon steel surface and corrosion processes.

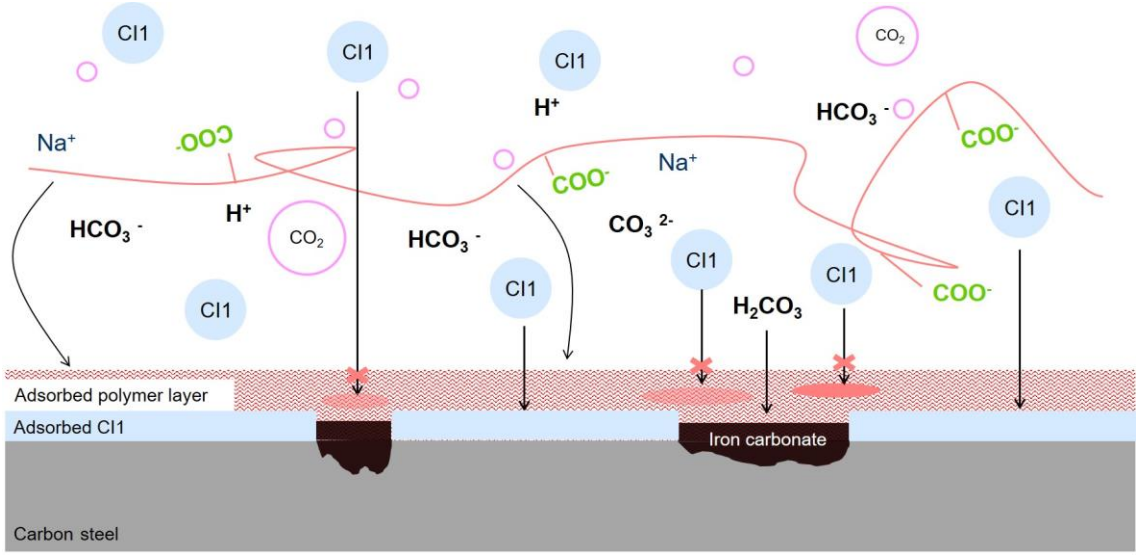

Figure 92: Competition for adsorption sites on carbon steel surface between polymer and corrosion inhibitor.

Table 12: pH for different PX-AfB in CO_2 saturated environment.

Brine	pH
AfB	6,25
P1-AfB	6,65
P5-AfB	6,76

4.9.1.2 Influence of the CI1 concentration on inhibited P1-AfB

To see if there is a threshold potential where corrosion processes start, PAC experiments with a stepwise potential interval increase were done. Figure 93 shows this interval measurement, the potential for P1-AfB with 20 ppm CI1 is increased gradually for certain time intervals by 10 mV starting at OCP+ 50 mV up to OCP+ 100 mV. For a potential shift at OCP+ 50 mV its observed that current density decreases over time and reaches a stable value after 10 h. For the intervals at OCP+ 60 mV and OCP+70 mV the current density increases steadily in Figure 93. The first steeper increase in current density is seen with OCP+ 80 mV after 30 h. With OCP+ 90 mV corrosion processes get accelerated however, the carbon steel specimen in Figure 94 shows only slight localized attack on the surface and edges despite the high anodic potential (OCP+ 100 mV) The time during the accelerated corrosion process (>OCP+ 70 mV) may have been too short to clearly localise the attack to cause visible effects.

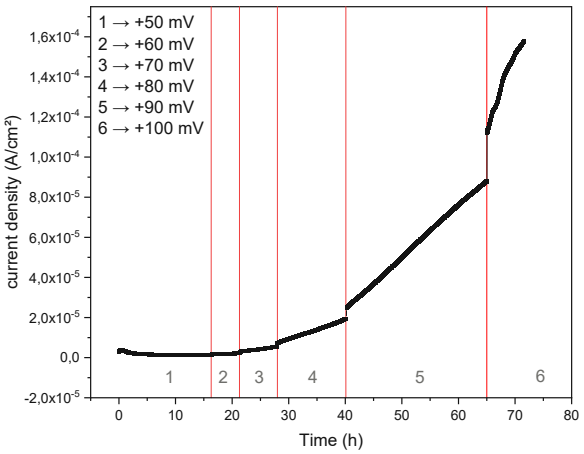

Figure 93: PAC experiment with stepwise increased potential shift for P1-AfB with 20 ppm CI1.

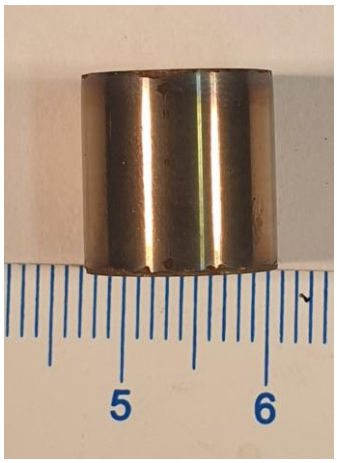

Figure 94: Carbon steel specimen after PAC experiment with stepwise potential increase for P1-AfB with 20 ppm CI1.

4.9.2 Influence of P1 and its chain length on PAC tests

In section 4.7.2 there is a brief discussion on the influence of P1 MW, chain length on the efficiency of corrosion inhibitor CI1.

To possible see corrosion patterns occurring due to the influence of the adsorbed polymer, PAC experiments were carried out. Figure 95 shows the current density curves over time. The current for inhibited P1-SLMW increases drastically during the first 10 h, reaching a stable value till it decreases again after 45 h, despite the high Rp values measured before (Figure 75). The specimen after the experiment, Figure 96, indicates severe localization. The pits were covered with iron carbonate before cleaning, which explains the decrease in current density measured. Although, the results for polymer sample P1-VLMW showing lowest Rp during uninhibited EIS measurements and highest values at inhibition with 20 ppm CI1 the specimen (section 4.7) suffered the same localization effect as P1 and P1-SLMW. A slight flatter ascent in the current density is observed compared to P1 due to better inhibition of CI1 in a P1-VLMW electrolyte. The green curve in Figure 95 represents CI1

inhibited P1-AfB, showing a steeper ascent in current density but a similar maximum and decrease in current density compared to P1-VLMW. This corresponds to observed phenomena in section 4.7.2. If polymer is present in the electrolyte, independent from the polymer chain length, the combination with CI1 leads to localized attack during PAC experiments. Although, different adsorption behaviour of polymers with different chain length and better inhibition with CI1 with medium molecular weight polymer, a heterogeneous surface state is achieved. Adsorption sites preferring polymer adsorption were insufficiently inhibited and favoured spots for anodic iron dissolution, whereas CI1 inhibited areas act as cathode promoting the corrosion till a stable iron carbonate layer is formed.

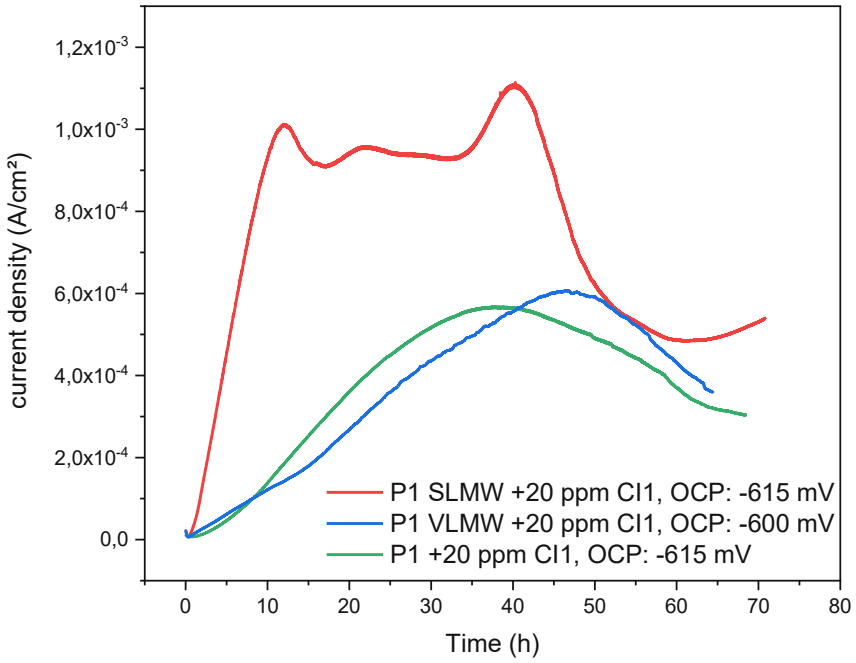

Figure 95: PAC experiments at OCP +100 mV for different P1-AfB electrolytes with 20 ppm CI1.

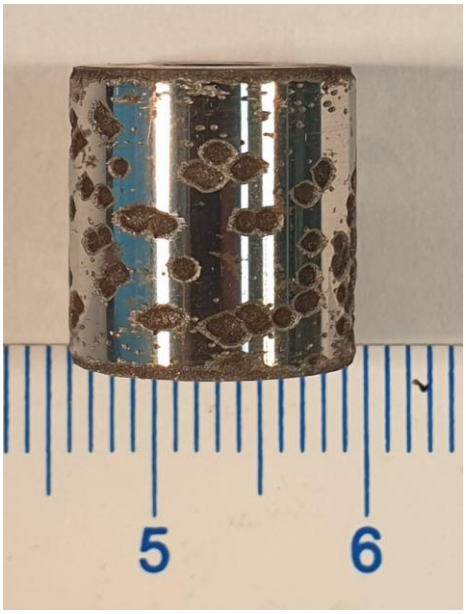

Figure 96: Cleaned test specimen after PAC experiments, P1 SLMW with 20 ppm CI1.

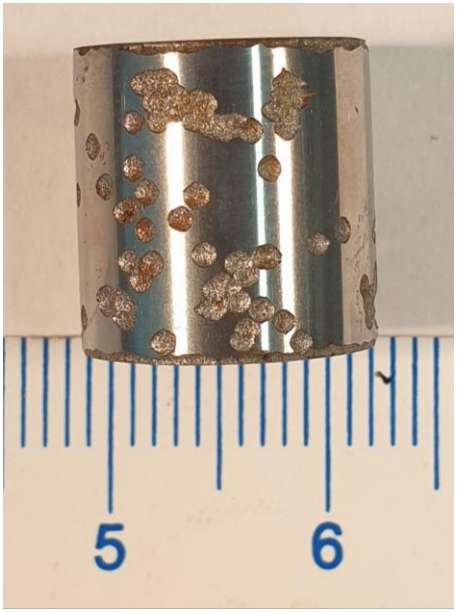

Figure 97: Cleaned test specimen after PAC experiments, P1 VLMW with P1.

4.9.3 Influence of P5 and its chain length on PAC tests

Polymer P5 and its chain length showed a higher corrosion resistance in uninhibited electrolytes and a synergistic effect with corrosion inhibitor CI1. Therefore, they were assumed to counteract the localization effects seen with P1-AfB. PAC experiments with P5 and 20 ppm CI1 (green curve in Figure 98) showing a less steep increase of the current density with time compared to P1 (green curve in Figure 95) and the resulting corrosion pattern at the carbon steel specimen in Figure 85 is located at the edges and some single spots on the surface. This supports the discussion of the synergistic effect for P5-AfB and CI1 given in section 4.7.2, based on the EIS experiments. A similar effect can be recognized with P5 MMW (Figure 98), the current density curve has a steeper ascent at the beginning, heading into a maximum after approx. 45 h and followed by a decrease due to carbonate layer formation. Again, the corrosion occurred on the interface metal/rubber-gasket/electrolyte shown in Figure 100. The polymer sample P5 VLMW with lowest Rp values, despite the presence of corrosion inhibitor (section 4.7.2), shows a different current density evolution and corrosion pattern at the specimen. The current increased immediately when PAC is started for the first 10 h, reaching a kind of stable current density. Between 33 h and 40 h a drastically drop can be observed, stabilising at low current densities. The specimen in Figure 99 indicates localized corrosion attack, the drop in current density may be related to the formation of protective iron carbonate reducing corrosion reaction speed. We may assume that the phase of pit growth was during the timespan with high current density.

To sum up and comparing EIS and PAC experiments for P5 and P5 molecular weight, a relation of the synergistic effects for P5 and CI1 can be seen. The sample with lowest molecular weight, i.e. shortest chain length, promoted the localization of corrosion processes, whereas higher MW in combination with CI1 show mostly non-attacked carbon steel surface. The corrosion on the specimen's edge, i.e. the interface metal/rubber gasket/electrolyte, may be related to diffusion and construction issues at the interface and a resulting crevice effect.

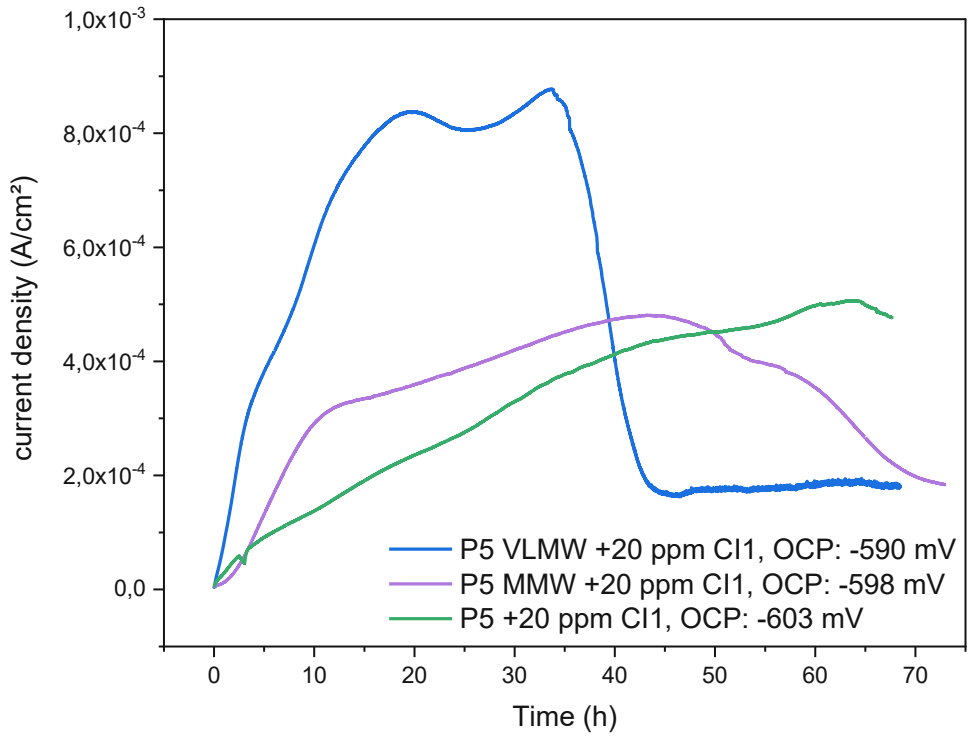

Figure 98: PAC experiments at OCP +100 mV for different P5-AfB electrolytes with 20 ppm CI1.

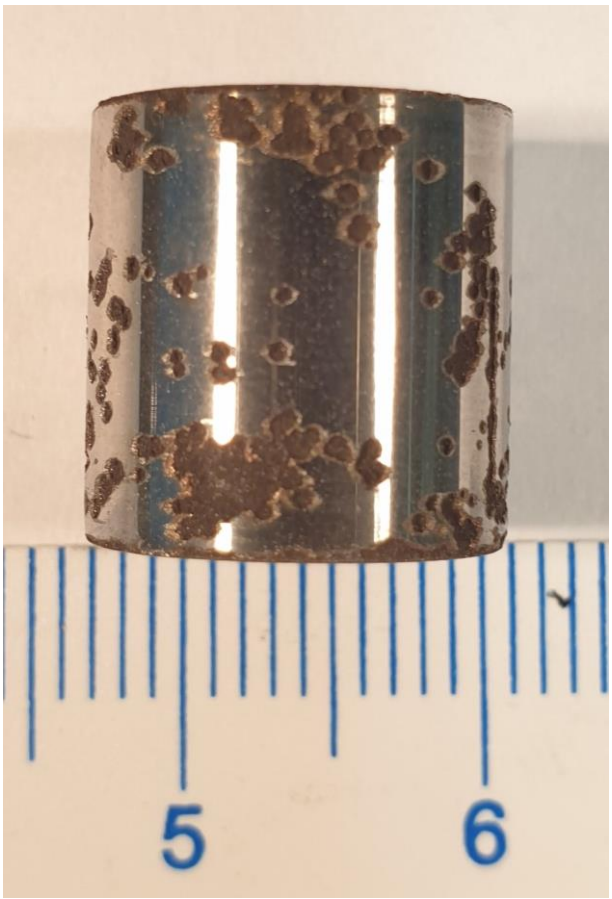

Figure 99: Cleaned test specimen after PAC experiments, P5 VLMW with 20 ppm CI1

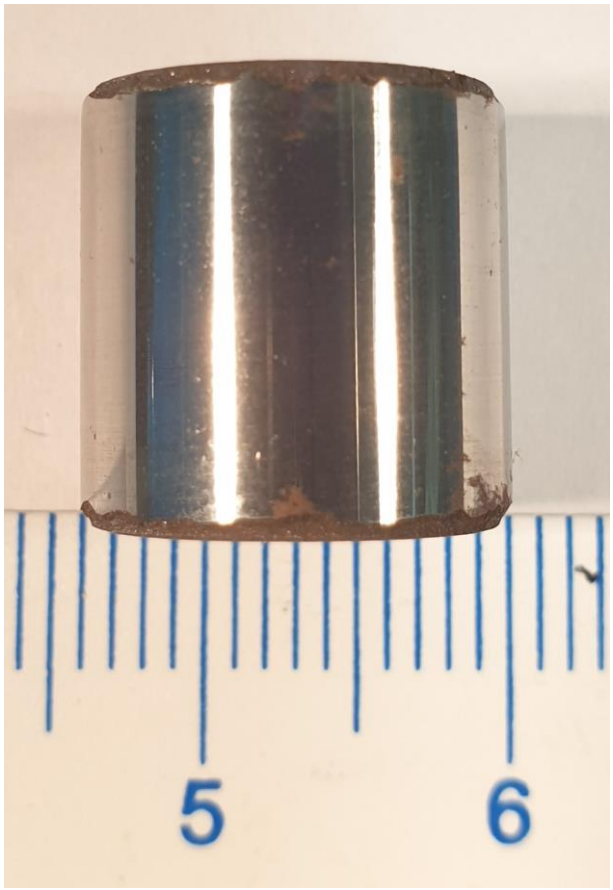

Figure 100: Cleaned test specimen after PAC experiments, P5 MMW with 20 ppm CI1

4.9.4 Influence of CI1 concentration on P1

Since in the tests carried out in section 4.9.1, we were able to reproduce the oil field phenomena and localisation of the corrosion attack with a polymer electrolyte, it was necessary to verify the possibility of suppressing corrosion by a sufficiently high inhibitor concentration. Corrosion monitoring in oil field installations indicated that two or three times the initial concentration of CI1 suppresses the antagonistic effect of P1 and the severe localisation that occurs on weight loss coupons, see Figure 16 and Figure 19.

Figure 101 shows PAC experiments with 100, 60 and 20 ppm CI1 concentration in a P1-AfB electrolyte. OCP at higher concentrations (>60 ppm) is shifted to a 20 mV more positive potential compared to 20 ppm, which is mentioned in the caption of the figure.

The black curve, P1-AfB with 20 ppm CI1, is described in section 4.9.1, a steep increase in the corrosion current density is observed until it reaches a maximum and decreases afterwards.

A similar behaviour is seen with 60 ppm CI1, for the first 25 hours the increase in current density is less steep due to the higher inhibitor concentration allowing more polymer to be replaced from adsorption sites on the metal surface. The current then increases to a maximum at around about 55 hours, followed by a decrease with the formation of a carbonate layer on the corrosion pits (Figure 103). 100 ppm of corrosion inhibitor CI1 was sufficient to replace polymer from adsorption sites or to penetrate the polymer layer and forming a homogeneous CI layer on the specimen's surface, similar to inhibited AfB experiments. The CI suppresses cathodic and anodic processes and hardly any corrosion current is measured during the 70 hour PAC experiment. The carbon steel specimen suffered no corrosion attack which can be seen in Figure 102.

With this experimental approach, we were able to demonstrate the effect of overdosing with CI1, where a high enough concentration of corrosion inhibitor provides effective corrosion protection despite the presence of polymer in the electrolyte. This agrees with the above-mentioned observations in oil field facilities. The antagonistic effect of P1 can be reduced by increasing the inhibitor concentration.

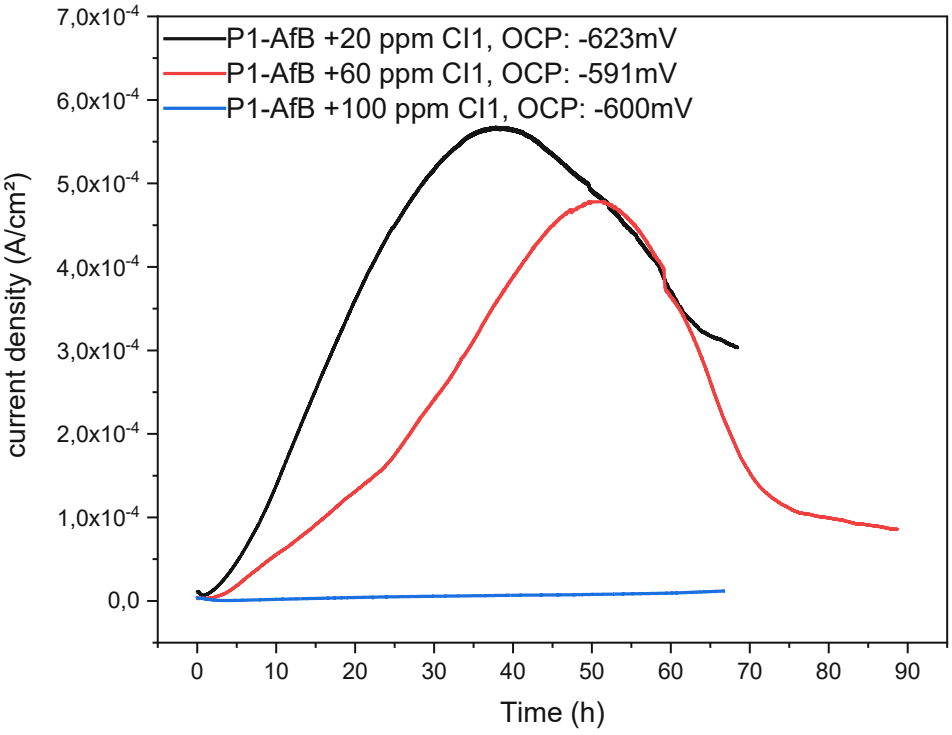

Figure 101: PAC tests at OCP+100 mV and different CI1 concentrations with P1-AfB.

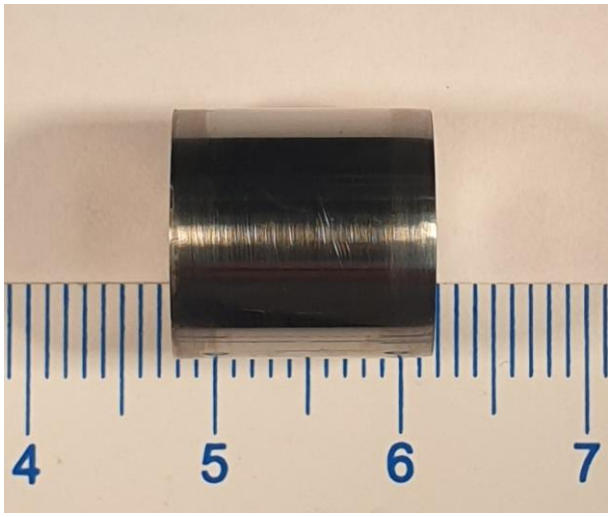

Figure 102: Carbon steel specimen after PAC with 100 ppm CI1 in P1-AfB, uncleaned.

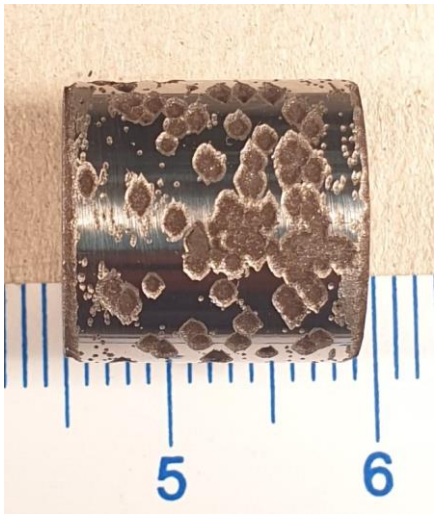

Figure 103: Carbon steel specimen after PAC with 60 ppm CI1 in P1-AfB, cleaned.

4.9.5 Influence of oxygen traces

Since oxygen ingress in the oil field cannot be fully excluded and, as described in section 1.1.4, oxygen has a major influence on corrosion processes in sweet gas environment, the question about its possible influence was addressed qualitatively using CI1 inhibited P1-AfB in PAC experiments. This was necessary because the available oxygen test kits and optical test methods were not applicable to the equipment used in the experiments. Therefore, for this experiment, no quantification of the oxygen concentration was performed.

Experimentally, a 40 cm silicone hose was inserted in the gas supply line (described in section 3.9.1), just before entering the cell in order to allow sufficient time for oxygen diffusion processes through the silicone. Figure 104 shows the adaptation of the CO_2 gas supply, the silicon hose is marked red and the standard gas supply is marked yellow. By the permeability of such silicone [82], traces of oxygen could permeate into the purge gas and accumulate to some degree in the electrolyte. Under the influence of oxygen introduced by this approach, OCP was found by ca. 25 mV more anodic compared to the oxygen-free experiments (section 4.9.1) and with the data from potentiodynamic scans it was decided to apply less polarization (+50 mV from OCP) for the projected PAC tests, in order not to leave the linear Tafel regime as discussed in section 4.8. To compare these experiments with oxygen free tests, which were done in triplicate, the resulting current traces are provided in Figure 105. The experiments with the voluntary ingress of oxygen were carried out in duplicate and the results are shown in Figure 107. Compared to oxygen free PAC experiments where the corrosion current decreases over time (45, 65 and 75 hours), the current was found higher by an order of magnitude and raise steadily throughout the duration of the experiments (45 and 65 hours, respectively) with oxygen present in the electrolyte.

The view of the specimen tested in oxygen free environment for 75 hours is presented in Figure 106. Optically no corrosion products can be seen on the specimen's surface. Compared to this observation, the specimen after 65 hours with oxygen ingress during the experiment shows severe localized corrosion after removal of the corrosion products (Figure 107). This corresponds to the observation from the oil field as described in section 2. Thus, these experiments resulted in very similar corrosion effects as found in the oxygen-free PAC experiments at OCP+100 mV (Figure 83 and Figure 85), although the applied potential was gradually lower. It may be interesting to note that, despite a quantitatively similar degree of corrosion damage, the current-time integral appears considerably lower in the experiments with oxygen ingress. This points to the participation of oxygen in the cathodic process, causing extra cathodic current, which is electrochemically bypassed in this way, inaccessible by the potentiostat.

To sum up, oxygen contaminations may participate in corrosion processes in sweet gas environment, leading to severe localization with polymer presence in the electrolyte.

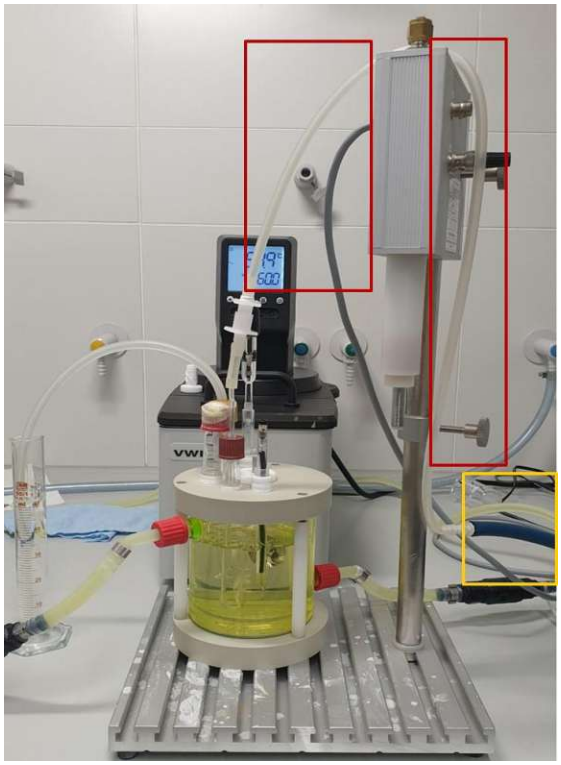

Figure 104: Silicon hose inlet for qualitative oxygen contamination through the CO_2 gas supply.

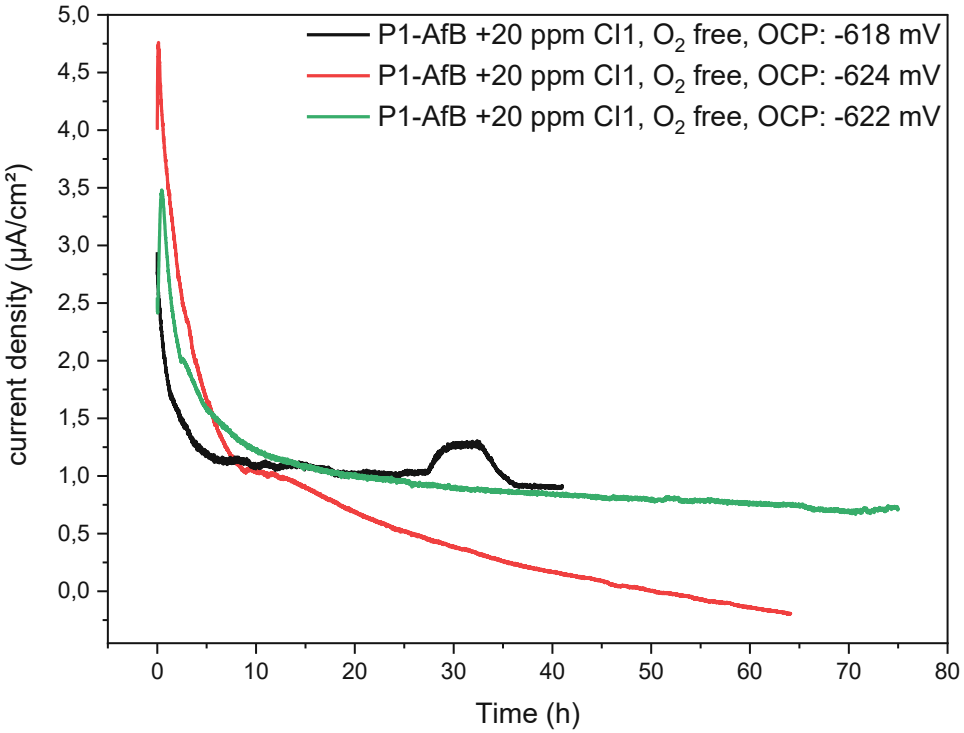

Figure 105: PAC tests with P1-AfB and inhibitor, without oxygen ingress, @OCP +50 mV.

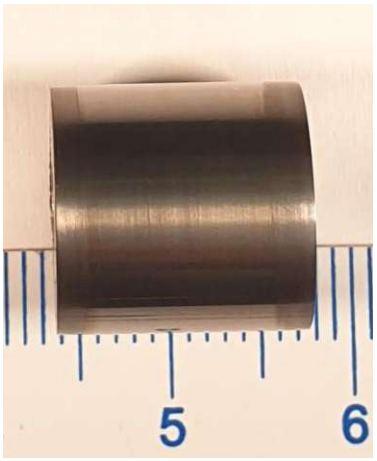

Figure 106: Test specimen @electrolyte without oxygen traces, uncleaned.

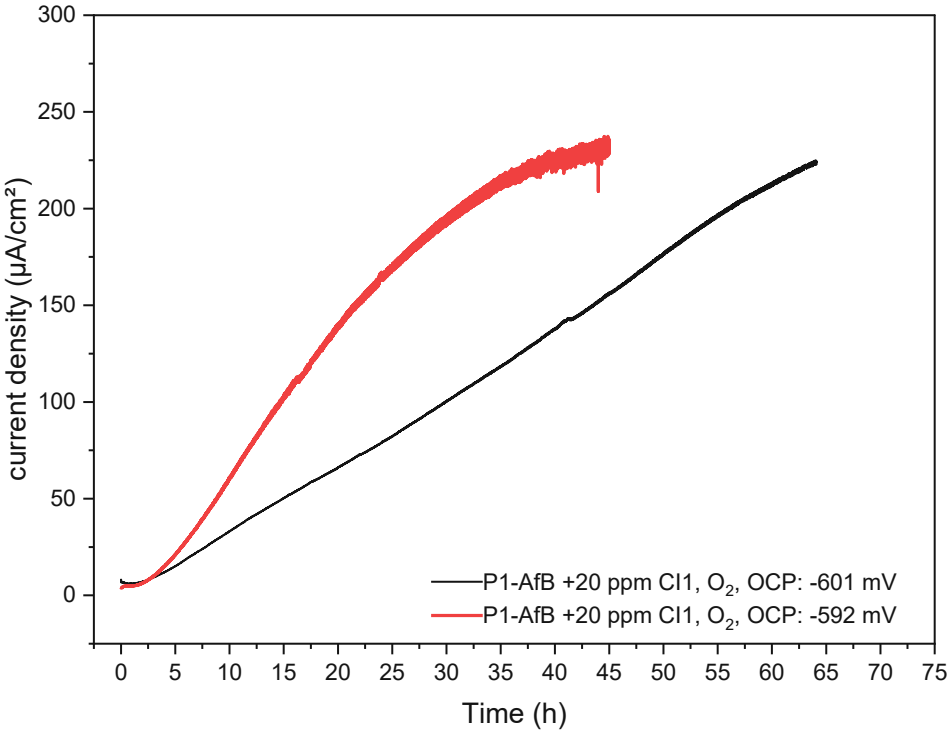

Figure 107: PAC tests with P1-AfB and inhibitor, with oxygen ingress, @OCP +50 mV.

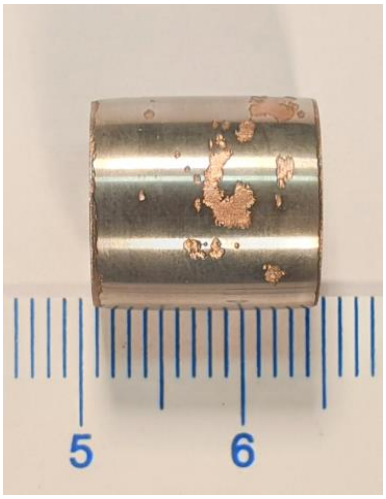

Figure 108: Test specimen @electrolyte with oxygen traces, cleaned.

5 Conclusions

With the test setup and procedure developed during this project we were able to collect sufficient data to conclude as follows:

- RCE-EIS is suitable for the assessment of influences on corrosion processes in specific environmental conditions. Electrolyte composition, temperature, gas saturation and materials for RCE cylinders could be varied easily. Evaluation of impedance spectra by data validation (z-Hit algorithm) and fitting by a Rp/CPE-ladder model was found sufficient for estimating Rp, i.e. the polarisation resistance.
- It's necessary to strictly follow the developed procedure to ensure a reproduceable and surface sensitive EIS result. Especially for measurements of corrosion inhibitor an equilibration time of approximately 20 hours is necessary to decrease the standard deviation σ of Rp.
- Traces of oxygen were found to influence the corrosion mechanism and therefore the EIS recorded. Polarisation resistances (Rp) appear to be lower by an order of magnitude with oxygen impurities present in the electrolyte, i.e. corrosion rates are higher. Leaking sealings and ports of measurement equipment must be avoided.
- Localized corrosion phenomena seen in the oilfield can be replicated by the developed RCE-EIS and PAC laboratory test procedures. For direct reference and comparison of laboratory experiments with field data, further data need to be generated and compared in the field and in the laboratory. In addition, adjustments are still required for PAC testing. These includes reducing the potential shift to provide a reliable method and achieving an optimum between accelerated corrosion and no change in the corrosion mechanism.
- The polymer hydrolysed Polyacrylamide (HPAM) or a polyacrylamide Ter-polymer itself is not corrosive, this applies to all tested products P1-P5. It rather acts slightly inhibitive in saturated CO_2 environment. Without corrosion inhibitor, all tested polymers, especially P1 and P5 were found to promote the formation of a uniform protective layer of corrosion products, supposedly by hindering the diffusion of iron ions through the viscous layer adhering to the steel, leading to precipitation of iron carbonate.
- All tested polymer containing electrolytes without corrosion inhibitor addition provide insufficient protection for carbon steel surfaces in oil field facilities, because the increase in Rp is negligible compared to an effective CI. PAC experiment showed that a combination of a uniform and stable iron carbonate layer and polymer can decrease corrosion rates over time. In a practical application, a uniform layer of corrosion product is unlikely to be preserved and defects could lead to a localisation of the corrosion attack.
- EIS experiments with polymer variants of lower molecular weight (P1 and P5 variants) show a drop in protective properties with lower MW, while extra low MW was found to increase the protection again. It is assumed that flexibility in alignment supports denser adsorption of the small molecules, while for the full-size polymer long-range spreading and coverage is beneficial with respect to the protective effect. Furthermore, it's important to be aware that

most of commercially available polymers consists of a certain range of molecular weight, influencing the adsorption at metal surfaces.

- Degradation of polymer influences the adsorption of the polymer chains and the interaction with different corrosion inhibitors, as degradation influences the chain length of polymer used.
- With inhibitor CI1, a synergistic effect on inhibition was seen with P5, while with P1 less inhibition was found. Different permeability of P1 and P5 for CI1, and a kind of complementary adsorption of P5 and CI1 to the steel surface are considered relevant for these observations.
- Best performing corrosion inhibitor and polymer combinations were P1-AFB with CI2 and P5-AfB with CI1, due to their synergistic effects found during laboratory experiments.
- By potentiostatic tests up to 75 hours, susceptibility to pitting was observed with both polymers when combined with CI1, with P1 being more critical than P5. Under the same conditions, CI1 without polymer provided full protection. Traces of oxygen were found to shift OCP in the anodic direction, thus increasing the risk for localized corrosion.
- The susceptibility to pitting was not revealed by potentiodynamic measurements, which is attributed to the slow kinetics of the localized corrosion process, relative to the duration of a potentiodynamic scan.
- All negative effects observed with polymer presence in the inhibited electrolyte, i.e. increasing corrosion rates and localization of corrosion, can be mitigated by a sufficient increase in corrosion inhibitor concentration.

To summarize, HPAM polymers alone were found not to cause but rather to protect from corrosion. Degradation of the polymer (P1 and P5 tested) weakens this beneficial effect. In combination with an corrosion inhibitor, however, polymer may hinder access of corrosion inhibitor to the steel and consequently incomplete surface coverage may occur. This results in some susceptibility to localized corrosion and provides a direct explanation for such observations from the field. In case of traces of oxygen being present in such a system, the risk for localized corrosion is increased. All these effects of HPAM on corrosion may vary gradually with different HPAM products as was noted in this study. The role of alternative corrosion inhibitors was addressed with the inhibitor comparison in 0, where CI2 performs best with the initially used P1. The standard corrosion inhibitor CI1 shows synergistic effects with P5, a field trial with these candidates is recommended. It has been shown that higher dosages (>100 ppm) of the inhibitor can suppress the negative effects of the polymer and provide sufficient corrosion protection of carbon steel surfaces in oil field facilities where EOR is used.
The possible influence of an oil phase was not considered in this study.
Corrosion testing with RCE-EIS is an option to characterize such combinations of products, and this seems justified from case to case as the commercial polymer products may contain various additives, and similarly inhibitors have in general rather complex formulations, likely causing different interactions with polymers. Careful selection and design of chemicals (polymer, corrosion inhibitor, additives etc.) and materials used in EOR by polymer flooding, is required. Further data from field trials, RCE-EIS and PAC experiments should be gathered and combined in the future to improve the developed procedure and finally by the methodology developed to gain relevant data which can be applied to the oil field.

6 References

[1] J. F. Hilyard, *The oil & gas industry : a nontechnical guide* (The oil and gas industry). Tulsa, Okla, 2012, p. 315 S.

[2] J. G. Speight, "Chapter 1 - Chemistry and Chemical Technology," in *Handbook of Industrial Hydrocarbon Processes*, J. G. Speight Ed. Boston: Gulf Professional Publishing, 2011, pp. 1-41.

[3] J. G. Speight, *An introduction to petroleum technology, economics, and politics*. Salem, MA : Hoboken, N.J.: Wiley, 2011, p. 336 p.

[4] D. W. Green and G. P. Willhite, *Enhanced oil recovery*. Richardson, TX: Henry L. Doherty Memorial Fund of AIME, Society of Petroleum Engineers (in English), 1998.

[5] S. Thomas, "Enhanced Oil Recovery - An Overview," *Oil & Gas Science and Technology - Revue de l'IFP,* vol. 63, pp. 9-19, 01/01 2007, doi: 10.2516/ogst:2007060.

[6] A. Thomas, *Essentials of polymer flooding technique*, First edition.. ed. Hoboken, NJ: Hoboken, NJ : : Wiley, 2019, p. 330 pages.

[7] L. W. Lake, *Enhanced oil recovery*. Englewood Cliffs, N.J.: Prentice Hall (in English), 1989.

[8] G. K. Pedraza Basulto, I. Carrillo, D. Ortega, L. Martinez, and J. Cantó, "Evaluation at Pipeline Corrosion at Oil Field," *ECS Transactions,* vol. 64, no. 26, 2015/04/07, doi: 10.1149/06426.0103ecst.

[9] R. Heidersbach, *Metallurgy and corrosion control in oil and gas production*, Second edition. ed. (Wiley series in corrosion). Hoboken, NJ: Wiley, 2018, p. 354 Seiten.

[10] O. Oyediran, "Mathematical modeling: an application to corrosion in a petroleum industry," 04/01 1999.

[11] L. T. Popoola, A. S. Grema, G. K. Latinwo, B. Gutti, and A. S. Balogun, "Corrosion problems during oil and gas production and its mitigation," *International Journal of Industrial Chemistry,* vol. 4, no. 1, p. 35, 2013/09/27, doi: 10.1186/2228-5547-4-35.

[12] F. W. H. Dean and S. W. Powell, "Hydrogen Flux and High Temperature Acid Corrosion," *Corrosion,* 2006.

[13] J. Kvarekvål and J. Moloney, "Sour corrosion," in *Trends in Oil and Gas Corrosion Research and Technologies*, A. M. El-Sherik Ed. Boston: Woodhead Publishing.

[14] J.-G. Shim, D. W. Lee, J. H. Lee, and N.-S. Kwak, "Experimental study on capture of carbon dioxide and production of sodium bicarbonate from sodium hydroxide," *Environmental Engineering Research,* vol. 21, no. 3, pp. 297-303, 09 2016, doi: 10.4491/eer.2016.042.

[15] L. Smith and B. Craig, "Practical Corrosion Control Measures for Elemental Sulfur Containing Environments," 2005.

[16] S. Papavinasam, *Corrosion Control in the Oil and Gas Industry*. Oxford: Elsevier Science & Technology, 2013.

[17] N. K., "Corrosion and its Mitigation in the oil and gas industry- An Overview," PM-Pipliner, PM-Pipliner, Report 2010.

[18] R. Puthalath, A. O. Surendranathan, and C. S. N. Murthy, "Corrosion mitigation of the oil well steels using organic inhibitors-A review," *Journal of Materials and Environmental Science,* vol. 3, pp. 856-869, 01/01 2012.

[19] J. G. Speight, "Chapter 6 - Corrosion Monitoring and Control," in *Oil and Gas Corrosion Prevention*, J. G. Speight Ed. Boston: Gulf Professional Publishing, 2014.

[20] E. McCafferty, *Introduction to corrosion science*. New York, NY: Springer, 2010, p. 575.

[21] AMPP. "The annual global cost of corrosion in USD2.5 trillion." AmppORG. https://twitter.com/AmppOrg/status/1537178966603497473 (accessed 15.02.2023, 2023).

[22] R. W. Revie and H. H. Uhlig, *Uhlig's corrosion handbook*, 3. ed.. ed. (Corrosion handbook). New York, NY, 2011, p. 1253.

[23] *Korrosion von Metallen und Legierungen –Grundbegriffe*, ISO 8044:2020, D. I. f. N. e.V., Brussels, 2020.

[24] N. Perez, *Electrochemistry and corrosion science*, Second edition. ed. Springer International Publishing, 2016, p. 455 Seiten.

[25] S. K. Dhawan, *Corrosion preventive materials and corrosion testing*. Boca Raton, 2020, p. 258 Seiten.

[26] P. Linhardt, "Lecture Korrosion," M. Schwingenschlögl, Ed., ed. TU Wien: Paul Linhard, 2019.

[27] L. Shreir and R. Cottis, *Shreir's corrosion : 2. Corrosion in liquids, corrosion evaluation*, 4. ed.. ed. Amsterdam: Elsevier, 2010.

[28] M. Pourbaix, *Atlas of electrochemical equilibria in aqueous solutions*, 2d English ed. ed. Houston, Tex: National Association of Corrosion Engineers, 1974.

[29] K. Patterson, Barker, and F. Walsh, *Electrochemical and physical techniques in support of the conservation of historic vessels in the solent*. 2002.

[30] A. Rahmel, *Korrosion und Korrosionsschutz von Stählen*, 1. Aufl.. ed. Weinheim: Verl. Chemie, 1977, p. 380

[31] M. G. Fontana, N. D. Greene, and J. Klerer, "Corrosion Engineering," *Journal of The Electrochemical Society,* vol. 115, no. 5, p. 142, 1968/05/01, doi: 10.1149/1.2411256.

[32] M. Stern and A. L. Geary, "Electrochemical Polarization I . A Theoretical Analysis of the Shape of Polarization Curves," *Journal of The Electrochemical Society,* vol. 104, 1957.

[33] M. Autolab, "Electrochemical corrosion studies of various materials," in "AN-COR-010," Metrom Autolab, AN-COR-010, September 2019. [Online]. Available: https://www.metrohm.com/de_at/applications/application-notes/autolab-applikationen-anautolab/an-cor-010.html

[34] E. E. Stansbury and R. A. Buchanan, *Fundamentals of Electrochemical Corrosion*. ASM International, 2004.

[35] L. L. Shreir, "Outline of Electrochemistry," 1994.

[36] S. Nešić, M. Nordsveen, and A. Stangeland, "A Mechanistic Model for C02 Corrosion with Protective Iron Carbonate Films," 2000.

[37] S. Nesic, J. Postlethwaite, and S. Olsen, "An Electrochemical Model for Prediction of Corrosion of Mild Steel in Aqueous Carbon Dioxide Solutions," *Corrosion,* vol. 52, no. 4, pp. 280-294, 1996, doi: 10.5006/1.3293640.

[38] A. Kahyarian, M. Achour, and S. Nesic, "CO 2 corrosion of mild steel," 2017, pp. 149-190.

[39] T. Tanupabrungsun, "Thermodynamics and Kinetics of Carbon Dioxide Corrosion of Mild Steel at Elevated Temperatures," Ohio University, 2012. [Online]. Available: http://rave.ohiolink.edu/etdc/view?acc_num=ohiou1355328679

[40] R. Barker, D. Burkle, T. Charpentier, H. Thompson, and A. Neville, "A review of iron carbonate (FeCO3) formation in the oil and gas industry," *Corrosion Science,* vol. 142, pp. 312-341, 2018/09/01, doi: https://doi.org/10.1016/j.corsci.2018.07.021.

[41] S. Nešić, "Key issues related to modelling of internal corrosion of oil and gas pipelines – A review," *Corrosion Science,* vol. 49, no. 12, 2007/12/01/, doi: https://doi.org/10.1016/j.corsci.2007.06.006.

[42] E. Van Hunnik, E. Hendriksen, and B. Pots, "The Formation of Protective FeCO3 Corrosion Product Layers in CO2 Corrosion," in *CORROSION 96*, 1996, NACE-96006.

[43] A. Dugstad, "Mechanism of Protective Film Formation During CO2 Corrosion of Carbon Steel," presented at the CORROSION 98, 1998.

[44] M. Gao, X. Pang, and K. Gao, "The growth mechanism of CO2 corrosion product films," *Corrosion Science,* vol. 53, no. 2, pp. 557-568, 2011/02/01/, doi: https://doi.org/10.1016/j.corsci.2010.09.060.

[45] C. Waard and D. E. Milliams, "Carbonic Acid Corrosion of Steel," *Corrosion,* vol. 31, pp. 177-181, 1975.

[46] V. C. Cāstiri, *Corrosion inhibitors : principles and applications / V.S. Sastri*. Chichester, New York: Wiley (in eng), 1998, p. 903.

[47] A. Singh, *Corrosion*. London: IntechOpen, 2020, p. 178 pages.

[48] *Corrosion tests in artificial atmospheres-Salt spray tests (ISO/DIS 9227:2021); German and Endlish Version prEN ISO 9227:2021*, Standard DE30092844, D. D. I. f. N. e.V, 01.07.2022 2022.

[49] S. Hurch, *Wirkung von Inhibitoren auf das Beizen von warmgewalzten Stahlbändern* (Mechanisms of pickling inhibition for hot rolled steels). Wien, 2017, p. 131.

[50] M. E. Orazem, *Electrochemical impedance spectroscopy* (Electrochemical Society series). Hoboken, N.J.: Wiley, 2008, p. 560.

[51] J. R. Macdonald and W. B. Johnson, "Fundamentals of Impedance Spectroscopy," in *Impedance Spectroscopy*, 2005, pp. 1-26.

[52] E. Gileadi, *Physical electrochemistry: fundamentals, techniques and applications* (Master). Weinheim: Wiley-VCH Verl., 2011, p. 373.

[53] A. Sadkowski, "CNLS fits and Kramers–Kronig validation of resonant EIS data," *Journal of Electroanalytical Chemistry,* vol. 573, no. 2, pp. 241-253, 2004/12/01/, doi: https://doi.org/10.1016/j.jelechem.2004.07.009.

[54] E. Barsoukov, J. R. Macdonald, W. John, and Sons, *Impedance spectroscopy : theory, experiment, and applications*, Third edition ed. Hoboken, NJ: Wiley, 2018, p. 528 Seiten.

[55] I. D. Raistrick, D. R. Franceschetti, and J. R. Macdonald, "Theory," in *Impedance Spectroscopy*, 2005, pp. 27-128.

[56] A. Sadkowski, "Unusual electrochemical immittance spectra with negative resistance and their validation by Kramers–Kronig transformation," *Solid State Ionics,* vol. 176, no. 25, pp. 1987-1996, 2005/08/15/, doi: https://doi.org/10.1016/j.ssi.2004.08.041.

[57] B. Mayr-Schmölzer, "Einfluss von Inhibitoren beim Beizen von warmgewalzten niedriglegierten Stählen," Effects of inhibitors on acid pickling of low-alloyed hot-rolled steels, Wien, Techn. Univ., Diss., 2014, 2013. [Online]. Available: https://permalink.catalogplus.tuwien.at/AC10775924

[58] *Wheel Test Method Used for Evaluation of Film-Persistent Corrosion Inhibitors for Oilfield Applications*, 1D182, I. NACE, 2017.

[59] F. Walsh, G. Kear, A. Nahlé, J. Wharton, and L. Arenas, "The rotating cylinder electrode for studies of corrosion engineering and protection of metals—An illustrated review," *Corrosion Science,* vol. 123, 03/01 2017, doi: 10.1016/j.corsci.2017.03.024.

[60] H. Ohba and S. Kuroda, "Numerical Analysis of Flows around a Rotating Square Cylinder," *JSME International Journal Series B,* vol. 36, no. 4, 1993, doi: 10.1299/jsmeb.36.592.

[61] M. Aparecida de Melo, E. F. Lucas, I. Fundão, M. Fernandes Santos De Melo, and E. F. Lucas, "Characterization and selection of polymers for future research on enhanced oil recovery," 2008.

[62] A. Thomas, N. Gaillard, and C. Favero, "Some Key Features to Consider When Studying Acrylamide-Based Polymers for Chemical Enhanced Oil Recovery," *Oil & Gas Science and Technology,* vol. 67, pp. 887-902, 11/01 2013, doi: 10.2516/ogst/2012065.

[63] A. Galio and C. Dariva, "Corrosion Inhibitors – Principles, Mechanisms and Applications," 2014, pp. 365-380.

[64] *API RP6 3*, A. P. Institute, Dallas, TX, 1990.

[65] C. FAVERO, N. GAILLARD, and B. GIOVANETTI, "Novel formulations of water-soluble polymers and stabilizing additives for injecting a single compound usable in injection fluids for chemical enhanced oil recovery," FR Patent Appl. PCT/EP2009/057270, 2010.

[66] T. G. Mezger, *Applied Rheology*. Austria: Anthon Paar GmbH, 2021, p. 196.

[67] *Warmgewalzte Erzeugnisse aus Baustählen- Teil 2: Technische Lieferbedingungen für unlegierte Baustähle*, Standard DIN EN 10025-2, D. I. f. Normung, 10/2019 2019.

[68] *Korrosion von Metallen und Legierungen-Entfernen von Korrosionsprodukten von Korrosionsprüfkörpern*, Standard DIN EN ISO 8407, D. I. f. Normung, Januar 2021 2021.

[69] W. Ehm, H. Göhr, R. Kaus, B. Röseler, and C. A. Schiller, "The evaluation of electrochemical impedance spectra using a modified logarithmic Hilbert transform," *ACH - Models in Chemistry,* vol. 137, pp. 145-157, 01/01 2000.

[70] F. Mansfeld, "Recording and Analysis of AC Impedance Data for Corrosion Studies," *Corrosion,* vol. 37, no. 5, 1981, doi: 10.5006/1.3621688.

[71] N. D. Cogger and N.J.Evans, "A Introduction to Electrochemical Impedance Measurement," in "Technical Report No.6," Solatron analytical, France, Technical Report 6, 05/1999 1999.

[72] F. Mansfeld, M. W. Kendig, and S. Tsai, "Recording and Analysis of AC Impedance Data for Corrosion Studies," *Corrosion,* vol. 38, no. 11, pp. 570-580, 1982, doi: 10.5006/1.3577304.

[73] A. Kahyarian, B. Brown, and S. Nesic, "Electrochemistry of CO2 corrosion of mild steel: Effect of CO2 on iron dissolution reaction," *Corrosion Science,* vol. 129, pp. 146-151, 2017/12/01/, doi: https://doi.org/10.1016/j.corsci.2017.10.005.

[74] W. Weißbach, *Werkstoffkunde : Strukturen, Eigenschaften, Prüfung*, 19., vollst. überarb. u. erw. Aufl. ed. (Lehrbuch). Wiesbaden: Wiesbaden : Springer Vieweg, 2015, p. 597 S.

[75] M. Jafarzadegan, A. Abdollah-zadeh, A. Feng, T. Saeid, J. Shen, and H. Assadi, "Microstructure and Mechanical Properties of a Dissimilar Friction Stir Weld between Austenitic Stainless Steel and Low Carbon Steel," *Journal of Materials Science & Technology,* vol. 29, pp. 367–372, 04/01 2013, doi: 10.1016/j.jmst.2013.02.008.

[76] *Metallic materials- Vickers Hardness test- Part 1: Test method*, Standard ISO/DIS 6507-1:2022, D. I. f. N. e.V., 15.07.2022 2022.

[77] D. R. Gabe, G. D. Wilcox, J. Gonzalez-Garcia, and F. C. Walsh, "The rotating cylinder electrode: its continued development and application," *Journal of Applied Electrochemistry,* vol. 28, no. 8, pp. 759-780, 1998/08/01, doi: 10.1023/A:1003464415930.

[78] D. R. Gabe, "The rotating cylinder electrode," *Journal of Applied Electrochemistry,* vol. 4, no. 2, pp. 91-108, 1974/05/01, doi: 10.1007/BF00609018.

[79] Y. J. Tan, S. Bailey, and B. Kinsella, "An investigation of the formation and destruction of corrosion inhibitor films using electrochemical impedance spectroscopy (EIS)," *Corrosion Science,* vol. 38, no. 9, pp. 1545-1561, 1996/09/01/, doi: https://doi.org/10.1016/0010-938X(96)00047-9.

[80] P. Altoé, G. Pimenta, C. F. Moulin, S. L. Díaz, and O. R. Mattos, "Evaluation of oilfield corrosion inhibitors in CO2 containing media: A kinetic study," *Electrochimica Acta,* vol. 41, no. 7, pp. 1165-1172, 1996/05/01/, doi: https://doi.org/10.1016/0013-4686(95)00467-X.

[81] R. Kelly, J. Scully, D. Shoesmith, and R. Buchheit, "Electrochemical Techniques in Corrosion Science and Engineering," 01/01 2003, doi: 10.1201/9780203909133.

[82] H. Zhang, "The Permeability Characteristics of Silicone Rubber," *SAMPE Fall Technical Conference,* 01/01 2006.

[83] M. Moshtaghi, M. Eškinja, G. Mori, T. Griesser, M. Safyari, and I. Cole, "The effect of HPAM polymer for enhanced oil recovery on corrosion behaviour of a carbon steel and interaction with the inhibitor under simulated brine conditions," *Corrosion Science,* vol. 217, 2023/06/01/, doi: https://doi.org/10.1016/j.corsci.2023.111118.

[84] O. M. A. Khamaysa *et al.*, "Hydrazone-based green corrosion inhibitors for API grade carbon steel in HCl: Insights from electrochemical, XPS, and computational studies," *Colloids and Surfaces A: Physicochemical and Engineering Aspects,* vol. 626, 2021/10/05/, doi: https://doi.org/10.1016/j.colsurfa.2021.127047.

[85] T. K. Sarkar, V. Saraswat, R. K. Mitra, I. B. Obot, and M. Yadav, "Mitigation of corrosion in petroleum oil well/tubing steel using pyrimidines as efficient corrosion inhibitor: Experimental and theoretical investigation," *Materials Today Communications,* vol. 26, 2021/03/01, doi: https://doi.org/10.1016/j.mtcomm.2020.101862.

[86] H. Viltres, O. F. Odio, M. C. Biesinger, G. Montiel, R. Borja, and E. Reguera, "Preparation of Amine- and Disulfide-Containing PAMAM-Based Dendrons for the Functionalization of Hydroxylated Surfaces: XPS as Structural Sensor," *ChemistrySelect,* https://doi.org/10.1002/slct.202000432 vol. 5, no. 16, 2020/04/30, doi: https://doi.org/10.1002/slct.202000432.

[87] E. Kolek, P. Simko, P. Simon, and A. Gatial, "Confirmation of polymerisation effects of sodium chloride and its additives on acrylamide by infrared spectrometry," *Journal of Food and Nutrition Research,* vol. 46, pp. 39-44, 01/01 2007.

[88] A. Lazareva, J. Owen, S. Vargas, R. Barker, and A. Neville, "Investigation of the evolution of an iron carbonate layer and its effect on localized corrosion of X65 carbon steel in CO2 corrosion environments," *Corrosion Science,* vol. 192, 2021/11/01/, doi: https://doi.org/10.1016/j.corsci.2021.109849.

7 Table of Figures

Figure 1: Formation and migration of oil and gas [1]. 2
Figure 2: Hydrocarbon recovery mechanisms[6]. 3
Figure 3: Bjerrum plot, pH vs. mole fraction of carbonate species[14]. 7
Figure 4: Schematic drawing of electrochemical processes at the metal/electrolyte interface modified after personal communication[26]. 12
Figure 5: Pourbaix diagram of iron in water (25°C) [29]. 13
Figure 6: Schematic Current-potential curve indicating possible effects of alloying elements and electrolyte compositions.[30]. 14
Figure 7: schematic experimental polarization curve [33]. 16
Figure 8: Polarization curve showing E_{pit} and E_r for a metal in a chloride solution[27]. 18
Figure 9: Pourbaix diagrams for Fe-CO2-H2O system; c(Fe^{2+})=10 ppm, c(Fe^{3+})=10 ppm at 25°C. 20
Figure 10:Pourbaix diagrams for Fe-CO2-H2O system; c(Fe^{2+})=10 ppm, c(Fe^{3+})=10 ppm at 80°C. 20
Figure 11:Pourbaix diagrams for Fe-CO2-H2O system; c(Fe^{2+})= 10 ppm, c(Fe^{3+})= 10 ppm at 100°C. 21
Figure 12: Phase shift of the sinusoidal current response[25]. 26
Figure 13: Randal circuit with elements: electrolyte resistance R_s, charge transfer resistance R_{ct} and double layer capacitance C_{dl}. [25] 26
Figure 14: Example of a Nyquist plot[25]. 27
Figure 15: Simulated pseudo-inductivity (reproduced from [57]). 27
Figure 16: Example of corrosion monitoring for wellhead 1. 29
Figure 17: Example of corrosion monitoring for wellhead 2. 29
Figure 18: Corrosion coupon without HPAM (P1) and uniform corrosion attack at low corrosion rates. 30
Figure 19: Corrosion coupon with HPAM (P1) at wellhead 1 and localized corrosion attack. 30
Figure 20: Corrosion coupon with HPAM (P1) at wellhead 2 and localized corrosion attack 30
Figure 21: Considerations how a polymer (HPAM) could influence the system: carbon steel/corrosion inhibitor/polymer. 31
Figure 22: Stirring unit for polymer brine preparation. 32
Figure 23: Propeller stirrer with diameter of 50 mm. 32
Figure 24: Specimen holder with seals and carbon steel sample. 35
Figure 25: Blueprint of the used cylinder specimen with dimensions and tolerances. 35
Figure 26: Schematic drawing of RCE cell. 38
Figure 27: impedance model used for data fitting, four stage ladder circuit. 39
Figure 28: Carbon steel specimen, etched with 1% Nital for 6 sec., 200x. 41
Figure 29: Carbon steel specimen, etched with 1% Nital for 6 sec., 1000x. 41
Figure 30: SEM BSE image of carbon steel specimen at magnification 5000x. 42
Figure 31: Dimensioning of hardness indentation at 200x magnification. 42
Figure 32: Nyquist plot of continuous EIS measurement for P1-AfB with 20 ppm CI1. 45
Figure 33: Comparison of Rp for AfB and P1-AfB with different concentrations of CI1 during continuous procedure. 45
Figure 34: Comparison of RP for AfB and P1-AfB with different concentrations of CRW85579 during single measurement procedure. 45
Figure 35: Bode plot for uninhibited AfB and P1-AfB during single measurment procedure. 46
Figure 36: OMV cell setup, l.t.r.: OMV-A (model 1), OMV-N1 (model 2), OMV-N2 (model 2). 47
Figure 37: TU Wien cell setup, l.t.r.: TU-A (prototype), TU-N (model 2). 47
Figure 38: OMV-N1, Test A, rusty brown electrolyte due oxygen contamination. 48

Figure 39: OMV-N1, Test A, corrosion layer on specimen after 24h EIS. 48
Figure 40: TU-A, Test A, electrolyte without O_2 contamination 48
Figure 41: Test A&D, Results from EIS measurements @ OMV Lab. 49
Figure 42: Test A&D, Results from EIS measurements @ OMV and TU Lab. 49
Figure 43: Test A, potentiodynamic scans. 50
Figure 44: Test D, potentiodynamic scans. 50
Figure 45: Test C, Results from EIS measurement @ OMV Lab. 51
Figure 46: Test B&C, Results from EIS measurements @ OMV and TU Lab. 51
Figure 47: Test B, potentiodynamic scans. 52
Figure 48: Test C, potentiodynamic scans. 52
Figure 49: Test C, different CO_2 supply lines. 53
Figure 50: Rp values of different electrolyte brines (AfB and P1) with CI1. 55
Figure 51: Inhibitor free Rp values of AfB and P1-AfB. 55
Figure 52: Bode plot, Impedance vs frequency for inhibited and uninhibited artificial brine with CI1. 55
Figure 53: Bode plot, phase vs. frequency for inhibited and uninhibited artificial brine with CI1. 55
Figure 54: Bode plot, Impedance vs frequency for inhibited and uninhibited P1-AfB with CI1. 55
Figure 55: Bode plot, phase vs frequency for inhibited and uninhibited P1-AfB with CI1. 55
Figure 56: schematic sketch of adsorbed polymer and the diffusion limitation. 56
Figure 57: Fitted Rp values of different corrosion inhibitor samples in P1-AfB. 58
Figure 58: Rp comparison of AfB and P1-AfB with CI1 and CI2. 59
Figure 59: Bode plot, frequency vs. phase for uninhibited and inhibited AfB with CI1. 59
Figure 60: Bode plot, frequency vs. phase for uninhibited and inhibited AfB with CI2. 59
Figure 61: Bode plot, frequency vs. phase for uninhibited and inhibited P1-AfB with CI1. 60
Figure 62: Bode plot, frequency vs. phase for uninhibited and inhibited P1-AfB with CI2. 60
Figure 63: Rp values of different polymer samples at inhibitor concentration 0. 61
Figure 64: Comparison of Rp for different polymer samples and CI1. 63
Figure 65: Comparison of Rp for different polymer samples and CI2. 64
Figure 66: Rp for different P5 batches. 66
Figure 67: Bode plot, phase vs. frequency for P5 batches. 66
Figure 68: Differences for uninhibited P5 batches. 66
Figure 69: FTIR measurement of P5 Batch 1 and Batch 2. 66
Figure 70: Rp values of AfB, P1 and P5 with different CI1 concentration 69
Figure 71: Rp values of uninhibited P1. 69
Figure 72: Bode plot, phase vs. frequency of uninhibited P1 and AfB. 69
Figure 73: Rp values of uninhibited P5. 69
Figure 74: Bode plot, phase vs. frequency of uninhibited P5 and AfB. 69
Figure 75: Rp values of polymer 1 with 20 ppm CI1. 71
Figure 76: Bode plot, frequency vs phase for inhibited P1 and Standards with CI1. 71
Figure 77: Rp values of polymer 5 with 20 ppm CI1. 71
Figure 78: Bode plot, frequency vs phase for inhibited P5 and Standards with CI1. 71
Figure 79: Potentiodynamic scan of uninhibited P1-AfB and inhibited AfB and P1-AfB. Only scans in anodic direction are displayed. 72
Figure 80: Potentiodynamic scan of uninhibited P5-AfB and inhibited AfB and P5-AfB. Only scans in anodic direction are displayed. 72
Figure 81: PAC tests at OCP+100 mV, in different solutions. 75

Figure 82: Carbon steel specimen after PAC with uninhibited P1-AfB, uncleaned. ... 76
Figure 83: Carbon steel specimen after PAC with 20 ppm CI1 inhibited P1-AfB, uncleaned. ... 76
Figure 84: Carbon steel specimen after PAC with uninhibited P5-AfB, uncleaned. ... 76
Figure 85: Carbon steel specimen after PAC with 20 ppm CI1 inhibited P5-AfB, cleaned. ... 76
Figure 86: Carbon steel specimen after PAC with 20 ppm CI1 inhibited AfB, uncleaned. ... 76
Figure 87: SEM picture of P1-AfB uninhibited, 20 kV, SE, 1500x. ... 76
Figure 88: SEM picture of P5-AfB uninhibited, 20 kV, SE, 1500x. ... 77
Figure 89 SEM picture of AfB uninhibited, 20 kV, SE, 1500x. ... 77
Figure 90: Adsorption of corrosion inhibitor on carbon steel surface. ... 77
Figure 91: Adsorption of polymer on carbon steel surface and corrosion processes. ... 78
Figure 92: Competition for adsorption sites on carbon steel surface between polymer and corrosion inhibitor. ... 78
Figure 93: PAC experiment with stepwise increased potential shift for P1-AfB with 20 ppm CI1. ... 79
Figure 94: Carbon steel specimen after PAC experiment with stepwise potential increase for P1-AfB with 20 ppm CI1. ... 79
Figure 95: PAC experiments at OCP +100 mV for different P1-AfB electrolytes with 20 ppm CI1. ... 80
Figure 96: Cleaned test specimen after PAC experiments, P1 SLMW with 20 ppm CI1. ... 80
Figure 97: Cleaned test specimen after PAC experiments, P1 VLMW with P1. ... 80
Figure 98: PAC experiments at OCP +100 mV for different P5-AfB electrolytes with 20 ppm CI1. ... 82
Figure 99: Cleaned test specimen after PAC experiments, P5 VLMW with 20 ppm CI1 ... 82
Figure 100: Cleaned test specimen after PAC experiments, P5 MMW with 20 ppm CI1 ... 82
Figure 101: PAC tests at OCP+100 mV and different CI1 concentrations with P1-AfB. ... 84
Figure 102: Carbon steel specimen after PAC with 100 ppm CI1 in P1-AfB, uncleaned. ... 84
Figure 103: Carbon steel specimen after PAC with 60 ppm CI1 in P1-AfB, cleaned. ... 84
Figure 104: Silicon hose inlet for qualitative oxygen contamination through the CO_2 gas supply. ... 86
Figure 105: PAC tests with P1-AfB and inhibitor, without oxygen ingress, @OCP +50 mV. ... 86
Figure 106: Test specimen @electrolyte without oxygen traces, uncleaned. ... 86
Figure 107: PAC tests with P1-AfB and inhibitor, with oxygen ingress, @OCP +50 mV. ... 87
Figure 108: Test specimen @electrolyte with oxygen traces, cleaned. ... 87